# Kamil Wojnicki

# The role of BLM and RecQL4 helicases in defining the response of glioma cells to chemotherapeutics

PhD thesis

Completed in the Laboratory of Molecular Neurobiology

of the Nencki Institute of Experimental Biology

Polish Academy of Sciences

**SUPERVISOR:**

**Prof. dr hab. Bożena Kamińska-Kaczmarek**

Warsaw, 2023

## ***Pragnę podziękować/I would like to thank:***

# Content

## 4. RESULTS

## 5. DISCUSSION

## ABSTRACT

Malignant gliomas are primary tumours of the central nervous system. They remain one of the hardest to treat brain tumours due to their invasive phenotype, the immunosuppressive microenvironment and anatomical localisation in vital areas of the brain. The intratumoural heterogeneity and overexpression of enzymes involved in DNA replication and repair, impair the effectiveness of commonly used therapies, leading to an inevitable relapse of the tumour.

The RecQ helicases are considered 'guardians of the genome', as they play the fundamental roles in DNA replication, repair and maintaining genome stability. The RecQ family is composed of several structurally related helicases, including BLM (Bloom Syndrome) helicase. The involvement of RecQ helicases in tumorigenesis and responses to therapies in malignant brain tumours is not fully understood, thus we aimed to elucidate the role of BLM in these processes.

The Cancer Genome Atlas (TCGA) dataset analyses and immunostaining of numerous tumour sections demonstrated that BLM is overexpressed in high grade gliomas (WHO grade 3 and 4). In malignant gliomas BLM localisation was detected in the cytoplasm whereas in benign tumours BLM was present mostly in the nuclear compartment. High BLM levels were detected in several glioma cell lines and primary patient derived cultures. To decipher the role of BLM in gliomas, BLM deficient LN18 and LN229 cells were generated using CRISPR/Cas9 genome editing technology. BLM deficiency (KO) had minor effects on basal cell viability and proliferation. However, the cell responses to chemotherapeutics, in particular to the combination of temozolomide (TMZ, a DNA methylating agent common used in glioblastoma therapy) and olaparib (OLA, a PARP inhibitor) were changed. Unexpectedly, BLM KO cells were more resistant to the combined treatment than wild type (WT) cells that underwent apoptosis. Moreover, this effect was exclusive for TMZ combined with PARP inhibitors. The BLM KO cells were not sensitive to PARP inhibitors, in contrast to expected the synthetic lethality. BLM KO cells displayed the therapy induced cellular senescence (LN229) or polyploidy (LN18). The polyploidy in p53-deficient LN18 cells was reversed by forced p53 expression.

Interestingly, RecQL4-depleted LN18 and LN229 cells responded to TMZ+OLA similarly to WT cells which indicates specialised and non-overlapping functions of RecQ family helicases.

To obtain more insights into the functions of distinct RecQ helicases we generated *blm* and *recql4* knock-out in *Xenopus* frogs to evaluate roles of the helicases in the embryonic development. Considerable mortality of tadpoles was noted and helicase-depleted tadpoles displayed morphological and functional developmental abnormalities.

Altogether, the present study demonstrates important and specific functions of BLM and RecQL4 helicases in glioma cell responses to chemotherapy. As BLM expression was highly elevated and inversely correlated with survival of patients with malignant gliomas, we postulate that BLM could be a therapeutic target. The assessment of BLM levels, p53 and MGMT, a DNA repair enzyme, status might be helpful in choosing the proper therapy against malignant gliomas.

## STRESZCZENIE

Glejaki złośliwe są pierwotnymi nowotworami ośrodkowego układu nerwowego i pozostają jednymi z najtrudniejszych do leczenia guzów mózgu ze względu na inwazyjny fenotyp, immunosupresyjne mikrośrodowisko i anatomiczną lokalizację w ważnych obszarach mózgu. Heterogenność nowotworu i zwiększona ekspresja enzymów biorących udział w replikacji i naprawie DNA, osłabia skuteczność powszechnie stosowanych terapii, co prowadzi do nieuchronnego nawrotu nowotworu.

Helikazy RecQ są uważane za „strażników genomu" i odgrywają fundamentalną rolę w procesach replikacji DNA, naprawie i utrzymaniu stabilności genomu. Rodzina helikaz RecQ składa się z kilku, strukturalnie podobnych enzymów, do których należy helikaza BLM (Bloom Syndrome). Zaangażowanie helikaz RecQ w powstawanie nowotworów i odpowiedzi na terapie złośliwych guzów mózgu nie jest w pełni poznane, dlatego podjęliśmy badania, aby wyjaśnić rolę BLM w tych procesach.

Analiza danych z repozytorium The Cancer Genome Atlas (TCGA) i barwienie immunohistochemiczne skrawków licznych guzów wykazały, że ekspresja BLM zarówno na poziomie mRNA i białka jest podwyższona w glejakach o wysokim stopniu złośliwości (stopień 3 i 4 wg Światowej Organizacji Zdrowia). W glejakach złośliwych obecność BLM wykryto w cytoplazmie, podczas gdy w guzach łagodnych i tkance prawidłowej BLM był obecny głównie w jądrze komórkowym. Wysoki poziom białka BLM wykryto w kilku liniach komórkowych glejaka i pierwotnych hodowlach pochodzących od pacjentów. Aby wyjaśnić rolę BLM w glejakach, usunięto gen *BLM* w komórkach glejaków linii LN18 i LN229 stosując technikę edycji genomu CRISPR/Cas9. Usunięcie BLM (KO) miało niewielki wpływ na żywotność i proliferację komórek w warunkach podstawowych, jednak zmieniało odpowiedzi komórek na chemioterapeutyki. Było to szczególnie widoczne po zastosowaniu temozolomidu (TMZ, środek metylujący DNA, powszechnie stosowany w terapii glejaka wielopostaciowego) i olaparibu (OLA, inhibitor PARP). Nieoczekiwanie, komórki BLM KO były bardziej oporne na kombinację obu leków niż komórki z funkcjonalną helikazą BLM (WT), które umierały na drodze apoptozy. Co więcej, efekt ten występował tylko w przypadku

połączenia TMZ z inhibitorami PARP. Komórki BLM KO nie były wrażliwe na inhibitory PARP, w przeciwieństwie do oczekiwanej syntetycznej śmiertelności. Komórki BLM KO wykazywały indukowane terapią starzenie komórkowe (LN229) lub poliploidię (LN18). Występowanie poliploidii w komórkach LN18 z niedoborem p53 było obniżone po przywróceniu funkcjonalnego białka p53. Co ciekawe, komórki LN18 i LN229 pozbawione helikazy RecQL4 reagowały na TMZ+OLA podobnie jak komórki WT, co wskazuje na wyspecjalizowane i niejednakowe funkcje helikaz z rodziny RecQ.

W celu uzyskania informacji na temat funkcji różnych helikaz RecQ, przeprowadzono usunięcie genów *blm* i *recql4* u zarodków żab *Xenopus*, aby ocenić rolę helikaz w rozwoju embrionalnym. Odnotowano znaczną śmiertelność kijanek, a kijanki pozbawione funkcjonalnych helikaz wykazywały morfologiczne i funkcjonalne nieprawidłowości rozwojowe.

Niniejsze badania pokazują ważne i specyficzne funkcje helikaz BLM i RecQL4 w odpowiedzi komórek glejaka na chemioterapię. Status mutacyjny i poziom ekspresji BLM jest szczególnie ważny przy łączeniu terapii TMZ z inhibitorami PARP. Ze względu na podwyższoną ekspresję BLM, która odwrotnie korelowała z przeżyciem pacjentów z glejakami złośliwymi, postulujemy, że BLM może być celem terapeutycznym. Proponujemy, że ocena poziomu BLM oraz statusu p53 i MGMT, jednego z enzymów naprawczych DNA, może być pomocna w wyborze właściwej terapii przeciw glejakom złośliwym.

## ABBREVIATIONS

**3-ABA** – 3-aminobenzamide

**6-TG** - 6-thioguanine

**β-gal** – β-galactosidase

**ALT** - Alternative Lengthening of Telomeres

**APE1** - DNA-(APurinic or APyrimidinic site) Endonuclease

**ATM** - serine-protein kinase ATM

**ATR** - serine/threonine-protein kinase ATR

**BER** – Base Excision Repair

**BGS** - Baller-Gerold Syndrome

**BLM KO** – BLM knock-out

**BRCA1/2** - BReast and ovarian CAncer susceptibility protein 1/2

**DDR** - DNA Damage Response

**DOX** - doxorubicin

**DSB** – DNA Double-Strand Breaks

**ETO** – etoposide

**EXO1** – EXOnuclease 1

**FEN1** - Flap ENdonuclease 1

**GBM** – glioblastoma, WHO grade 4 glioma

**H2AX** - histone H2AX

**HR** – Homologous Recombination

**IDH1/2** - Isocitrate DeHydrogenase 1/2

**INI** - iniparib

**MGMT** – O$^6$-MethylGuanine MethylTransferase

**MMR** – mismatch repair

**NER** – Nucleotide Excision Repair

**NHEJ** - Non-Homologous End Joining

**OLA** – olaparib

**p53** - cellular tumour antigen p53

**PARP** –Poly(ADP-Ribose) Polymerase

**PARPi** – Poly(ADP-Ribose) Polymerase inhibitors

**PCNA** - Proliferating Cell Nuclear Antigen

**PFA** – paraformaldehyde

**POT1** - Protection Of Telomeres protein 1

**RAD51** - DNA repair protein RAD51 homolog 1

**RTS** - Rothmund-Thomson Syndrome

**RUCA** - rucaparib

**RQ4** – RecQL4 helicase

**RQ4 KO** – RecQL4 knock-out

**SASP** – Senescence-Associated Secretory Phenotype

**SSB** – DNA Single-Strand Break

**T+O** – temozolomide with olaparib

**TCGA** – The Cancer Genome Atlas

**TIS** – Therapy Induced Senescence

**TMZ** – temozolomide

**TRF1/2** - Telomeric Repeat-binding Factor 1/2

**WHO** - World Health Organisation

**WT** – Wild Type

# 1. INTRODUCTION

## 1.1. Structure and biological roles of helicases

Helicases belong to a large group of ubiquitous enzymes that utilise the energy from nucleoside triphosphate (NTP) hydrolysis to disrupt complementary hydrogen bonds and separate double-stranded DNA, RNA duplexes or amino acid complexes with proteins. The separation of a DNA strand allows each strand to be copied, maintaining the integrity of all cellular processes (Gorbalenya and Koonin 1993; Cordin et al. 2006). Based on sequence and structure homology, helicases are divided into super families: SF1-SF6, and further into families. Helicases from super families 1 and 2 (SF1-2) can act as a single protein or dimers while helicases encompassing super families 3-6 (SF3-6) occur in ring-shaped hexameric structures (Medagli and Onesti 2013). While divergent in the overall protein sequence, the structural similarities of helicases indicate that they have similar enzymatic activities. The examples of DNA (black) and RNA (green) helicases of SF1-6 are presented in figure 1.
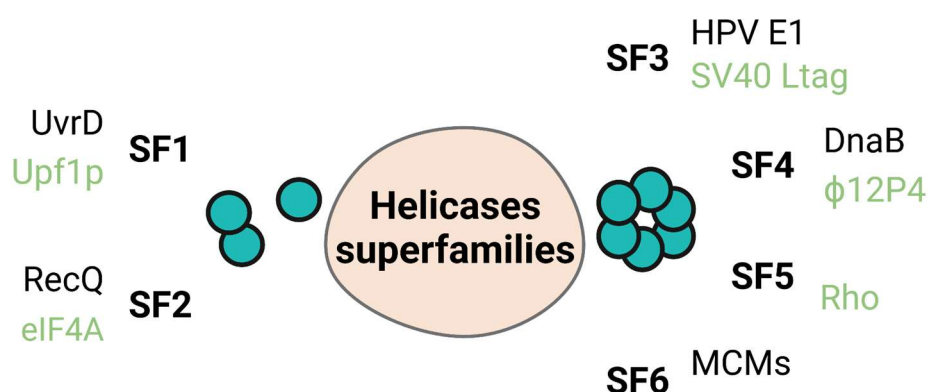


**Figure 1. DNA and RNA helicases superfamilies.**
DNA helicases (black) and RNA helicases (green) are divided into 6 superfamilies (SF1-6) and display the functions as monomers/dimers (SF1/SF2) or form hexameric-ring structures (SF3-SF6). Figure adapted from Jankowsky and Fairman-Williams 2010.

Basic parameters characterising the helicases are: translocation rate, directionality, processivity, step size and "active" or "passive" mechanism of action (Singleton et al. 2007). The 'processive, zipper-like' protein with unwinding activity was discovered by Abdel-Monem et al. in 1976 in *Escherichia coli* (*E.coli*) DNA helicase (Abdel-Monem et al. 1976).

There are 95 helicases or putative helicases (31 DNA- and 64 RNA helicases) encoded by the human genome (Umate et al. 2011). DNA and RNA helicases

are found in prokaryotes, eukaryotes and viruses. The enzymes participate in many cellular processes from DNA replication, recombination and repair, through disrupting G-quadruplexes and other DNA secondary structures, to all aspects of RNA metabolism such as duplex unwinding, secondary structure resolving, and protein displacement from DNA/RNA strands (Jankowsky and Fairman-Williams 2010; Brosh and Matson 2020).

Helicases are involved in many vital processes, thus the activity of DNA/RNA helicases must be tightly regulated. The overexpression and mutations can affect the cellular homeostasis and contribute to cancer development or progression due to disruption of genome stability and integrity (Heerma van Voss et al. 2017; Datta and Brosh 2018; Xie et al. 2022).

### 1.2. Functions of RecQ Family of DNA Helicases

The first RecQ helicase was discovered nearly 40 years ago in *E.coli* through screening of thyminless-death resistant mutants and its function was connected with the RecF pathway of recombinational repair (Nakayama et al. 1984). RecQ activity prevented the illegitimate recombination in *E.coli*, rescuing the stalled replication forks and ultimately promoting the SOS (stands for 'save our soul') repair response (Killoran and Keck 2006). In human cells there are five RecQ helicases: RecQL1, BLM (Bloom syndrome helicase), WRN (Werner syndrome), RecQL4 and RecQL5 (Bernstein et al. 2010). RecQL5 exists in different forms due to alternative mRNA splicing (Shimamoto et al. 2000). RecQ helicases belong to the SF2 super family. The enzymes bind to DNA and translocate along a single strand in a 3' to 5' direction and notably, the single-stranded DNA (ssDNA) stimulates the double-stranded DNA (dsDNA) unwinding activity.

All RecQ helicases exist in several pathways and the function is to maintain the integrity of the genome; thus RecQ helicases are named 'guardians of the genome'. These enzymes take part in DNA replication, recombination and repair, influencing base excision repair (BER) and are indirectly involved in DNA double-strand break repair (Croteau et al. 2014; Newman and Gileadi 2020). Mutations in genes coding for the three helicases (BLM, WRN and RecQL4) have been associated with rare, aging- and cancer-predisposing related diseases: Bloom Syndrome ([BS] in the *BLM* gene), Werner Syndrome ([WS], in the *WRN* gene), and Baller-Gerold (BGS)-, RAPADILINO- and Rothmund-Thomson (RTS) Syndromes

(in the *RecQL4* gene) (Monnat 2010). Recently, the mutations in *RecQL1* gene have been identified and associated with a novel, human genome instability disorder named RECON (RECql ONe) Syndrome (Abu-Libdeh et al. 2022). Only RecQL5 is currently not associated with any genetically determined syndromes, however the gene has been implicated in a hereditary breast cancer susceptibility (Tavera-Tapia et al. 2019).

The RecQ helicases share three conserved sequence regions across bacterial and eucaryotic proteins: the helicase domain, the RecQ carboxy-terminal (RecQ-Ct, RQC) domain and the Helicase-and-RNaseD-like-C-terminal (HRDC) domain. The helicase domain is responsible for ATP binding and hydrolysis, and also defines the RecQ family. The RQC domain provides the protein structural integrity, dsDNA binding and mediates the interactions with other proteins. The HRDC domain plays an auxiliary role in binding to nucleic acids and is present only in BLM and WRN helicases. Moreover, the HRDC domain is found in other helicase families or nucleases digesting RNA (Bennett and Keck 2004; Guo et al. 2005; Lee et al. 2005; Killoran and Keck 2006; Chu and Hickson 2009). Notably, only WRN contains the Exo domain with 3'-5' exonuclease activity, helping to process telomeric D-loop substrates and telomere maintenance (Romero-Zamora and Hayashi 2023). The N-terminal Sld2 domain of RecQL4 shows the sequence similarity to the yeast Sld2, plays a role in the initiation of DNA replication in *Saccharomyces cerevisiae* (Masumoto et al. 2002) and displays an ATP-dependent DNA unwinding activity *in vitro* (Xu and Liu 2009; Abe et al. 2011). Structures of RecQ family members are depicted in the figure 2.
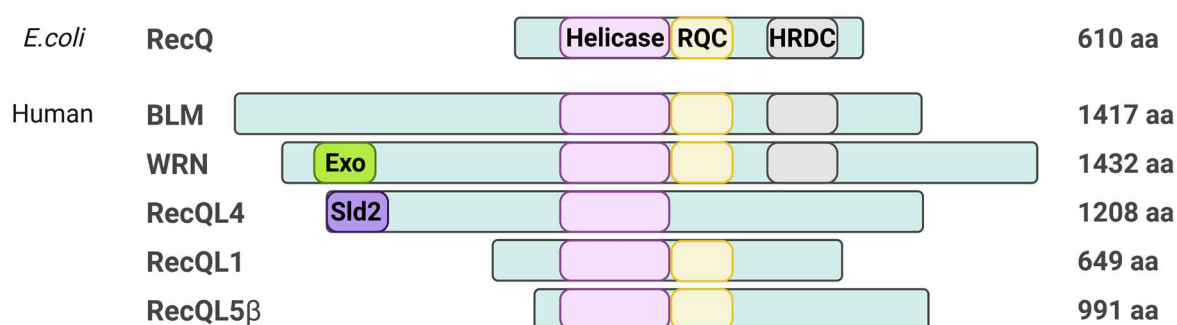


**Figure 2. Domain structure of the RecQ helicases.**
The conserved and exclusive domains are indicated by coloured shapes. The length of enzymes is given in the amino acids number [aa]. Figure adapted from Chu and Hickson 2009.

### 1.3. Functional characteristics of the BLM helicase

#### 1.3.1. Functions of BLM helicase

BLM is a prominent member of the RecQ helicases family. It is encoded by the *BLM* gene located at the chromosome 15q26.1 (Kaur et al. 2021). The highest level of *BLM* expression in synchronised leukemic K562 cell cultures was found during the late S and G2 phase of the cell cycle (Kitao et al. 1998). BLM is localised on telomers and promyelocytic leukaemia (PLM) bodies in the nucleus (Bischof et al. 2001). In fibroblasts, BLM was recruited to difficult-to-replicate regions, where it facilitated resolution of latent DNA structures in the anaphase (Barefield and Karlseder 2012). Mutations in the *BLM* gene cause the Bloom Syndrome, a rare autosomal recessive genetic disease characterised by the genetic instability due to numerous chromosomal breaks and increased events of sister chromatid exchanges. Moreover, patients suffering from a Bloom syndrome exhibit high rates of heterozygosity, increased mitotic recombination (Langlois et al. 1989), chromatid gaps and breaks (German et al. 1974), aberrant quadriradical chromosomes (Groden and German 1992), anaphase bridges (German et al. 1965) and telomere defects (Barefield and Karlseder 2012). Growing evidence shows that the Bloom Syndrome predisposes to development of various cancers at early age (German et al. 1965; German 1997; Ababou 2021).

Further insights regarding a role of BLM in cell biology came from studies of blm-deficient mice. Notably, a disruption of the *blm* gene in mice resulted in the embryonic lethality at 13.5 days gestation in homozygous mutant mice. $Blm^{-/-}$ mice displayed growth retardation and embryonic fibroblasts derived from those animals demonstrated increased sister chromatid exchange events (Chester et al. 1998). Defects in *blm* were linked to a high incidence of cancer in adult animals due to the hyperrecombination phenotype and chromosomal instability (Luo et al. 2000; McDaniel et al. 2003; Nicholas et al. 2006). In yeast, a lack of *sgs1*, a *BLM* homolog, induced a hyperrecombination and increased vulnerability to DNA-damaging chemical agents (Watt et al. 1996). Altogether, BLM ensures a proper control of recombination events and is vital for normal embryonic development, preventing the occurrence of cancer.

BLM expression significantly correlates with levels of Ki67 and PCNA (Proliferating Cell Nuclear Antigen) in various tumours, which points to its role in cancer development and progression. Furthermore, the exploration of TCGA

database showed overexpression of the *BLM* mRNA in comparison to normal tissue in many types of malignancies. The highest *BLM* levels were found in glioblastoma (GBM) samples (Chandrashekar et al. 2017). Elevated levels of BLM protein were associated with poor overall survival in patients suffering from acute myeloid leukaemia (AML) with the normal karyotype, in gastric- and lung cancers. This suggests that BLM could be a prognostic marker in these tumours (Viziteu et al. 2016; Chandrashekar et al. 2017).

Biological consequences of BLM mutations or its mRNA/protein overexpression are summarised in the figure 3.
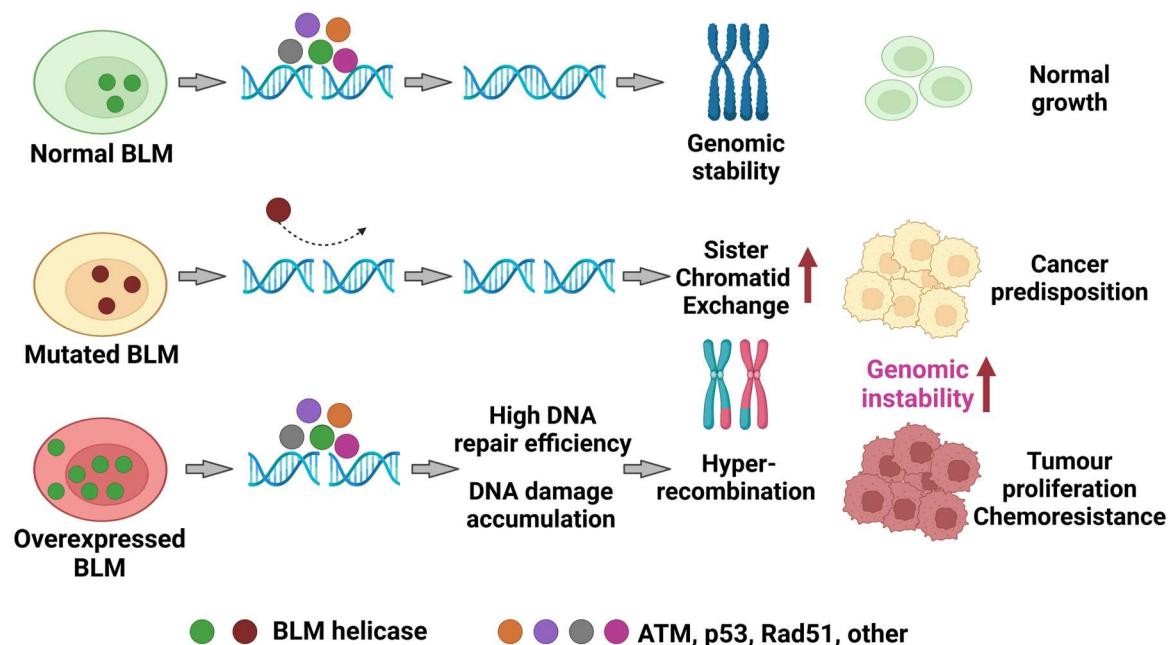


**Figure 3. BLM impairments and biological consequences.**
BLM maintains the genome integrity by repairing DNA breaks. Mutations and/or overexpression of BLM leads to genomic instability and uncontrolled cell growth. Figure adapted from Kaur et al. 2021.

### 1.3.2. Roles of the BLM helicase in DNA replication and repair

BLM takes part in DNA replication and repair, cooperating with various homologous recombination (HR) factors. HR pathway is engaged in DNA double-strand breaks (DSB) and inter-strand crosslinks (ICL) repair (Li and Heyer 2008). BLM stabilises the replication fork during undisturbed DNA replication and under the replication stress, assisting by the replication restart (Sengupta et al. 2004; Ahamad et al. 2021). At the early stages of replication perturbations induced by transcription-stalling drugs, BLM is recruited together with BRCA2 (BReast

and ovarian CAncer susceptibility protein 2) and FANCD2 (Fanconi ANaemia Complementation group D2) to damaged foci solve the conflict (Shao et al. 2020).

Moreover, BLM can bind and unwind unconventional guanine-quadruplex (G4) structures present in telomers, ribosomal DNA or gene regulatory regions, promoting fork progression in guanine-rich regions (Drosopoulos et al. 2015). BLM cooperates with POT1 (Protection Of Telomeres protein 1) (Opresko et al. 2005) and TRF2 (Telomeric Repeat binding Factor 2) (Opresko et al. 2002) in resolving DNA structures at telomeric ends. Furthermore, BLM is involved in the alternative lengthening of telomeres (ALT) pathway, which is frequently activated in cancer and involves homologous recombination to lengthen telomeres (Bryan et al. 1995). The aberrant R-loops structures, triggered by reactive oxygen species (ROS) at actively transcribed sites, could be also targeted and resolved by a BLM helicase (Tan et al. 2020).

The role of BLM as a sensor to various types of DNA damage is well established. In response to physically (IR radiation, laser) induced DSB BLM assembles along with RAD51 (DNA repair protein RAD51 homolog 1), p53 (cellular tumour antigen p53), γH2AX (histone H2AX) and ATM (serine-protein kinase ATM) proteins at the damaged sites (Wu et al. 2001; Karmakar et al. 2006; Ouyang et al. 2009). BLM is a part of a large BRCA1-associated genome surveillance complex (BASC) composed of BRCA1 (BReast and ovarian CAncer susceptibility protein 1) and MRN complex (MRE11-RAD50-NBS1). BASC is co-recruited together with PCNA during DNA replication-associated repair (Wang et al. 2000).

BLM plays multiple roles in the homologous recombination pathway of DSB repair, interacting with EXO1 (EXOnuclease 1) and DNA2 (DNA replication helicase/nuclease 2) in the initial stages of the process and promoting an extensive end resection (Nimonkar et al. 2008; Sturzenegger et al. 2014). The generated 3' single-stranded fragment serves as a scaffold for a RAD51 protein to form nucleofilaments (Mimitou and Symington 2009). Markedly, BLM exhibits a regulatory role in HR due to its ability to disrupt the RAD51 filaments (Patel et al. 2017). Further, together with TOPIIIα (TOPoisomerase IIIα), RMI1, RMI2 (RecQ-Mediated genome Instability proteins 1 and 2) BLM forms a BTRR complex called the 'BLM dissolvasome' to process the double Holiday Junctions (dHJs) occurring at the strand invasion step of HR, resulting in non-crossover recombinants (Daley et al. 2014). This complex is also recruited to the sites of the stalled replication

forks due to replication stress and abundant RPA (Replication Protein A) units on ssDNA to restart the ongoing replication (Shorrocks et al. 2021). Recently, the co-recruitment of BLM and XRCC4 (DNA repair protein XRCC4), a classical non-homologous end joining (c-NHEJ) pathway protein, has been reported suggesting the role of the helicase in discriminating between HR and c-NHEJ repair pathways (Tripathi et al. 2018). Noticeably, BLM prevents the error-prone microhomology-mediated end joining (MMEJ), also known as alternative nonhomologous end-joining (alt-NHEJ) pathway in mice and humans (Gaymes et al. 2002). Altogether, BLM *via* interactions with various partners protects the genome stability and integrity, ensuring the most accurate HR way of DNA repair. The examples of BLM interacting partners are summarised in the figure 4.
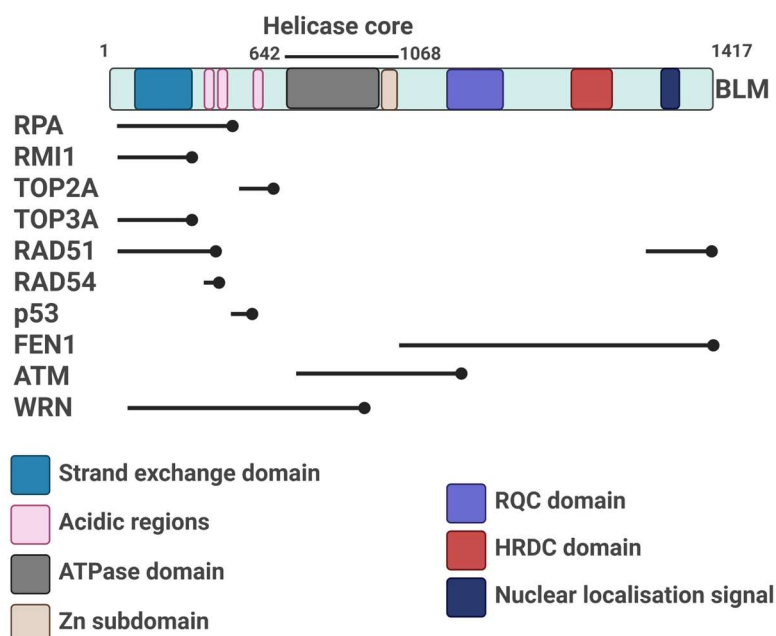


**Figure 4. BLM interacting partners.**
BLM interacting partners with marked binding regions. BLM domains are depicted by coloured shapes. Figure adapted from Kaur et al. 2021.

### 1.4. Inhibitors of BLM

Despite the prominent role of the helicase in important cellular processes, there is only one well described potent BLM inhibitor, ML216. The inhibitor is not fully BLM specific as the compound affects the WRN helicase activity at higher concentrations. The mechanism of action is a competition with BLM binding to DNA. ML216 treatment results in cellular alterations inducing the sister chromatin exchanges and enhancing its susceptibility to aphidicolin. ML216

exhibits an anti-proliferative activity exclusively towards cells expressing BLM, confirming its high specificity (Nguyen et al. 2013).

There are a few less characterised compounds predicted to act *via* BLM inhibition. An isaindigotone derivate, a natural alkaloid used in Chinese medicine disrupts the BLM/DNA interactions. The 'compound 29' efficiently inhibits the BLM recruitment to DSB, promoting an accumulation of RAD51 proteins and attenuating the HR process. Moreover, the compound evokes apoptosis and cell cycle arrest in HCT116 colon cancer cells (Yin et al. 2019). Furthermore, synthetic lethal interactions of BLM have been discovered, shedding the light upon potential therapeutical approaches. In BLM KO cells, the depletion of the one of proteins such as MUS81 (crossover junction endonuclease MUS81), GEN1 (flap endonuclease GEN homolog 1) or SLX4 (structure-specific endonuclease subunit SLX4) reduced the cell viability (Sarbajna et al. 2014). In SLX4 null cells, a lack of BLM induced a synthetic lethality in the absence of any DNA damaging agents (Garner et al. 2013). A subset of cancer cells uses the telomerase-independent and HR-dependent, ALT pathway to preserve telomere lengths and desensitise cells to telomerase inhibitors (Henson and Reddel 2010; Ivancich et al. 2017). In ALT cells co-deletion of the FANCM (Fanconi ANaemia Complementation group M) and BLM led to a synthetic lethality. Deletion of BLM in the FANCM KO ALT negative HCT116 cells led to a strong reduction of cell viability (Wang et al. 2018). Interestingly, a lack of an homologous protein sgs1 together with mutations in the *sod1* gene encoding superoxide dismutase (SOD) induced a synthetic lethality in yeast (Pan et al. 2006). Similarly, SOD1 depletion in BLM deficient HCT116 human cells resulted in cytotoxicity, elevated DNA damage rate and apoptosis (Sajesh and McManus 2015).

## 1.5. Posttranslational BLM regulation

Due to numerous functions of BLM in the cell, its activity must be tightly regulated. A number of biochemical studies have demonstrated various post-translational modifications such as acetylation, phosphorylation, SUMOylation (small ubiquitin-like modifier) or ubiquitination of the BLM. $Thr^{99}$ and $Thr^{122}$ phosphorylation of the BLM by ATM/ATR (serine/threonine-protein kinase ATR) is crucial for stalled replication forks restarting after chemical treatments (Davies et al. 2004). Chk1 (serine/threonine-protein kinase Chk1) ensures constitutive

phosphorylation at Ser$^{502}$ during interphase, which prevents cullin-3 mediated degradation and stabilises the BLM level in colon cancer cells (Petsalaki et al. 2014). Furthermore, NEK11 (serine/threonine-protein kinase NEK11) phosphorylates Ser$^{338}$ in the BLM attenuating its interaction with TopBP1 (DNA Topoisomerase 2-Binding Protein 1). This event sustains the appropriate BLM level in the S and G2 cell cycle phases (Wang et al. 2013a). Relocation to the stalked replication forks requires the ubiquitination at Lys$^{105}$, Lys$^{225}$ and Lys$^{259}$ BLM by RNF8/RNF168 (E3 ubiquitin-protein ligase RNF8/RNF168) (Tikoo et al. 2013). The SUMOylation at Lys$^{317}$, Lys$^{331}$, Lys$^{334}$ and Lys$^{347}$ is necessary for intra-nuclear trafficking of BLM to DNA damage-induced foci (Eladad et al. 2005). Furthermore, BLM function is also regulated by the interacting proteins such as RPA (Replication Protein A) proteins, forming an abundant, high-affinity ssDNA-binding complex. BTRR complex is recruited to the replication forks only when the number of RPA units increased under the pathological conditions, indicating the role of RPA in regulating the BLM activity (Shorrocks et al. 2021). The indicated processes regulating a helicase activity and translocation ensure the intact replication, adequate DNA repair and maintaining the homeostasis in the cells.

### 1.6. The RecQL4 helicase, its functions and interactions with BLM

The RecQL4 helicase is encoded by the *RecQL4* gene localised on chromosome 8q24.3 and mutations in this gene have been detected and contribute to BGS, RAPIDILINO and RTS syndromes, and are linked to a predisposition to cancer due to the impaired genome stability maintenance (Luong and Bernstein 2021). RecQL4 was mainly detected in the cytoplasm, nucleus, and - uniquely among RecQ helicase family members - in the mitochondria where it participates in upkeeping the mitochondrial genome (Croteau et al. 2014). *Hrq1*, a yeast *RecQL4* homolog, has an ability to unwind DNA structures like D-loops, bubbles and poly(dT) forks (Rogers et al. 2017).

Many biological models have been employed to reveal the RecQL4 functions. The gene knock-out (KO) of RecQL4 caused the embryonic lethality in mice (*M. musculus*) and flies (*D. melanogaster*) (Ichikawa et al. 2002; Wu et al. 2008). Due to such early lethality other organisms such frogs (*X. laevis*) or yeasts (*S. cerevisiae*) have been used in studies of RecQL4 functions. A role of RecQL4 in the replication initiation of *Xenopus* eggs and mosaic flies has been

established. The N-terminus fragment of the RecQL4 protein was similar to the essential Sld2 replication initiation factor in yeast (Sangrithi et al. 2005; Wu et al. 2008; Germani et al. 2018) Human RecQL4 cooperates with the GMC complex composed of the CD45 (Cell Division control protein 45 homolog) and MCM2-7 (DNA replication licensing factor MCM2-7) to initiate the replication. The lack of RecQL4 in KO cells diminishes the interaction with the GMC complex and results in the chromatin loading failure (Xu et al. 2009).

Similarly to BLM, RecQL4 plays an important role in protecting telomers from DNA damage, interacting with the shelterin complex. The shelterin complex is composed of six polypeptides and assembles through binding of the double stranded TTAGGG repeats binding proteins TRF1 (Telomeric Repeat-binding Factor 1) and TRF2 which facilitates the recruitment of RAP1 (Ras-Associated Protein1), TIN2 (TERF1-Interacting Nuclear factor 2), TPP1 (TriPeptidyl-Peptidase 1) and POT1 proteins. TRF1 and TRF2 proteins stimulate the RecQL4-dependent D-loop unwinding at normal and oxidised telomeres. Moreover, RecQL4 interacts with WRN helicase and stimulates its resolving activity, preferably on oxidised telomeric D-loops (Singh et al. 2012). Co-localisation of RecQL4 with 53BP1 (TP53-Binding Protein 1) and γH2AX proteins at DNA DSB lesions induced by laser beam has been detected, and RecQL4 deficient cells maintain longer the 53BP1 foci, which implicates the helicase in the DSB repair (Singh et al. 2010). Notably, the absence of a molecular partner of RecQL4 – BLM, diminished the RecQL4 retention at DSB sites, and thus confirming the importance of the interaction between two helicases (Singh et al. 2012).

RecQL4 can act in main pathways of DSB repair (NHEJ and HR) depending on the cell cycle phase. Interactions between the helicase and KU80/KU70 proteins (X-ray repair cross-complementing protein 6/5) confirm its involvement in the NHEJ pathway, predominantly active in the G1 phase. RecQL4 deficient cells had diminished end joining *in vivo* and *in vitro*, and decreased KU80 recruitment to damaged lesions, preventing the DNA repair (Mao et al. 2008; Shamanna et al. 2014; Tan et al. 2021) In contrast, in the S/G2 cell cycle phase RecQL4 interacts with MRE11 (double-strand break repair protein MRE11) and CtIP (DNA endonuclease RBBP8), promoting the 5' end resection, which is the crucial step of early HR. The interaction between RecQL4 and MRE11 is mediated by RecQL4 phosphorylation

at Ser[89] and Ser[251] by CDK1 and CDK2 (Cyclin-Dependent Kinase 1/2) (Lu et al. 2016; Lu et al. 2017a).

RecQL4 participates also in base excision repair (BER) and nucleotide excision repair (NER) pathways. BER is activated by DNA damage resulting from DNA alkylation, deamination and oxidation, which does not necessarily cause the DNA structure distortion (Krokan and Bjørås 2013). Upon treatment with oxidative DNA damaging agents, RecQL4 is found at nuclear foci and co-localises with the key BER enzymes: APE1 (DNA-(APurinic or APyrimidinic site) Endonuclease) and FEN1 (Flap ENdonuclease 1) (Schurman et al. 2009). The immunoprecipitation experiments detected the new RecQL4 partners such as OGG1 (N-glycosylase/DNA lyase) and a core member of the BER pathway - PARP1 (Poly [ADP-Ribose] Polymerase 1). RecQL4 interactions with OGG1 are mediated by the helicase acetylation by the CBP (CREB-Binding Protein) complex. The opposite process, deacetylation, is regulated by a deacetylase SIRT1 (NAD-dependent protein deacetylase SIRTuin-1) and reduces the RecQL4-OGG1 interactions (Petkovic et al. 2005; Schurman et al. 2009; Duan et al. 2020).

The NER pathway ensures the repair of bulky DNA lesions such as cyclobutene pyrimidine dimers (CPD) or 6-4 photoproducts induced by environmental mutagens, UV light and some chemotherapeutics. RecQL4 participates in the repair of CPD adducts, cooperating with the key protein XPA (DNA repair protein complementing XP-A cells) in the pathway (Schärer 2013).

RecQL4 is the only RecQ helicase member having the mitochondria localisation sequence. This feature enables RecQL4 to protect the mitochondrial genome integrity. Under normal conditions RecQL4 recruits p53 and mitochondrial polymerase Polγ responsible for replication of mitochondrial DNA. Interestingly, upon DNA damage both proteins fail to interact and migrate to the nucleus, where they contribute to the DNA damage response (De et al. 2012; Gupta et al. 2014). Depletion of RecQL4 in human glioma cells perturbated the functionality and morphology of the mitochondrial network, pointing out the role of the helicase in malignant cells (Król et al. 2020).

**1.7. Basic facts about human gliomas and their therapy**

**1.7.1. Molecular classification of GBM and patient survival**

Gliomas are the central nervous system (CNS) tumours that arise from neural stem or progenitor cells. Gliomas encompass a wide of spectrum of tumours ranging from benign, slow growing pilocytic astrocytomas (World Health Organisation, WHO grade 1) to the most aggressive, malignant and incurable glioblastomas (GBMs, WHO grade 4) (Germano et al. 2010). Gliomas accounts for 2% of all human tumours and for 75% of primary malignant brain tumours in adults, with the most frequent GBMs (>50%) (Ostrom et al. 2019). While 91% of patients with non-malignant brain tumours have a 5-year survival rate in all age groups, it amounts to only 5% in GBM patients (Barnholtz-Sloan et al. 2018).

The recent WHO classification (2021) of CNS tumours included a set of molecular markers in the CNS tumour diagnosis. One of the important molecular features is the *IDH* mutational status. *IDH1* and *IHD2* genes encode the isocitrate dehydrogenase 1 and 2, and conservative mutations result in a 'gain of function', resulting in the production of the oncometabolite 2-hydroxygluatarate and the DNA hypermethylator phenotype. Based on 2021 WHO recommendations, adult-type diffuse gliomas are divided into: *IDH*-mutant astrocytomas (WHO grades 2,3,4), *IDH*-mutant and 1p/19q-codeleted oligodendrogliomas (WHO grades 2,3) and *IDH*-wildtype glioblastoma (WHO grade 4) (Louis et al. 2021).

GBMs display considerable genomic and cellular heterogeneity driven by microenvironmental, epigenetic and genetic cues. Studies based on bulk expression profiles distinguished three distinct GBM subtypes described as classical (CL), mesenchymal (MES) and proneural (PN), characterised by some prominent alterations. Oncogenic *EGFR* (Epidermal Growth Factor Receptor) alterations occur in the CL type, the *NF1* (NeuroFibromin) mutations in the MES subtype, and *PDGFRA* (Platelet-Derived Growth Factor Receptor Alpha) amplification, *IDH1* and *p53* mutations in the PN subtype (Verhaak et al. 2010). Notably, these subtypes can co-exist in different regions across the same tumour and change over time and through therapy (Verhaak et al. 2010; Wang et al. 2017).

Other approaches used single-cell RNA sequencing (scRNA-seq) of glioblastoma and cell type-based deconvolution of TCGA database to detect

states of GBMs characterised by transcriptional signatures: oligodendrocyte-progenitor like (OPC-like), neural-progenitor like (NPC-like), mesenchymal-like (MES-like) and astrocyte-like (AC-like) with genetic alterations in *PDGFRA*, *CDK4* (Cyclin Dependent Kinase 4), *NF1* and *EGFR*, respectively (Neftel et al. 2019). Regarding prognosis prediction, three subtypes have been identified by analysing the TCGA RNA-seq transcriptome and survival time: a mitotic (favourable), intermediate and invasive (poor). Notably, the favourable prediction markers i.e. the *MGMT* gene promoter methylation, mutations in *IDH1*[R132H] and *ATRX* (transcriptional regulator ATRX) are enriched exclusively in the mitotic type GBMs (Park et al. 2019b).

### 1.7.2. Therapeutic treatment modalities in glioblastoma

The standard approach for newly diagnosed GBMs remains unchanged since 2005 when the Stupp protocol had been published. It proposed a maximal surgical resection followed by radiotherapy and adjuvant temozolomide (TMZ) treatment. TMZ is a pharmacologically inactive prodrug that is rapidly converted to an active anticancer metabolite at physiological pH. TMZ metabolites exert alkylating effects on DNA, which causes structural changes and fragmentation of DNA chains, and consequently, disturbance of DNA and RNA synthesis, and the inhibition of cell division. These changes ultimately lead to cell death. TMZ crosses the blood brain barrier (BBB) and its active form, as a methyldiazonium ion (MI), and is transferred to DNA forming multiple adducts leading to cytotoxicity (Mohammad and Hopfinger 1980; Stupp et al. 2014; Arora and Somasundaram 2019). The reactive MI methylates preferably the $O^6$- and $N^7$ position of guanine, and $N^3$ position of adenine (Chien et al. 2021). Methylation of $O^6$-guanine is a main mechanism of TMZ toxicity, however the most frequent methylation occurs at $N^7$-guanine (70%) (Barciszewska et al. 2015).

Despite therapy the tumour frequently recurs and the overall survival (OS) of GBM patients is 14.6 months (Stupp et al. 2005). Recently, several new drugs or therapies entered clinical trials, however a significant extension of OS over 14 months still remains challenging (Rapp et al. 2017). From 2010 to 2020, among 568 unique therapeutic entities that underwent drug discovery clinical trials in brain tumours, the three most common classes were: kinase inhibitors,

chemotherapeutic agents and tumour vaccines. The most frequently applied in clinical trials were: TMZ, cyclophosphamide, and lomustine.

Interestingly, PARP inhibitors (PARPi) used in breast cancers with BRCA1/2 deficiency, were also tested in brain tumours. Out of seven drugs from this class, the most common were olaparib (OLA), pamiparib and veliparib (Sokolov et al. 2021).

Nonetheless, GBM recurrence is inevitable due to radio- and chemoresistance of glioma cells. Also due to the infiltrative nature of tumour, the relapse decreases the life expectancy to 6-10 months (Lamborn et al. 2008; Stupp et al. 2009; Wu et al. 2010; Lima et al. 2012). One of the reasons for a recurrence is the presence of a rare population of glioma stem cells (GSC) among bulk tumour cells. GCSs contribute to the treatment resistance and relapse due to its ability to self-renew and recreate the bulk tumour. Recently, such cells were categorised as proliferative GSCs (pGSC) with a rapid cell division, and quiescent GSCs (qGSC). GBM patients exhibiting the enriched pGSC population had poor clinical outcome (Yan et al. 2023). Moreover, GBMs are considered as immunologically "cold" characterised by poor lymphocyte infiltration and the immunosuppressive microenvironment responsible for therapeutic resistance (Tomaszewski et al. 2019). The accumulation of glioma- associated microglia and macrophages (GAMs) in the tumour microenvironment supports the tumour progression and therapy resistance. A high number of immunosuppressive macrophages has been reported as a poor prognosis factor for many cancer variants. Tumour-educated macrophages stimulate angiogenesis, suppress anti-tumour immunity and support tumour invasion, which all result in tumour progression (Ochocka et al. 2021).

## 1.8. Temozolomide and PARP inhibitors – a promising combination?
### 1.8.1. Mechanism of TMZ action

Most of anti-tumour therapies eliminate neoplastic cells by introducing DNA damage which ultimately triggers cell death. These effects are counteracted by activated DNA repair pathways that efficiently diminish therapeutic effects. Therefore, the enhancement of anti-tumour effects could be achieved by simultaneous DNA damage and blockade of DNA repair pathways. The combinations of drugs and repurposing are well known approaches in clinical

trials. Recently, the combination of TMZ and PARPi, was tested in clinical trials in patients with primary or secondary GBMs (NCT05463848, NCT04614909, NCT01390571).

TMZ is a first choice chemotherapeutic for newly-diagnosed GBMs since its approval by Food and Drug Administration (FDA) in 2005. However, the standard Stupp regimen with radiotherapy and TMZ (Stupp et al. 2014) prolongs the median overall survival for only 3 months (Stupp et al. 2005; Wilson et al. 2014). Moreover, prolonged TMZ treatment leads the acquired resistance to the treatment, contributing to further progression of the disease (Higuchi et al. 2020). There are multiple ways to repair the introduced DNA adducts. The methyl group bound to $O^6$-guanine can be removed by $O^6$-methylguanine DNA methyltransferase (MGMT), therefore MGMT expression is an important factor in TMZ treatment response. The expression of MGMT is regulated mainly by a CpG methylation status in the *MGMT* gene promoter (Rivera et al. 2010; Feldheim et al. 2019). Unfortunately, only ~50% of patients have the methylated *MGMT* gene promoter and can benefit from TMZ therapy (Yin et al. 2014) irrespectively of age (Vuong et al. 2020). The best response rates to TMZ display GBM patients bearing the *MGMT* promoter methylation and *IDH* mutations (Yang et al. 2015). Notably, the initial *MGMT* promoter methylation may decrease upon the recurrence following the treatment and the malignant cells may acquire a therapeutic resistance, diminishing the drug effectiveness (Park et al. 2012).

Another DNA repair pathway targeting $O^6$-methylguanine ($O^6$-meG) is a mismatch repair (MMR) involving: MSH2 (DNA mismatch repair protein Msh2), MSH6 (DNA mismatch repair protein Msh6), MLH1 (DNA mismatch repair protein Mlh1) and PMS2 (mismatch repair endonuclease PMS2) proteins (von Bueren et al. 2012). MSH2/6 protein complex recruits MLH1/PMS2 to a DNA damage site, facilitating removal of an improper base. Next, the synthesis of a new DNA strand is carried out by EXO1, DNA polymerase δ/ε (DNA-polδ/ε), RPA, PCNA and FEN1 proteins (Jiricny 2006). Due to incorrect pairing $O^6$-meG with a thymine, instead of cytosine, the MMR system recognises the mispairing and excises the newly synthesised strand without processing the parental strand with $O^6$-meG residue. The repeated futile cycles lead to cell cycle arrest and ultimately to apoptosis (Jiapaer et al. 2018). However, in recurrent malignant gliomas with *IDH*-wildtype (Hunter et al. 2006; The Cancer Genome Atlas Research Network 2008)

or *IDH*-mutant (Johnson et al. 2014; Choi et al. 2018) previously treated with TMZ, the genes related to MMR are frequently inactive, which results in the resistance to the treatment (Higuchi et al. 2020). Interestingly, MMR alterations are rare in primary tumours (Maxwell et al. 2008; van Thuijl et al. 2015) and do not have impact on survival of high-grade glioma patients (Caccese et al. 2020).

$N^3$ and $N^7$-methyl residues are recognised, excised by DNA glycosylases and subjected further to a base excision repair (BER) pathway. PARP1/2 translocate to the abasic site, facilitating the recruitment of additional BER factors as XRCC1 (DNA repair protein XRCC1). XRCC1 recruits the APE1 nuclease to cleave the abasic site. Finally, RFC engages PCNA and DNA-polδ/ε to resynthesise missing nucleotides and the endonuclease FEN1 cleaves the dislodged nucleotide, enabling the LIG1 (DNA LIGase 1)to reseal the single strand break (Dietlein et al. 2014) The inhibition of the BER pathway in cancer cells augments their sensitivity to alkylating agents and radiotherapy (Neijenhuis et al. 2005; Gao et al. 2019). The primary therapeutic targets to inhibit BER pathway are APE1 and PARP (Li et al. 2020b). The combination of TMZ with PARPi enhanced the effectiveness of TMZ (Erice et al. 2015; Jue et al. 2017). The main TMZ-related DNA damage and repair pathways are presented in the figure 5.
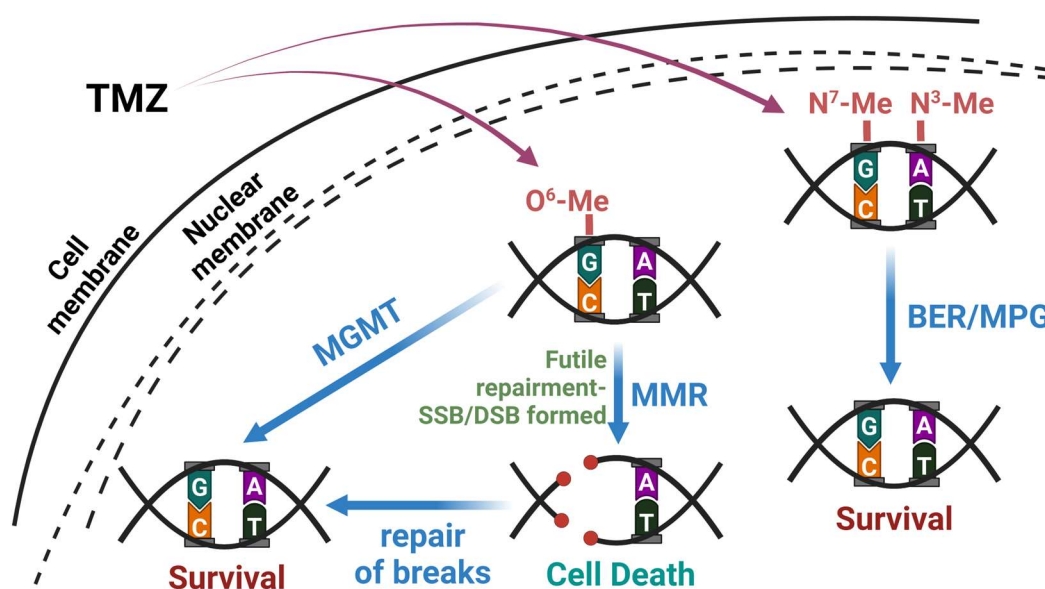


**Figure 5. Mechanisms of toxic TMZ action and related DNA damage repair pathways.** TMZ alkylates the guanine and adenine residues. Different mechanisms are involved in cell death and TMZ resistance due to enhanced DNA repair. Abbreviations: **TMZ**- temozolomide, **MGMT**- $O^6$-methylguanine methyltransferase, **MMR**- mismatch repair pathway, **BER**– base excision repair, **MPG**- N-methylpurine-DNA glycosylase, **SSB**– single strand breaks, **DSB**– double strand breaks. Figure adapted from Chien et al. 2021.

### 1.8.2. PARP1 as a therapeutic target

PAPR1 is the best characterised protein among 18 members of the PARP family that is involved in many biological processes from DNA repair to cell death. Interestingly, PARP1 is the second, most abundant protein in the eukaryotic nucleus after histones (Thomas et al. 2019). The upregulation of PARP1 is observed in many malignancies, including lung; breast; skin; endometrial and ovarian cancers (Ossovskaya et al. 2010), and non-cancer diseases such as diabetes; arthritis, and certain neurogenerative diseases (Obrosova et al. 2004; García and Conde 2015; Mao and Zhang 2022). Upon activation, PARP1 introduces poly ADP-ribose (PAR) residues nicotinamide adenine dinucleotide (NAD$^+$) to target proteins in a process called PARylation (Amé et al. 2004). PARylation regulates the function of proteins entangled in cell proliferation, DNA repair and cell death (Wei and Yu 2016; Krüger et al. 2020). PARP1 is mainly associated with major DNA repair pathways and the maintenance of replication fork stability. Moreover, PARP1 is involved in RNA processing, inflammation, aging, anti-viral protection, transcriptional- and cell cycle regulations (Kumar et al. 2022). Interestingly, severe and unrepairable DNA damage leads to auto-PARylation of PARP1, which is substrate for PARG (Poly(ADP-Ribose) Glycohydrolase), an enzyme with an endoglycosidase activity releasing PAR units that translocate to the cytoplasm and evoke caspase-independent cell death called parthanatos (Andrabi et al. 2006; Zhou et al. 2021). The functions of PARP1 are summarised in the figure 6.
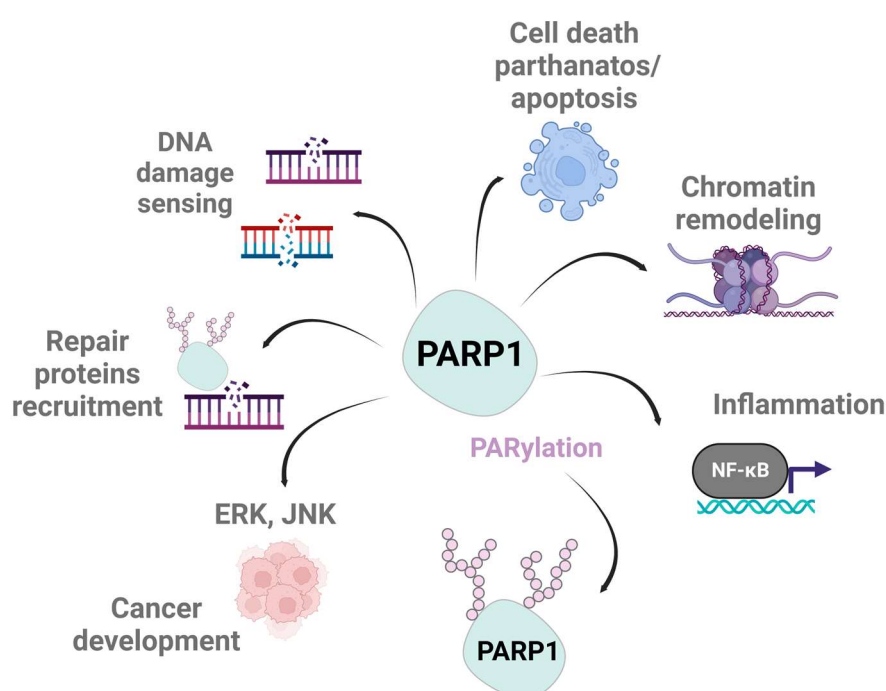
> **Figure 6. The multiple roles of PARP1.**
> PARP1 is involved in many biological processes. The round pink circles represent the polyADP-ribose (PAR) units. The main mechanism of PARP1 action. Abbreviations: **ERK**- extracellular signal-regulated kinase, **JNK**- c-Jun NH2-terminal kinase. Figure adapted from Kang et al. 2022 and Kumar et al. 2022.

### 1.8.3. PARP1 in DNA repair

The role of PARP1 in DNA single-strand break repair is better known than in case of double-strand breaks. Single strand break repair pathway is the important way to fix the ongoing damage occurring due to direct attack of intracellular metabolites and/or spontaneous DNA decay (Caldecott 2008). In BER pathway, single strand breaks are rapidly detected by APE1 and DNA glycosylases, recruiting PARP1. Next, PARP1 auto-PARylation is launching the recruitment of XRCC1 responsible for further enrolment of DNA polβ (DNA polymerase beta) and LIG3 (DNA ligase 3) acting in BER (Ray Chaudhuri and Nussenzweig 2017; Koczor et al. 2021). In the initial step of NER pathway, auto-PARylated PARP1 serves as a scaffold for DDB1-DDB2 (Damage specific DNA Binding protein 1/2) protein complex. The PARylation of XPC-RAD23B (DNA repair protein complementing XP-C cells-UV excision repair protein RAD23 homolog B) protein complex, modulates its activity to recognise UV-damaged lesions (Maltseva et al. 2015). Moreover, DDB2 enhances histone PARylation, thus inducing nucleosome displacement and triggering the NER pathway (Luijsterburg et al. 2012; Ray Chaudhuri and Nussenzweig 2017). In MMR pathway PARP1 exhibits its activity by poli-ADP-ribosylation of MSH6 protein (Ray Chaudhuri and Nussenzweig 2017), however the exact role of this modification has to be elucidated. Interestingly, the action of PARP1 in double-strand breaks is still debatable as single strand breaks can be considered as two independent single strand breaks on opposite DNA strands, and the precise localisation of those breaks remains unknown (Liu et al. 2017). Nevertheless, PARP1 was shown to sense the double-strand breaks within 100 ms after damage introduction (Caron et al. 2019) and its activity increases rate of the MRN complex recruitment (Haince et al. 2008) to orchestrate the pathway choice in repair of double-strand breaks between HR and NHEJ (Bian et al. 2019). In HR pathway, PARP1 is implicated in the attenuation and recruitment of BRCA1 (Gong et al. 2022) that controls the initial steps of double-strand breaks resection and is involved in RAD51 loading

onto DNA, essential for strand exchange (Li and Yu 2013). Moreover, PARP1 interacts with Ku70/80 complex, characteristic for the NHEJ pathway, building the functional complex with DNA-PK (DNA-dependent Protein Kinase catalytic subunit) (Dong et al. 2010). Notably, PARylation of DNA-PK increases its kinase activity (Ruscetti et al. 1998).

### 1.8.4. Synthetic lethality and PARP1 inhibitors

The synthetic lethality (SL) is a concept based on the interaction between two genes, suggesting that a loss of function of both elements affects cellular viability, while a loss of one of them is compensated by the other (Ashworth and Lord 2018). The most successful clinical use of this concept is the application of PARP1 inhibitors (PARPi) in the treatment of the BRCA1/2-deficient breast and ovarian cancers (Bryant et al. 2005; Farmer et al. 2005; Lord and Ashworth 2017). FDA approved four PARPi to be used in the clinics: olaparib, rucaparib, niraparib and talazoparib (Kumar et al. 2022). There are many ongoing and completed clinical trials using PARPi alone or with combination with other drugs to treat different malignancies. Niraparib (as a monotherapy) is present in clinical studies of recurrent gliomas (NCT05297864, recruiting) and in the combination with durvalumab, an immune checkpoints inhibitor, to treat *IDH*-mutated solid tumours (glioma, cholangiocarcinoma and others; NCT03991832, recruiting) (Hunia et al. 2022). Interestingly, *IDH* mutations reflect a HR deficiency phenotype, proficient for PARPi to treat brain tumours, particularly lower grade gliomas (70% harbour the *IDH1* mutation) (Yan et al. 2009; M et al. 2023). *IDH1*[R132H] xenografts were sensitive to PARPi (Sulkowski et al. 2017). Moreover, the blockade of PARP dependent DNA repair pathways led to a significant boost of TMZ toxicity in *IDH*-mutated glioma cells (Lu et al. 2017b).

The other concept is a synthetic dosage lethality (SDL) interaction, where a gene function loss influences cell viability only when a second gene is overactivated. This therapeutic modality is particularly interesting in case of upregulated helicase encoding genes in many types of cancers (Arna et al. 2022).

### 1.9. Drug-induced senescence and polyploidy as mechanisms of cell death evasion

### 1.9.1. Characteristics of cellular senescence

In 1961, Hayflick and Moorhead described a cellular senescence as an irreversible growth arrest state, in which normal human fibroblasts, remain metabolically active after exhausting the replicative potential (Hayflick and Moorhead 1961). Cellular senescence can be induced by stressors such as DNA or organelle damage, loss of tumour suppressor functions, oncogene activation, telomere shortening and epigenetic changes (Herranz and Gil 2016). Moreover, senescence occurs during physiological conditions as wound healing or embryonic development (Demaria et al. 2014; Herranz and Gil 2016). There are many types of cellular senescence: replicative, DNA damage-induced, oncogene-induced, oxidative stress-induced, chemotherapy-induced, mitochondrial dysfunction-associated, epigenetically-induced and paracrine senescence (Hernandez-Segura et al. 2018). The hallmark of senescent cells is the cell cycle arrest mediated by cyclin-dependent kinase (CDK) inhibitors 1 and 2A (p21 and p16 $^{INK4a}$) blocking the CDK-cyclin complexes involved in the G1-S phase transition (Fagagna et al. 2003). The retinoblastoma protein (RB) is a downstream target of p16 $^{INK4a}$/RB and p53/p21 $^{CIP1}$ axes and displays a crucial role in the cell cycle regulation. Hypophosphoryated RB binds to an E2F transcription factor, neutralising its function thus locking the cells into a proliferative halt (Ben-Porath and Weinberg 2005). Chronic activation of DNA damage response (DDR) results in double strand DNA breaks and the ATM kinase recruitment to the damaged lesion driving the phosphorylation of H2AX histone and facilitating an assembly of the repair complexes (Ayrapetov et al. 2014).

Several metabolic and structural changes occur frequently in senescent cells. Elevated activities of the senescence-associated β-galactosidase (SA-β-gal) and senescence-associated α-fucosidase (SA-α-fuc) reflect the augmented activities of lysosomal enzymes (Sugrue et al. 1997; Li et al. 2023). Senescent cells accumulate the lipid-containing granules, lipofuscin, resulting from lysosomal abnormalities (Lloyd 2013). The structural changes include enlarged cell body, increased nuclear size and multinucleation which prevents the complete mitosis and cytokinesis (Dikovskaya et al. 2015). Moreover, chromatin rearrangements appear as dense structures known as senescence-associated heterochromatin

foci (SAHF) with subsequent loss of the lamin-B1 in the nuclear envelope (Di Micco et al. 2011; Freund et al. 2012). The changes in plasma membrane of senescent cells involve upregulation of caveolin-1, the component of cholesterol-enriched microdomains (Zou et al. 2011). All those changes alter cell-autonomous signalling and interactions with the microenvironment resulting in the senescence-associated secretory phenotype (SASP) (Schmitt et al. 2022). The SASP comprises a number of factors, such as matrix-remodelling metalloproteases (e.g. MMP1, MMP2), growth factors (e.g. HGF, EGF, TGFα), chemokines (e.g. CCL2, CCL5, CXCL1), pro-inflammatory cytokines (e.g. IL-1α, IL-1β, IL-6, IL-8), various oxylipins and extracellular vesicles (Coppé et al. 2008; Wiley et al. 2021).

The induction of SASP is dependent on persistent, unresolved DDR signalling, activation of transcription factor NF-κB, and phosphorylation of p38MAPK (Chien et al. 2011; Freund et al. 2011). SASP plays a role in tumorigenesis, tumour metastasis and aging (Krtolica et al. 2001; Zlotnik 2004). In cancer SASP exhibits a dual role. On one hand, SASP suppresses tumour progression *via* the cell cycle arrest, activation of the immune surveillance, recruitment of natural killer (NK) cells, and polarising macrophages to eliminate senescence tumour cells (Kang et al. 2011; Yang et al. 2021).

On other hand, SASP promotes the tumour progression by the release of components enhancing invasion and metastasis, maintaining a stem-cell phenotype, tissue remodelling, evoking drug resistance, stimulating epithelial-mesenchymal transition (EMT) and creates the immunosuppressive environment (Rao and Jackson 2016; Li et al. 2020a; Yang et al. 2021).

The main hallmarks of cellular senescence are presented in the figure 7.
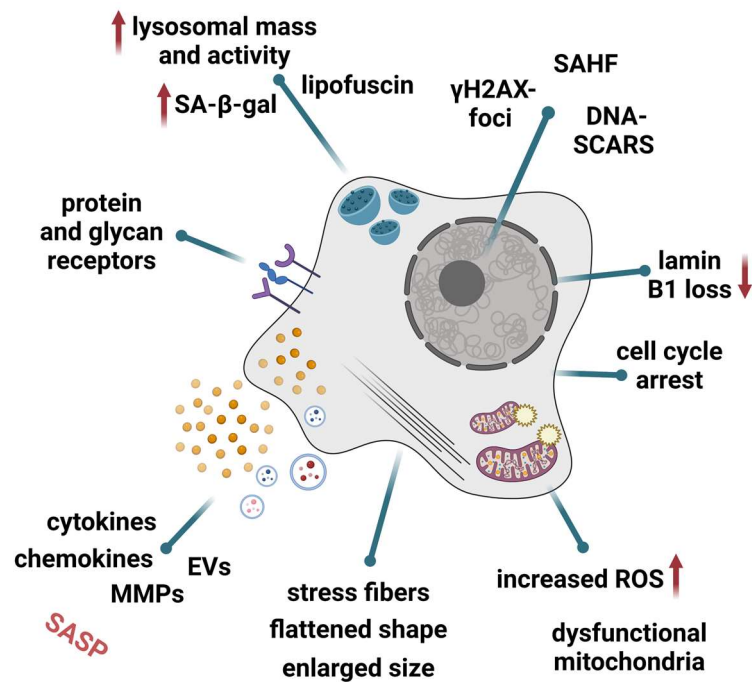
**Figure 7. Hallmarks of cellular senescence.**
A senescent cell displays many changes in morphology, lysosomal activity, DNA structure and cell cycle regulators. Numerous factors are deregulated including: **SA-β-gal**- senescence-associated β-galactosidase, **MMP**- metalloproteinase, **EV**- extracellular vesicle, **ROS**- reactive oxygen species, **DNA-SCARS**- DNA segments with chromatin alterations reinforcing senescence, **SAHF**- senescence-associated heterochromatin foci. Figure adapted from González-Gualda et al. 2021.

### 1.9.2. Therapy induced senescence

Therapy-induced senescence (TIS) is evoked by pharmacological drugs or radiation and the process is mediated by increasing the level or activity of tumour suppressors, mainly p16, p21, p27, p53 and PTEN (Kalathur et al. 2015; Park et al. 2019a). In the absence of p53 activity, other genes such as *skp2* serve as a backup pathway to induce TIS (Childs et al. 2015). Many chemotherapeutics induce cellular senescence in tumour cells: alkylating agents (Peiris-Pagès et al. 2015) (e.g. cisplatin, temozolomide), microtubule inhibitors (Hu et al. 2016) (e.g. paclitaxel), topoisomerase inhibitors (Han et al. 2002) (e.g. etoposide, doxorubicin, camptothecin) and others (Demaria et al. 2017; Schmitt et al. 2022). Aforementioned chemical agents were extensively examined in cellular and animal models, i.e. temozolomide in glioma, melanoma, colorectal cancer cells and in p16-3Mr mice-models (Wang et al. 2020a). For example, olaparib induced a reversible, p21 and Chk2-mediated senescence like phenotype in high-grade serous epithelial ovarian cancer cell (Fleury et al. 2019).

Senescent cells have been detected in cancer patients after therapy. Various senescence-associated genes and SASP markers have been found in mitotraxone-treated prostate cancer patients (Coppé et al. 2008). Breast cancer patients treated with cyclophosphamide, doxorubicin and 5-fluorouracil accumulated SA-β-gal⁺, p16⁺ and p53⁺ cells in tumour tissues (PMID:11912168). Breast cancer patients treated with different chemodrugs had T-cells with elevated levels of p16 [INK4a] reflecting the immune-senescence as a bystander effect of the treatment (Sanoff et al. 2014; Mitin et al. 2022). Senescent cells have been found in non-malignant lung tissues in patients with non-small-cell lung cancer after chemotherapy (Roberson et al. 2005).

### 1.9.3. Polyploidy as a link between senescence and cancer

Polyploidy is a condition where the cells have more than one pair of homologous chromosomes. Syncytiotrophoblasts, multinucleated cells formed by fusion of diploid cytotrophoblast cells or megakaryocytes that develop by DNA replication without cell division (endoreplication) serve as an example of polyploidy normal cell in the human body (Machlus and Italiano 2013; Knöfler et al. 2019). Many antiproliferative, DNA-targeting (e.g. anthracyclines, etoposide) and microtubule-targeting (e.g. vinca alkaloids, taxanes) drugs induce polyploidy. Some polyploid cells die during treatment, but the remaining cells may undergo cell divisions (Niu et al. 2016). A subpopulation of polyploid cancer cells known as polyploid giant cancer cells (PGCC) appear in malignant tumours (Lv et al. 2014) following radiotherapy (Mirzayans et al. 2017), chemotherapy (Sirois et al. 2019), hypoxic treatment (Lopez-Sánchez et al. 2014), virus infection (Nehme et al. 2022) or other stimuli leading to the DSB (Zhang et al. 2022a). PGCC are present in approximately 37% of human tumours and may arise from endoreplication, cell fusion (self- and heterogenous fusion between cancer and non-cancer cells) and recombinatorial reproduction *via* meiotic-like genome reductional division (Zack et al. 2013). Some PGCC have cancer stem cell features and express markers of stemness: CD44 and CD133 (Zhang et al. 2014b), OCT4, NANOG and SOX2 (Erenpreisa et al. 2011; Jackson et al. 2013). The presence of PGCC is a poor prognostic marker in multiple cancers including lymphomas, myelomas, melanomas, breast- and prostate cancer, gliomas, and others (Lopez-Beltran et al. 2005; Qu et al. 2013; Fei et al. 2015; Liu et al. 2018; Shimono et al. 2018; Sidana et al.

2019). Gene copy number alterations facilitate generation of the adaptive phenotype of PGCC and acquiring resistance to the therapies (Potapova and Gorbsky 2017) through production of tumour growth proteins (Chen et al. 2019), metabolic reprogramming, secretion cytokines and chemokines that remodel the tumour microenvironment (Sirois et al. 2019). PGCC have been implicated in the tumour recurrence and therapy resistance (Zhang et al. 2014b). In contrast, daughter cells are generate *via* depolyploidisation (Zhang et al. 2022a). PGCC can rapidly divide by asymmetric divisions (budding, splitting and bursting) producing small-sized progeny typical for aggressive phenotype (Zhang et al. 2014a).

## 2. RATIONALE AND AIMS

Most of anti-tumour therapies eliminate neoplastic cells by introducing DNA damage which ultimately triggers cell death. These effects are counteracted by activated DNA repair pathways that efficiently diminish therapeutic effects. Human RecQ helicases participate in all DNA dependent processes, including replication stress, DNA damage and repair. Glioblastoma (GBM) is deadly, primary brain tumour, resistant to conventional treatments encompassing surgery, radio- and chemotherapy. Expression and functions of the BLM helicase in tumorigenesis and GBM progression have not been fully elucidated. The main objective of this study was to evaluate the expression of the BLM helicase in gliomas, assess the effects of the BLM deficiency on cell function and cell responses to therapy and to explore a possibility of targeting BLM for the treatment of the malignant gliomas.

**The specific aims were as follow:**
1. Evaluation of the BLM helicase expression in gliomas and glioma cell lines/cultures.
2. Development of BLM deficient human glioma cells using CRISPR/Cas9 genome editing.
3. Characterisation of the effects of BLM knock-out on behaviour of glioma cells.
4. Evaluating the effects of chemotherapeutics TMZ and/or PARP1 inhibitors on wild type and BLM deficient glioma cells.
5. Elucidating mechanisms of therapy-induced senescence or polyploidy depending on BLM, MGMT and p53 status in glioma cells.
6. Comparing the functions of RecQL4 and BLM after the treatment with TMZ and PARP1 inhibitors.

## 3. Materials and Methods

### 3.1. Cell Culture

The LN18, LN229, T98G (T98), U87-MG (U87) and U251 cells were purchased from the ATCC, USA, and cultured in DMEM medium (Dulbecco's modified Eagle medium, ThermoFisher). Primary glioblastoma cell cultures (WG4 and WG9) were derivedby Iwona Ciechomska, PhD as described (Ciechomska and Wojnicki et al. 2023) and cultured in DMEM/F12 GlutaMAX media (ThermoFisher). Normal human astrocytes (NHA) (Lonza) were cultured in medium containing ABM™ Basal Medium (CC-3187) and AGM™ SingleQuots™ Supplements (CC-4123) from Lonza. LN18 and LN229 RecQL4 knock-out cells (LN18 RecQL4 KO, LN229 RecQL4 KO) were generated previously by Agnieszka Kaczmarczyk, PhD as described (Król et al. 2020). The cells were cultured in DMEM media. All culture media were supplemented with 10% FBS (Gibco), antibiotics (100 U/mL penicillin, 100 μg/mL streptomycin). Cells were cultured in a humidified atmosphere of $CO_2$/air (5%/95%) at 37 °C.

### 3.2. Drug treatments and exposure to UV-C irradiation

Cells were treated with Temozolomide (Sigma-Aldrich) alone or with combination with: Olaparib (MedChemExpress), 3-aminobenzamide (Cayman Chemicals), Rucaparib (Cayman Chemicals), 6-thioguanine (Cayman Chemicals) or Doxorubicin (Sigma-Aldrich). Doxorubicin was dissolved in water, whereas the other compounds were dissolved in DMSO. Control cells were exposed to DMSO at a dose corresponding to the highest drug concentrations.

Cells were irradiated with UV-C light and delivered at the 30 J/m$^2$ dose using the transilluminator (UltraLum UVC508). Prior to the experiment, cells were washed with PBS (phosphate buffered saline). Next, PBS was replaced by a fresh growth medium, and after 30 min cells were fixed with 4% PFA (paraformaldehyde) for 15 min, washed with PBS and stained according to the immunofluorescent staining protocol.

### 3.3. CRISPR/Cas9 mediated knock-out of *BLM* in human glioma cells

BLM knock-out cells were generated using the custom designed CRISPRCLEAR™ Transfection Ready Kit (Applied Stem Cell) for the human *BLM* gene. The kit included the commercial, validated gRNA (BLM.g1 GTTGGGTAGAGGTTCACTGA)

in the expression vector targeting the *BLM* exon 2 and Cas9-Puro plasmid (co-expressing hSpCas9 and puromycin resistance genes). Glioma cells were seeded at a density of $1.2 \times 10^5$ cells/well (24-well plate). Prior to transfection, the cells were washed with PBS and 500 µL antibiotic-free growth medium was added. Each plasmid (0.75 µg) was diluted in 50 µL of clear Opti-MEM I Reduced Serum Medium and mixed gently. Next, 2 µL of Lipofectamine 2000 (Invitrogen) was diluted in 50 µL of clear Opti-MEM and incubated for 5 min at RT. The plasmids and lipofectamine mixture were incubated for 20 min at RT and added to the cells for 6 h. Following the washes, the cells were grown for 5 days in a presence of puromycin (2 µg/mL in a growth medium) to select edited clones. Next, the cells were cultured in puromycin-free media for additional 72 h and the surviving cells (resistant to puromycin) were plated onto 100 mm petri-dishes as a single cell-derived clones to form colonies. After culturing, the colonies were validated for the *BLM* gene editing by Western blotting and ultra-deep Next Generation Sequencing. For two cell lines two independent clones with the deletion of *BLM* gene fragments and the lowest expression of the BLM protein were taken for further experiments.

### 3.4.    Cell viability assay

Cell viability was determined using a MTT metabolism test, measuring the mitochondrial dehydrogenase activity in living cells. The enzyme reduces a yellow tetrazolium salt MTT (3-[4,5-dimethylthiazol-2-yl]-2,5-diphenyltetrazolium bromide) to its purple, insoluble formazan crystals. This reaction takes place only in viable cells and the amount of formazan is proportional to the number of viable cells. In brief, cells were seeded at the density of $4 \times 10^3$ cells/well (in a 96-well plate) and at given times after treatment, MTT stock solution at a final concentration of 0.5 mg/mL in a fresh medium was added. After 1 h cells were washed with PBS and formazan crystals were dissolved in 100 µL of DMSO. Optical densities were measured at 570 nm and 620 nm (reference wavelength) using a scanning multiwell spectrophotometer.

### 3.5. Cell proliferation assay

Cell proliferation was assessed using ELISA BrdU kit (Roche Diagnostics) according to the manufacturer's protocol. The assay is based on the measurement of bromodeoxyuridine (BrdU), a thymidine analogue, incorporated into DNA strand during DNA synthesis. The reaction product is quantified by measuring the absorbance which values reflect DNA synthesis and are proportional to a number of proliferating cells. For BrdU assays, cells were seeded at a density of $4x10^3$ cells/well (in a 96-well plate) and BrdU was added for 2 h.

### 3.6. Cell cycle and cellular granularity analyses

For the cell cycle and cellular granularity analysis, cells were seeded at the density of $2x10^5$ cells/well (in a 6-well plate) and grown for the indicated times under specific conditions. Cell cycle analysis was performed by flow cytometry using BD Pharmingen PI/RNase Staining Buffer (BD Biosciences). In brief, cells were collected by trypsinization, re-suspended in a growth medium, spun down, washed with PBS, spun down again and re-suspended in 200 μL cold PBS and fixed in ice-cold 70% ethanol (2 mL/sample) for 2 h in 4 °C. Next, the cells were spun down, washed with cold PBS, spun down again, re-suspended in 1 mL of cold PBS and run at the flow cytometer. $1.0x10^6$ cells were taken for staining in PI buffer (500 μL, BD Pharmingen) for 30 min at RT in darkness. DNA content analyses were performed using the FACScalibur flow cytometer (BD Biosciences) and the BD CellQuest Pro 6.0 software (BD Biosciences). At least 10,000 events were analysed for each sample.

### 3.7. Ectopic p53 expression and functional analyses

LN18 cells ($2.5x10^5$ cells/well, in a 6-well plate) were co-transfected with the plasmid carrying the gene encoding a wildtype p53 under the CMV promoter (pC53-SN3, 0.1 μg) (Baker et al. 1990) or empty vector (pcDNA3.1, 0.3 μg) and the plasmid encoding EGFP protein (pEGFP-N1, 0.3 μg). Prior to the transfection, the culture medium was replaced with 900 μL antibiotic-free growth medium. Each plasmid was diluted in 50 μL of clear Opti-MEM I Reduced Serum Medium and mixed gently. Next, 6 μL of Lipofectamine 2000 (Invitrogen) was diluted in 50 μL of clear Opti-MEM and incubated for 5 min at RT. The plasmids and lipofectamine mixture were incubated for 20 min at RT

and added to the cells for 6 h. The medium was changed, and the cells were incubated overnight prior to the experiment. After treatments, the cells were trypsinised, fixed and stained in 15 µM DRAQ5 in 4% PFA solution and a cell cycle was analysed using FACScalibur flow cytometer (BD Biosciences) and the BD CellQuest Pro 6.0 software (BD Biosciences). At least 10,000 events of GFP$^+$ cells were analysed for each sample. The gating strategy and a scheme of the experiment are presented in the figure 1.
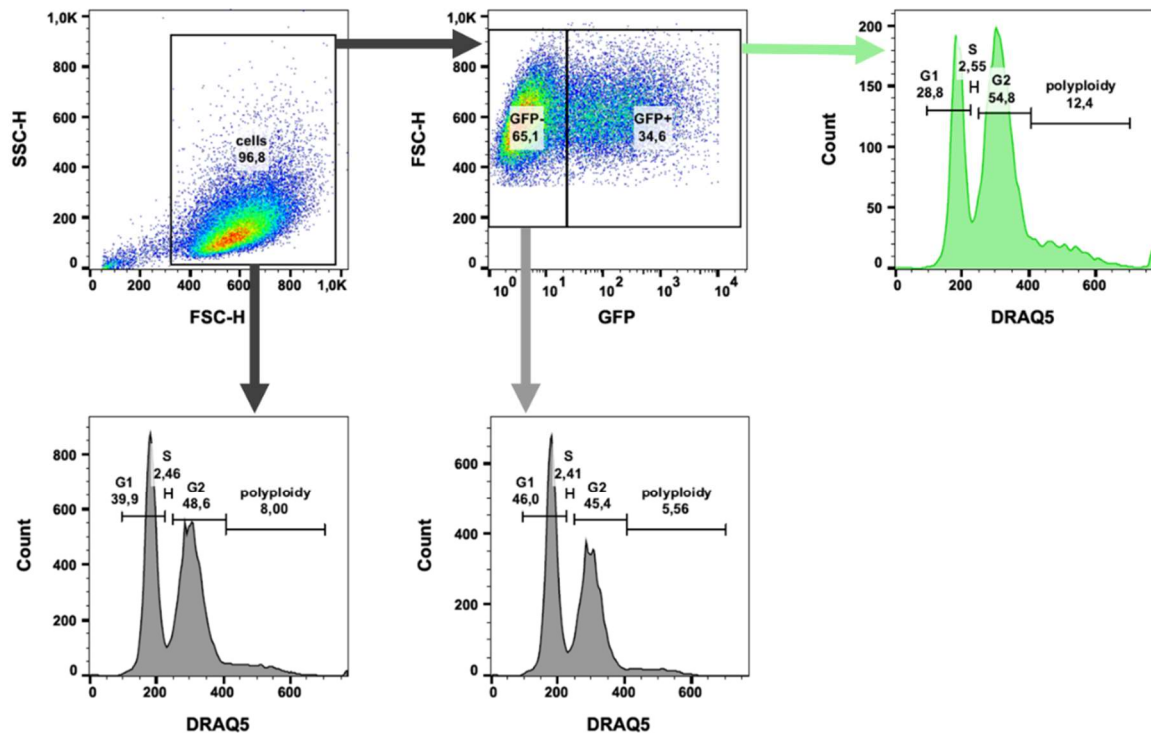


**Figure 1. Gating strategy for a cell cycle analysis of the p53-WT transfected cells.**

Transfection efficiency and the p53 transcriptional activity were assessed using two reporter constructs encoding firefly luciferase under a p53-responsive promoter (pPG13-Luc) containing 13 copies of the p53-binding sequence, or a promoter (pMG13-Luc) containing mutated sequence with no ability to bind p53. The constructs were kindly provided by M. Hetman, PhD (University of Louisville, USA) (Kern et al. 1992). In brief, LN18 cells (8x10$^4$ cells/well, 24-well plate) that were deficient for p53 activity were co-transfected with the plasmid carrying the gene encoding a wildtype p53 under the CMV promoter (pC53-SN3, 0.1 µg) with either pPG13-Luc plasmid (0.5 µg) or pMG13-Luc (0.5 µg) using Lipofectamine 2000 (Invitrogen). Prior to transfection, the cells were washed and 400 µL antibiotic-free growth medium was added. Each plasmid was diluted

in 50 µL of clear Opti-MEM I Reduced Serum Medium and mixed gently. Next, 1.5 µL of Lipofectamine 2000 (Invitrogen) was diluted in 50 µL of clear Opti-MEM and incubated for 5 min at RT. The plasmids and lipofectamine mixture were incubated for 20 min at RT and added to the cells for 6 h. After changing the medium, cells were incubated overnight. 24 h after transfection cells were lysed in 50 µL of a passive lysis buffer (Promega) and the luciferase activities were measured with the Dual-Luciferase Reporter System (Promega) using luminometer (Turner BioSystems). The results were normalised to the protein amount in the lysates, determined with BCA Protein Assay Kit (ThermoFisher).

### 3.8. Total RNA isolation

Glioma and NHA cells were lysed using RLT buffer containing 1% (v/v) β-mercaptoethanol and total RNA was extracted using RNeasy Mini kit (Qiagen) according to the manufacturer's protocol. QIAshredder columns (Qiagen) and DNase digestion step were employed to facilitate cell lysis and the depletion of genomic DNA, respectively. Next, RNA was eluted in 30 µL of high-purity nuclease free water. Quantity and quality were determined using NanoDrop 2000 spectrophotometer (ThermoFisher). Samples were stored at -80 °C.

### 3.9. Reverse Transcription Quantitative Polymerase Chain Reaction (RT-qPCR)

Reverse transcription was performed using 1 µg of RNA. The reaction mix contained RNA (1 µg), oligo(dT)$_{20}$ (1 µL of 50 µM stock), dNTPs (1 µL of 10 mM stock) and sterile RNase-free water (up to 13 µL of total volume). This mix was incubated at 65 °C for 5 min. Next, a mixture containing 5X First-Strand Buffer (4 µL), DTT (1 µL of 0.1 M stock), SuperScript III Reverse Transcriptase (200 U/µL; 0.5 µL, Invitrogen) and sterile RNase-free water (1.5 µL) was added followed by 1 h incubation at 50 °C for cDNA synthesis, and 70 °C for 15 min to inactivate the enzyme.

Gene expression was evaluated by real-time quantitative PCR (RT-qPCR) on Quantum Studio with 20 ng of cDNA in duplicates using TaqMan™ Fast Universal PCR Master Mix (ThermoFisher) in 10 µL reaction with a BLM (Hs00172060_m1) and GAPDH (Hs02758991_g1) TaqMan probes. The PCR program is given in table 1. The amplified product was normalised to the endogenous

expression of glyceraldehyde-3-phosphate dehydrogenase mRNA (*GAPDH*) and represented as delta Ct values.

| Step | Temp. | Time | Cycles |
|---|---|---|---|
| 1 | 95 °C | 20 sec | |
| 2 | 95 °C | 1 sec | 40 |
| 3 | 60 °C | 20 sec | |

**Table 1. Thermocycler settings for RT-qPCR.**

### 3.10. RNA-sequencing library preparation

To assess the RNA integrity before sequencing step, RNA samples were run on Agilent 2100 Bioanalyzer using RNA 6000 Nano Kit (Agilent). Next, 100 ng of intact total RNA (RIN > 8.5, diluted in 50 µL of water) and KAPA Stranded RNA-Seq Library Preparation Kit (KAPA Biosystems) were used to prepare libraries according to manufacturer's protocol (KR0960-38 v5.17). In brief, mRNA capture was performed using the mRNA capture beads that were washed once on a magnet with mRNA bead binding buffer. mRNA capture beads were mixed with a RNA sample and incubated at 65 °C for 2 min, then 20 °C for 5 min for 1st mRNA capture. The beads with captured mRNA were washed with 200 µL on a magnet and re-suspended in 50 µL of RNase-free water. 2nd capture was performed by incubating the samples at 70 °C for 2 min, then 20 °C for 5 min. 50 µL of bead binding buffer was added to the mixture and incubated at 20 °C for 5 min. Beads with captured RNA were washed with 200 µL of mRNA bead wash buffer and re-suspended in 22 µL of the Fragment, Prime and Elute buffer (1X). To obtain a library of 201 – 300 bp insert size, the samples were fragmented for 5 min at 94 °C. Immediately following incubation, the strips containing beads and eluted fragmented mRNA were placed on a magnet and 20 µL of supernatant was transferred into fresh PCR-strip on ice.

First strand synthesis was performed by incubating 20 µL of eluted mRNA and 10 µL of 1st strand synthesis master mix in a thermocycler. Following first strand synthesis, 2nd strand synthesis master mix was prepared and added into each sample, and incubated at 16 °C for 60 min on ice then hold at 4 °C. The product was then cleaned up using 1.8X bead-based cleanup, by combining 60 µL of the reaction and 108 µL of KAPA Pure Beads. The mixture was pipetted gently.

The strips were then incubated at room temperature for 10 min, and placed on a magnet for bead capture and cleanup using fresh 80% EtOH. The cleanup was performed twice, and beads were re-suspended in 15 µL of A-tailing buffer (1X) and stored overnight at 4 °C. A-tailing was performed by adding 15 µL of A-tailing master mix (final volume 30 µL), and incubating the mix at 30 °C for 30 min, then 60 °C for 30 min, and hold at 4 °C. Immediately following a completion of the run, NEBNext adaptor for Illumina (#E7337AA, NEB) diluted 1:30 was ligated at 20 °C for 15 min. 2.5 µL of USERTM enzyme (#E7500L, NEB) was added and incubated at 37 °C for 30 min to cleave the looped adaptors. Beads with ligated adapters were washed by adding PEG/NaCl solution 1:1, followed by two washes with 80% EtOH. The beads were re-suspended in 50 µL of 10 mM Tris-HCl (pH 8.0 - 8.5) and incubated for 2 min to elute the DNA. Second post-ligation cleanup was performed as described above, and DNA was eluted in 22 µL of 10 mM Tris-HCl. 20 µL of clear supernatant was transferred into fresh PCR strip and library amplification master mix was prepared using the NEBNext Multiplex Oligos for Illumina (#E7500L, NEB) with 2.5 µL NEBNext Universal PCR Primer for Illumina and 25 µL KAPA HiFi HotStart ReadyMix (2X). Unique NEBNext Index Primers (2.5 µL) were added into each sample and library was amplified using thermocycler with the program shown in the table 2.

| Step | Temp. | Time | Cycles |
|---|---|---|---|
| Initial denaturation | 98 °C | 45 sec | |
| Denaturation | 98 °C | 15 sec | |
| Annealing | 60 °C | 30 sec | 14 |
| Extension | 72 °C | 30 sec | |
| Final extension | 72 °C | 5 min | |
| Hold | 4 °C | ∞ | |

**Table 2. Thermocycler settings for amplification of the libraries.**

Libraries were purified using 1X bead-based cleanup with KAPA Pure Beads, and washed twice with 80% EtOH. Elution was performed in 22 µL of 10 mM Tris-HCl. Amplified libraries were stored at -20°C. Library QC was performed by running Bioanalyze High Sensitivity DNA Assay (Agilent) and Quantus ONE DNA (Promega). Sequencing was performed using Illumina HiSeq 1500, with pair-end sequencing resulting in 75 bases from each end. Reads were aligned, counted and raw read

counts were processed for further analysis using R software. The RNA sequencing was performed in collaboration with Bartłomiej Gielniewski, PhD.

### 3.11.  Bioinformatic analysis

Transcriptomic data were analysed as follows: fastq files were aligned to hg38 human reference genome with STAR program (Farmer et al. 2005), and reads were counted to genes using feature Counts algorithm SUBREAD package (Bryant et al. 2005). Gene counts were normalised with the FPKM method, and differential analysis was performed using the DESeq2 (https://genomebiology.biomedcentral.com/articles/10.1186/s13059-014-0550-8). Genes were considered to be differentially expressed (DE) with FDR corrected p-value<0.05. Kyoto Encyclopedia of Genes and Genomes (KEGG) pathway analyses were performed using R package clusterProfiler (Mo et al. 2016) to annotate the functions of differentially expressed (DE) mRNAs. The bioinformatic analyses were performed in collaboration with Bartosz Wojtaś, PhD.

### 3.12.  Ultra-deep sequencing library preparation.

DNA was isolated from BLM knock-out cells using QIAamp DNA Blood Mini Kit (Qiagen) according to manufacturer's protocol. 20 ng of DNA was used for PCR reaction to amplify the *BLM* gene region of interest using specific primers (F: ATGTGTCAGTAGCAAAAACACC,     R: CTGTCCTGCTGGAGCATTTTT,     0.5 mM/each) and Q5 High-Fidelity DNA polymerase (12.5 µL) in 25 µL total reaction volume. Thermocycler settings for a PCR are given in the table 3.

| Step | Temp. | Time | Cycles |
|---|---|---|---|
| Initial denaturation | 98 °C | 30 sec | |
| Denaturation | 98 °C | 10 sec | |
| Annealing | 67 °C | 30 sec | 30 |
| Extension | 72 °C | 15 sec | |
| Final extension | 72 °C | 2 min | |
| Hold | 4 °C | ∞ | |

**Table 3. Thermocycler settings for amplification of the *BLM* region.**

Purity of the product was determined by agarose gel electrophoresis. DNA libraries were prepared using the QIAseq Ultra Low Input Library Kit (Qiagen) following

the manufacturer's protocol. Firstly, PCR products were subjected to an end-repair reaction, then the 3' ends of the dsDNA molecules were adenylated, followed by an adapter attachment reaction (NEB). The loop structure in the attached adapters was digested with the USER enzyme (NEB). Next, the PCR products was amplified by PCR using NEB primers (NEB) complementary to the adapter sequence. The library concentration was measured using a Nanodrop spectrophotometer (ThermoScientific) and a Quantus fluorometer (Promega). Library quality was assessed by capillary electrophoretic separation using an Agilent 2100 Bioanalyzer and an Agilent DNA High Sensitivity reagent kit (Agilent). The average length of the DNA molecules constituting the library was 280 bp. Sequencing was performed using Illumina HiSeq 1500 with pair-end sequencing resulting in 75 bases from each end. Reads were aligned and counted, and raw read counts were processed for further analysis using R software. The amplicon sequencing was performed in collaboration with Bartłomiej Gielniewski, PhD and Bartosz Wojtaś, PhD.

### 3.13. Data availability

Data that support findings of this are available in NIH GEO database with the accession number GSE214931.

### 3.14. Protein isolation and Western blotting

Whole-cell protein extracts were prepared using a lysis buffer containing phosphatase and protease inhibitors (20 mM Tris HCl, pH 6.8, 137 mM sodium chloride, 25 mM β-glycerophosphate, 2 mM sodium pyrophosphate, 2 mM EDTA, 1 mM sodium orthovanadate, 1% Triton X-100, 10% glycerol, 5 µg/mL leupeptin, 5 µg/mL aprotinin, 2 mM benzamidine, 0.5 M DTT, 1 mM PMSF) and the protein concentration was determined with the Pierce BCA Protein Assay Kit (ThermoScientific). Total protein extracts were prepared in 4×Laemmli sample buffer (250 mM Tris-HCl pH 6.8, 8% SDS, 40% glycerol, 0.04% bromophenol blue, 400 mM DTT) and denatured for 5 min at 95 °C. Next, the protein extracts were resolved by SDS-PAGE electrophoresis and transferred to a nitrocellulose membrane (Amersham Biosciences) in a transfer buffer containing 10% of MeOH and 0.1% of SDS (sodium dodecyl sulphate). After blocking with 5% non-fat milk in TBST (Tris-buffered solution pH 7.6, 0.01% Tween-20), the membranes were

incubated overnight with primary antibodies diluted in a TBST with 3% bovine serum albumin (BSA) or 1 h with horseradish peroxidase (HP) – conjugated anti-β-actin antibody diluted in 5% non-fat milk in TBST. The primary antibody reaction was followed by 1 h incubation with HP-conjugated anti-rabbit IgG or anti-mouse IgG, which were diluted in TBST. Immunocomplexes were detected using an enhanced chemiluminescence detection system (ECL) and Chemidoc (Biorad). Membranes were stripped in 100 mM glycine and 20% SDS buffer, pH 3.0 for 30 min at RT, washed, blocked and re-probed with antibodies. Band intensities were measured by a densitometric analysis of immunoblots using the BioRad Image Lab (ver. 5.2) software. For antibody specifications and dilutions, see table 4.

| Antibody | Company | Cat. number | Dilution |
|---|---|---|---|
| anti-cleaved PARP | Cell signaling | 9541S | 1:1000 |
| anti-cleaved Caspase3 | Cell signaling | 9661S | 1:1000 |
| anti-cleaved Caspase7 | Cell signaling | 9491S | 1:1000 |
| anti-GAPDH | Millipore | MAB374 | 1:1000 |
| horseradish peroxidase conjugated anti-β-actin | Sigma Aldrich | A3854 | 1:40000 |
| horseradish peroxidase-conjugated anti-rabbit IgG | Vector | PI-1000 | 1:10000 |
| horseradish peroxidase-conjugated anti-mouse IgG | Vector | PI-2000 | 1:10000 |

**Table 4. Antibodies used for Western blot.**

### 3.15. Immunohistochemistry on tissue microarrays (TMA)

BLM expression across glioma samples was evaluated using immunohistochemistry on glioma tissue microarrays (US Biomax). Paraffin-embedded tissue sections (5 µm) were incubated at 60 °C for 30 min and deparaffinised by incubation in xylene, followed by incubation in ethanol (100, 90, 70%), and then rehydrated. Epitopes were retrieved by oven boiling in a pH 6.0 citrate buffer for 30 min. Endogenous peroxidase was blocked in 0.3% $H_2O_2$ in 10% methanol for 30 min followed by blocking with 10% horse serum. Sections were incubated overnight at 4 °C with the rabbit anti-BLM primary antibody 1:200 (ab2179, Abcam). Next, the specimens were washed in PBS, incubated with biotinylated horse immunoglobulin, then with HP-conjugated avidin for 60 min, and finally with 3,3′-diaminobenzidine (DAB). Sections were counterstained with

haematoxylin (Sigma-Aldrich), washed, dehydrated and mounted in a mounting medium. Images were acquired with the Leica DM4000 B microscope operating with the Application Suite ver. 2.8.1 software (Leica Microsystems CMS). The scoring was performed by two independent scientists based on positive staining of the BLM protein in the nucleus or cytoplasm, and marked as 1 if staining was present or 0 if absent.

### 3.16. Immunofluorescence staining

Cells were seeded onto glass coverslip at a density of $3 \times 10^5$ cells. After 24 h the cells were fixed with 4% PFA pH 7.2, washed, permeabilised with 0.1% Triton-X100 in PBS and blocked in PBS with 2% donkey serum and 1.5% fetal bovine serum, followed by 2 h incubation with rabbit anti-BLM and mouse anti-γH2AX or mouse anti-γ-tubulin primary antibodies. Cells were then washed in PBS, incubated with donkey anti-rabbit Alexa Fluor A555 and donkey anti-mouse Alexa Fluor A488, or donkey anti-mouse Alexa Fluor A555, counterstained with DAPI and mounted. When mouse anti-β-tubulin antibody conjugated with FITC was used, incubation with secondary antibodies was omitted. For antibody specifications and dilutions, see table 5.

| Antibody | Company | Cat. number | Dilution |
|---|---|---|---|
| anti-BLM | Abcam | ab2179 | 1:200 |
| Anti- RecQL4 | Novus Biologicals | 25470002 | 1:200 |
| anti-γ-tubuline | SantaCruz | sc-17787 | 1:100 |
| anti- γH2AX | Abcam | ab26350 | 1:1000 |
| anti-β-tubulin-FITC | Sigma-Aldrich | F-2043 | 1:100 |
| donkey anti-rabbit A555 | ThermoFisher | A31572 | 1:1000 |
| donkey anti-mouse A488 | ThermoFisher | A21202 | 1:1000 |

**Table 5. Antibodies used for immunofluorescent staining.**

### 3.17. Phalloidin staining

Cells were seeded onto glass coverslip at a density of $3 \times 10^4$ cells. Following 24 h incubation, cells were treated with TMZ and OLA for 48 h. Next, the cells were washed with PBS, fixed with 2% PFA in PBS and permeabilised with 0.1% Triton X-100. Rhodamine-Phalloidin (1:1000 in PBS) was used to stain F-actin for 25 min at room temperature and then co-stained with DAPI (1 μg/mL) to visualise nuclei.

### 3.18. Quantification of senescence-associated β-galactosidase-positive cells

The activity of senescence-associated β-galactosidase (SA-β-gal) was detected. Cells were seeded at density $2x10^4$ cells onto glass coverslips, and after the treatment, fixed with 2% formaldehyde and 0.2% glutaraldehyde in PBS, washed, and incubated overnight at 37 °C (without $CO_2$) in the solution containing 1 mg/mL 5-bromo-4-chloro-3-indolyl-β-D-galactopyranoside (X-gal), 5 mM potassium ferrocyanide, 5 mM potassium ferricyanide, 150 mM NaCl, 2 mM $MgCl_2$, and 0.1 M phosphate buffer, pH 6.0. Thereafter, the cells were washed, mounted and counted under a light Nikon Eclipse 50i microscope (Minato). The percentages of SA-β-gal-positive cells were calculated.

### 3.19. *Xenopus* Care

Nigerian strain *Xenopus tropicalis* were housed and maintained within the European *Xenopus* Resource Centre, at the University of Portsmouth, in re-circulating systems (25°C) with 15% daily water changes on a 13-11 h light-dark cycle. All procedures were conducted in accordance with the Home Office Code of Practice, under PPL 70/8983 with approval from the University of Portsmouth's Animal Welfare and Ethical Review Body. Adult female *X. tropicalis* were primed the evening prior to egg collection with 10 IU hCG (Chorulon, Intervet) and received a boosting dose of 100 IU hCG the following morning. Egg clutches were obtained by gentle abdominal massage and fertilised with cryopreserved sperm. Frozen *X. tropicalis* spermatozoa were generated within the European *Xenopus* Resource Centre from 12- to 15-month-old male *X. tropicalis* exhibiting enhanced nuptial pads. Sperm cryopreservation follows an adapted protocol initially developed by Sargent and Mohun (Noble et al. 2021).

### 3.20. Generating knock-out animals using CRISPR/Cas9

Target regions within *blm* and *recql4* exon1 and exon2 were identified using Xenbase (http://www.xenbase.org/entry; V9.1 of the genome) and three single-stranded oligonucleotides for generating sgRNAs, were selected based on the following criterion: high mutagenic activity and minimal predicted off-target events (CRISPRscan - http://www.crisprscan.org). Due to the uncertainty

of the nature of exon1 as identified in that genome version, only two of the three single-stranded oligonucleotides were selected for subsequent work.

Single guide RNAs (sgRNA) were synthesised from single-stranded oligonucleotides (Invitrogen, above) containing the T7 promoter as described in the Taq-based method by (Nakayama et al. 2014) then by using the T7 megashortscript kit as described in the manufacturer's instructions (Invitrogen, USA). Embryos for injection were prepared and cultured as described previously (Guille 1999). To maximise the chance of randomising eggs to the test and control groups, a Petri dish of eggs had all of the damaged ones removed under the microscope. The dish was removed from under the microscope, swirled to mix the eggs and then the eggs were distributed to each group without further visualisation. Each sgRNA was co-injected with Cas9 at 1-cell, 2-cell and 4-cell stages into *X. tropicalis* embryos from both a wildtype strain and a transgenic line. Genotyping PCR reactants consisted of lysate, GoTaq® DNA Polymerase (Promega), forward and reverse primer and molecular biology grade water. PCR amplicons were obtained using the standard PCR parameters.

A T7 Endonuclease I (NEB) assay (Fu et al. 2013) was used to indicate the proportion of positive samples and indel formation was confirmed using Sanger sequencing (Genewiz) and Tracking of Indels by Decomposition (https://tide.nki.nl/). Morphological differences between un-injected and crispant embryos were identified using a Zeiss Axio Zoom.V16 Stereomicroscope.

### 3.21. Microtomography of *Xenopus* tadpoles

Tadpoles for MicroCT were fixed in PFA following the method described for wholemount *in situ* hybridisation of *Xenopus* Embryos (Guille 1999). These fixed specimens were immediately contrast stained in phosphotungstic acid (PTA) following an adapted protocol from Metscher, (Metscher 2009) Briefly, the samples were stained in 1% PTA (in water) for 24 h, washed in methanol and placed in 1% PTA for a further 24 h. The specimens were allowed to rest in methanol for one week, before the samples were embedded in 0.7% agarose within a 20 μL pipette tip (to prevent movement during imaging). The samples were imaged using the ZEISS Xradia Versa 520 (Carl Zeiss Microscopy, Pleasanton, CA, USA) set to operate at a voltage of 50 kV and a current of 75 mA. A 4x objective lens was used, resulting in an effective isotropic voxel size of 3.1 μm. In total,

1601 projections were collected over 360° with an exposure time of 2.0 s per projection. Each tomogram was reconstructed to 16-bit grey-level images using the manufacturer's software (Scout and Scan Reconstructor, Carl Zeiss Microscopy, Pleasanton, CA, USA) which employs a filtered back projection algorithm. The imaged volumes were then visualised using TXM3DViewer (Carl Zeiss Microscopy, Pleasanton, CA, USA).

### 3.22. Statistical analysis

All biological experiments were performed on 3-5 independent cell passages. The results were expressed as means ± standard deviation (SD). P-values were calculated using chi-square, two-tailed t test; one-way ANOVA or linear contrast ANOVA analysis followed by appropriate post-hoc test using GraphPad Prism v6 (GraphPad Software). Differences were considered statistically significant for p values < 0.05. The effect sizes, Cohen's '$d$' and Hedge's '$g$', were calculated as follows: $d = \frac{\overline{X_1} - \overline{X_2}}{\sqrt{M_{SE}}}$, $g = d \times \left(1 - \frac{3}{4(n_1 - n_2) - 9}\right)$; $\overline{X}$ - mean of the group, $M_{SE}$ - error mean square, n - sample size.

Cohen's '$d$' describes the standardised mean difference of an effect and can be used to compare effects across studies when dependent variables were measured in different ways. The formula for Cohen's '$d$' is based on sample averages bears a risk for a biased estimate of the population effect size, particularly for small samples (n < 20), thus Cohen's '$d$' is sometimes referred to uncorrected effect size. For corrected effect size, the Hedge's '$g$' is introduced with the formula given above. A commonly used interpretation for effect size is as follow: small (0.2), medium (0.5) and large (0.8), however these values are arbitrary and should not be considered rigidly (Thompson 2007; Lakens 2013)

Eta squared ($\eta^2$) computes the proportion of the variation in Y that is associated with membership of different groups defined by X, or the sum of squares of the effect divided by the total sum of squares $\eta^2 = \frac{SS_{effect}}{SS_{total}}$. The value closer to 1, the more accurate the studies. $\eta^2$ of.045 means that 45% of the total variance could be accounted for by group membership (Lakens 2013).

Linear contrast ANOVA was used to determine the dose-dependent response of glioma cells to chemotherapeutics using cell-viability MTT assay. $EC_{50}$ values were calculated from linear relationships between cell viability [%] and drug doses.

### 3.23. Illustrations

Graphical abstract and illustrations were created with BioRender.com.

# 4. RESULTS

## 4.1. *BLM* expression and mutations across the tumours

The BLM helicase is one of the enzymes needed to loosen the DNA structure before the cell division and is involved in DNA double-strand brakes repair. We analysed the publicly available databases to determine the *BLM* expression (Fig. 1A) and mutations (Fig. 1B) in various tumours. *BLM* expression was upregulated in all the analysed tumours. Notably, the frequency of the somatic *BLM* mutations was low (1.6%). It spreads across whole protein encoding regions, without any specific hotspot. The majority of *BLM* mutations were missense mutations, marked by green dots.
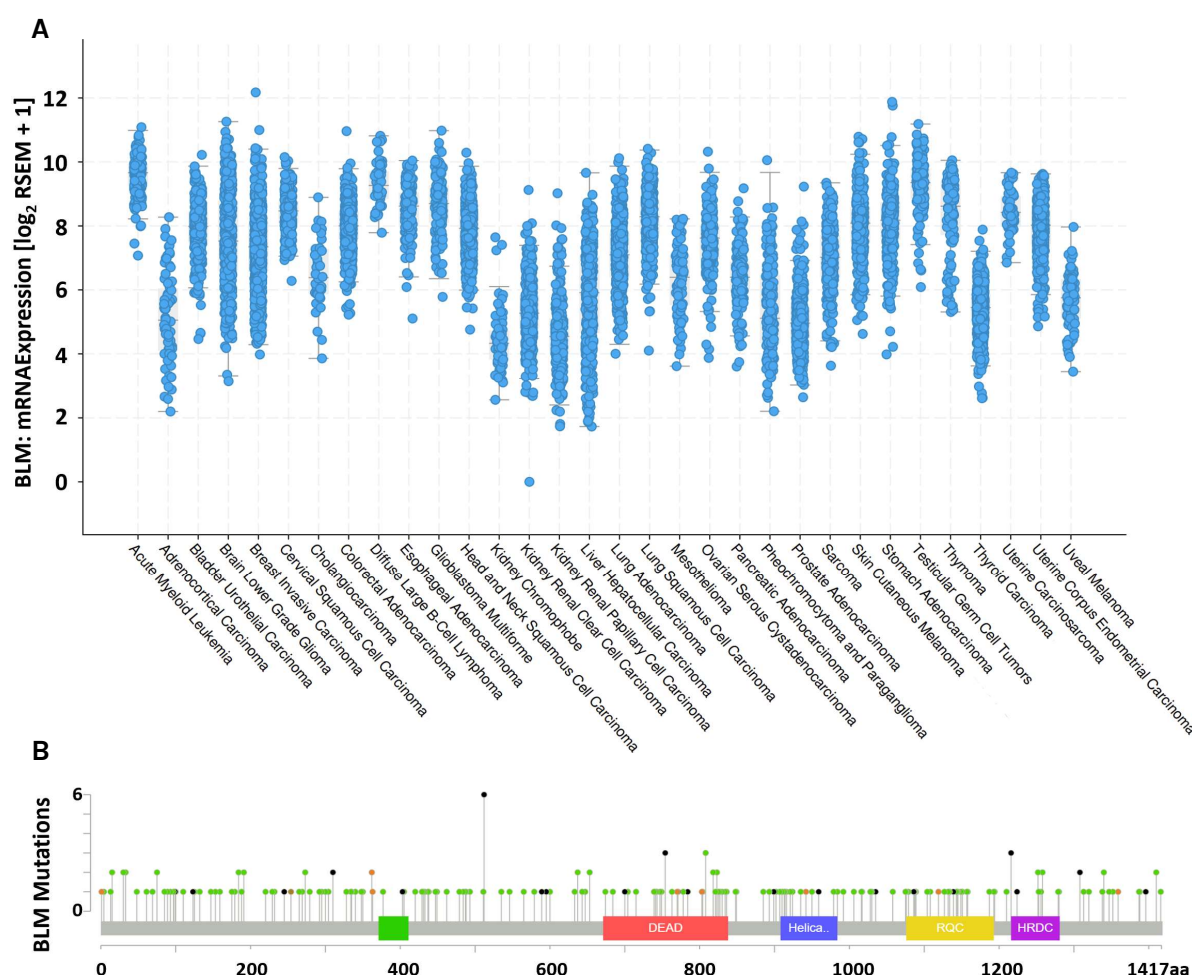


**Figure 1. BLM expression in various tumours.**
(**A**) Expression of the *BLM* mRNA and (**B**) *BLM* mutations across different types of tumours. Data obtained from cBioPortal. RSEM + 1 stands for batch normalised from Illumina HiSeq_RNASeqV2 $\log_2$ value + 1. Green box in (**B**) depicts the BDHCT domain (a C-terminal domain in Bloom's syndrome DEAD helicase subfamily). Coloured dots represent types of mutations: missense (green), splice (orange) and truncating (black). n=10,967. Prepared with the kind help of Bartosz Wojtaś, PhD.

Inspired by the findings that *BLM* is overexpressed in brain tumours, we investigated mutation rates in GBMs, as well as the *BLM* expression in low (G2)- and high (G3, G4) grades gliomas, using the transcriptomic dataset from The Cancer Genome Atlas (TCGA). The BLM mutations were found in GBMs, but the mutation rate was low (1%, Fig. 2). We found only 7 missense, and 1 mutation affecting splicing, which was considered as likely-oncogenic and likely-loss of functions.
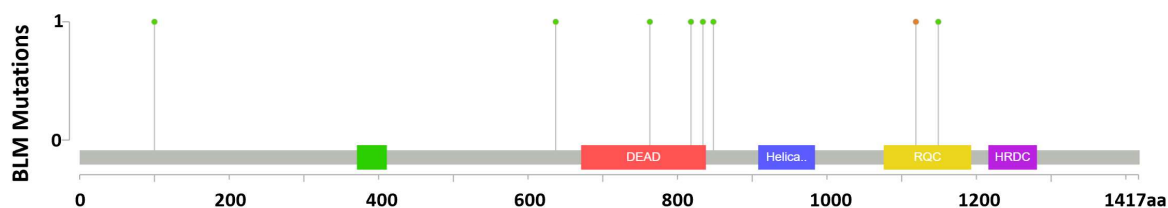


**Figure 2. The occurrence of *BLM* mutations in GBMs.**
Green box depicts BDHCT domain. Coloured dots represent types of mutations: missense (green) and splice (orange). Number of samples n=592.

We compared the *BLM* expression in gliomas from TCGA dataset and found the elevated *BLM* transcript level in gliomas of WHO grades 2-4, with the highest median expression of *BLM* in GBMs, in comparison to normal brain (NB). Notably, its expression in the low- and high-grades gliomas differed significantly (Fig. 3A). Moreover, the upregulated *BLM* expression correlated negatively with the patients' survival. The median survival (dashed lines) in high- and low-*BLM* expressing glioma patients was approximately 500 and 1,950 days, respectively (Fig. 3B). Ultimately, we investigated the correlations between all the helicases from RecQ family across the analysed tumours. The majority of helicases displayed a positive correlation with the other members of the RecQ family, nevertheless the expression of *BLM* correlated strongly with *RecQL4* (RQ4) and *WRN* helicases (Fig. 3C).
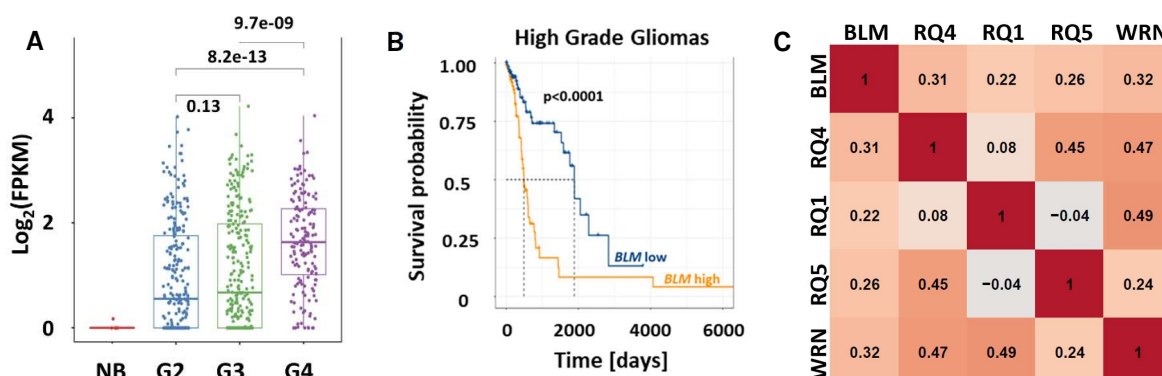
**Figure 3.** *BLM* **expression in human gliomas, its correlation with patients survival and with other RecQ family members.**

(**A**) *BLM* mRNA expression in normal brains (NB), WHO grade 2, 3 gliomas and WHO grade 4 glioblastomas in TCGA dataset. The expression is shown as $\log_2$ of FPKM (Fragments Per Kilobase of transcript per Million). The significance of BLM expression across gliomas with different grades was determined using the Wilcoxon rank-sum non-parametric test. (**B**) Kaplan-Meier censored overall survival analysis from TCGA data of patients with high-grade gliomas (WHO grades 3 and 4). The correlation between *BLM* expression and patient survival was assessed using the log-rank test and Kaplan-Meier estimators. (**C**) Correlation heatmap of RecQ helicases belonging to RecQ helicases family across G4 glioma tumours (TCGA dataset). With the kind help of Adrià-Jaume Roura, PhD.

We deciphered the expression of RecQ helicases family members across glioblastoma tumours using TCGA database with the Neftel signature referring to cellular states driving glioblastoma cell heterogeneity and defining more GBM specific subtypes (Neftel et al. 2019). We found that *BLM* expression positively correlated with astrocyte-like and oligodendrocyte-progenitor-like glioblastoma subtypes. Contradictory, the lower level of *BLM* mRNA correlated with proliferative tumours with the G1S and G2M signature. Those signatures reflect as AC-like and MES-like—GBMs which contains considerable subsets of proliferating cells (Fig. 4).
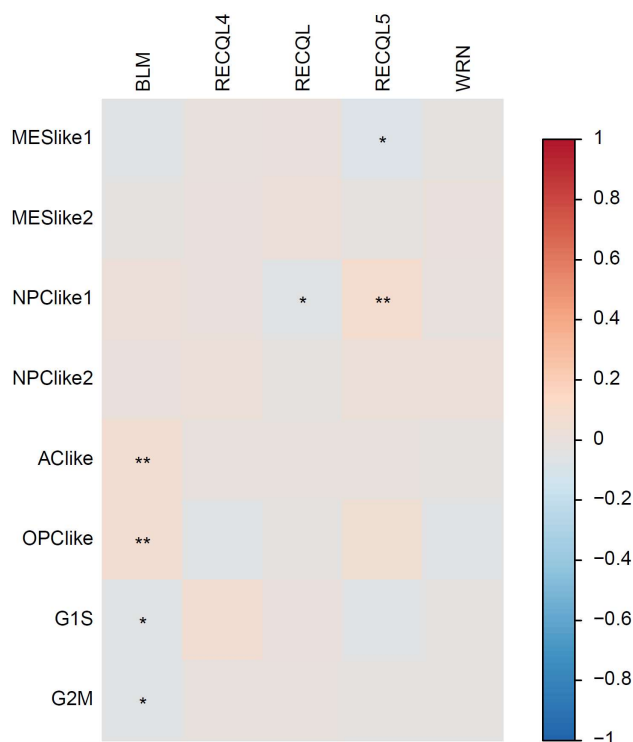


**Figure 4. Heatmap of RecQ helicases family members across glioma tumours.**
Abbreviations: **MESlike-** mesenchymal like, **NPClike-** neural progenitor like, **AClike-** astrocyte like, **OPClike-** oligodendrocyte-progenitor like, **G1S**, **G2M-** signatures of proliferating cells.
With the kind help of Bartosz Wojtaś, PhD.

For better characterisation of BLM localisation within the tumour tissues, the commercially available human glioma tissue microarrays were employed to verify the level of the BLM protein across the gliomas of different grades. In most cases, BLM was present in the tumour tissue whereas in the normal brain tissues, BLM staining was barely detectable (Fig. 5). In control brains and low-grade gliomas most of the BLM staining was nuclear whereas both nuclear and cytoplasmic localisation of BLM was detected in higher-grade gliomas. Quantification of the staining results revealed the negative correlation between nuclear BLM positive staining and glioma grades (Fig. 5, pie charts).
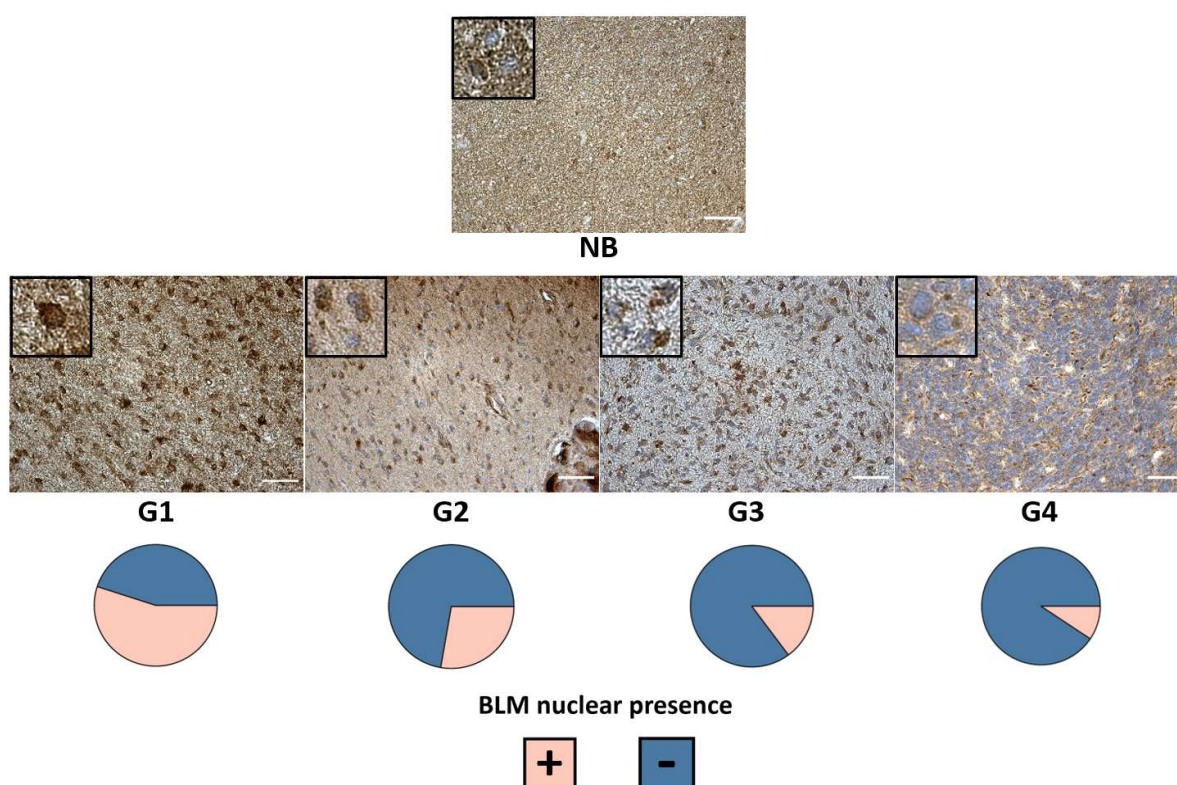


**Figure 5. Expression and localisation of BLM vary in gliomas of different grades.**
Representative images of BLM immunostaining in the control and glioma tissues on commercial tissue microarrays (TMAs). Pie charts represent a number of specimens with the nuclear localization of BLM across tumour grades. TMAs include spots of tissues from astrocytoma (n=127), glioblastoma (n=31), oligoastrocytoma (n=7), oligodendroglioma (n=9), ependymoma (n=11), ganglioglioma (n=1) and gliosarcoma (n=1), plus tumour adjacent and normal brain (NB) tissues (n=8). The immunohistochemistry results were evaluated by two researchers, with the kind help of Wiesława Grajkowska, Prof. Statistical significance of the nuclear BLM presence was determined by chi-squared test (p-val=$6.52\times10^{-5}$). Scale bar: 50 μm; insets show a tissue at higher magnification. Pie charts were calculated with the kind help of Jakub Mieczkowski, PhD.

Further, the BLM mRNA and protein levels were evaluated in seven human glioma cell lines: established T98, LN229, U251, LN18, U87 cell lines and patient-derived primary WG4, WG9 cell culture (Fig. 6). Cultured normal human astrocytes (NHA) served as a non-malignant control. *BLM* mRNA was uniformly significantly overexpressed in malignant cells in comparison to Normal Brain (NB) control as evidenced by qPCR (Fig. 6A). The BLM protein levels differed between the glioma cells (Fig. 6B), the highest level of BLM protein was detected in LN18 and LN229 cells. Due to the highest BLM levels these cell lines were employed for further experiments.

Using immunocytochemistry, we visualised BLM in glioma cells exposed to the UV-C light that introduces double strand breaks (DSB) into DNA. Numbers of BLM foci were increased when LN229 cells were exposed to UV-C. Double immunofluorescent staining of exposed cells showed that BLM is co-localized with γH2AX, a marker of DSB (Fig. 6C). These results show overexpression of BLM in human gliomas and cells, and rapid response of BLM to DSB in glioma cells.
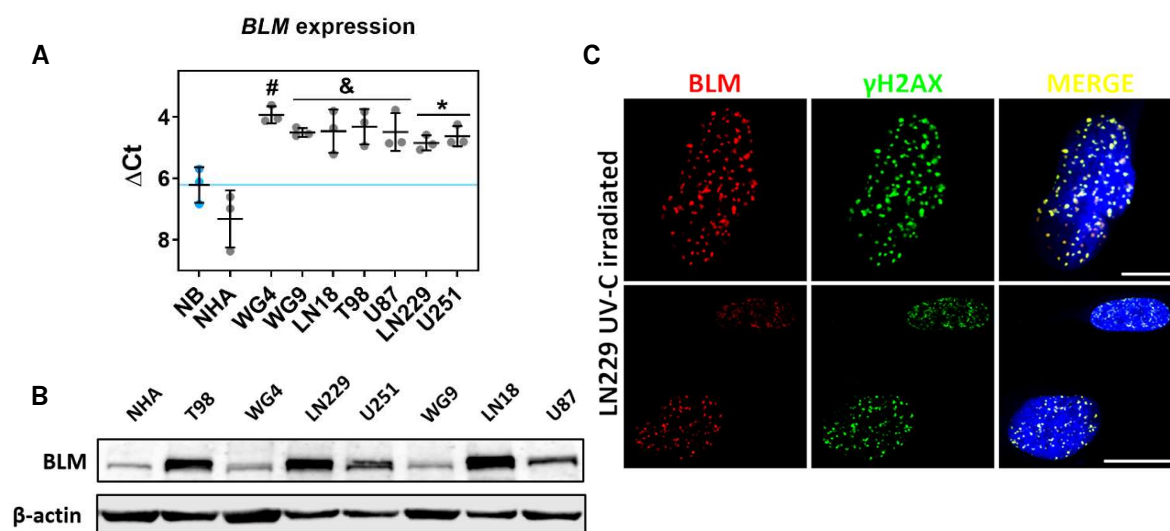


**Figure 6. BLM protein is upregulated in glioma cells and rapidly responds to UV-C induced DNA damage.**
(**A**) Expression of *BLM* in human established glioma cell lines (T98, LN229, U251, LN18, U87), patient-derived primary cultures (WG4, WG9), normal human astrocytes (NHA) and human normal brain (NB). RT-qPCR data are shown as delta Ct values relative to *GAPDH* expression in the same samples. Statistical analysis was performed using one-way ANOVA with Dunnett's post-hoc test to NB (*p<0.05, & p<0.01, # p<0.001), mean ± SD, n=3. (**B**) Immunoblot showing BLM levels in various glioma cells and NHA. β-actin was used as a protein loading control. (**C**) Representative images showing immunofluorescent staining of BLM and γH2AX in LN229 cells irradiated with 30 J/m² UV-C light. DAPI staining of cell nuclei shown in blue. Mean Pearson correlation coefficient=0.9183 CI95(0.86-0.98). Mean Manders overlap coefficient=1.0, n=4. Scale bar: 10 μm.

## 4.2. Identification of BLM-related gene expression networks in glioma cells

To decipher the role of BLM in the human glioma cells, the CRISPR/Cas9 genome editing to knock-out BLM has been used. The efficiency of knock-out in LN18 and LN229 cells was verified by Western blotting (Fig. 7A,B) on two clones of cells after 3 consecutive passages. Ultra-deep sequencing of DNA amplicons from KO cells confirmed the presence of effective gene editing (Fig. 7C). The lack of nucleotides, marked by orange frame, resulted in a frame shift and disruption of BLM protein structure due to an inappropriate amino acids incorporation. Two clones per cell line with the complete BLM knock-out were selected for further studies.
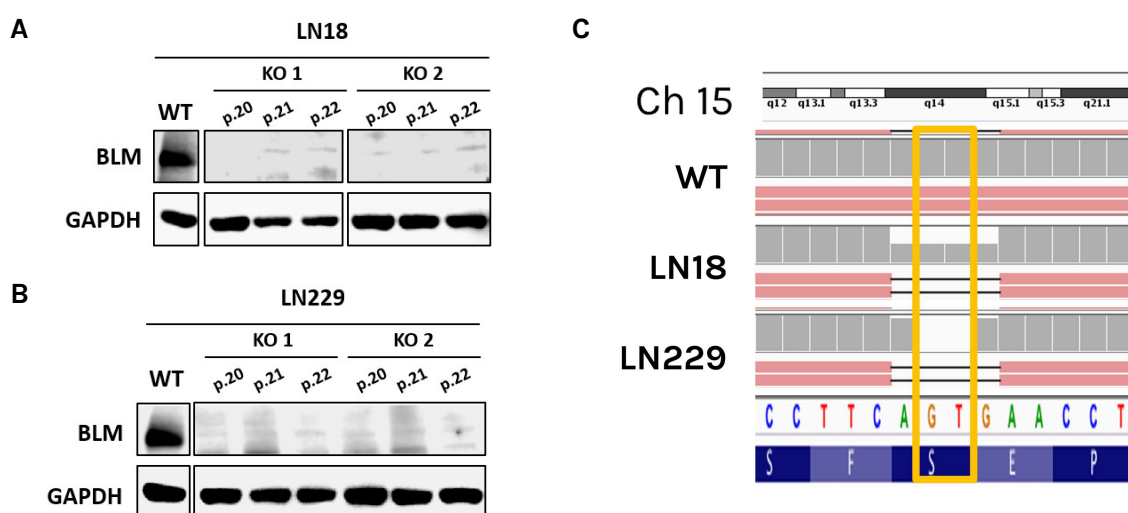


**Figure 7. Efficient _BLM_ gene knock-out in LN18 and LN229 glioma cells.**
(**A,B**) Immunoblots showing BLM levels in two independently derived LN18 (**A**) and LN229 (**B**) clones of BLM knock-out (BLM KO) cells developed using a CRISPR/Cas9 method, in three consecutive passages. Parental (wild type, WT) cells were used as a control. (**C**) Ultra-deep sequencing of WT and BLM KO LN18 and LN229 cells. Orange frame indicates effective knock-out of 2 nucleotides in chromosome 15 (Ch15) resulting in a frame shift.

Cell viability (Fig. 8A) and proliferation (Fig. 8B) of wild type (WT) and BLM KO cells was determined with MTT metabolism assay and BrdU, respectively. MTT is based on the reduction of a yellow tetrazolium salt by the mitochondrial NAD(P)H-dependent oxidoreductase enzymes in metabolically active viable cells. The viability was reduced by 20% in BLM KO LN18 cells and by 31% in BLM KO LN229 cells. The proliferation was significantly reduced only in BLM KO LN18 cells (by 21%), whereas non-significant 16% was found in BLM KO LN229 cells.

**A**



**B**
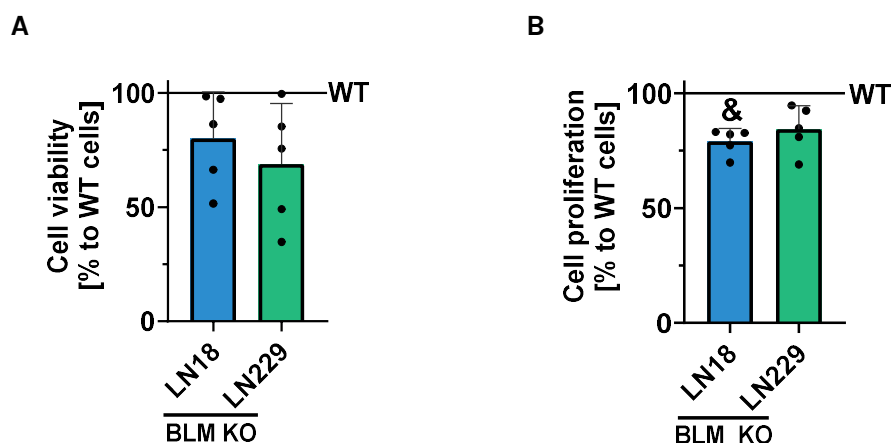


**Figure 8. Cell viability and proliferation of BLM KO LN18 and LN229 glioma cells is slightly affected.**
(**A**) Cell viability and (**B**) proliferation of BLM KO LN18 and LN229 glioma cells was measured using MTT and BrdU assay for 72 h. WT cell viability or proliferation was set to 100% and is represented by a black solid line. Statistical analysis was performed using t-test (& p<0.01), mean ± SD, n=5.

To obtain more insights into functions of BLM in glioma cells, BLM KO and WT glioma cells were subjected to RNA sequencing and the computational analysis was performed to identify differentially expressed genes (DEG). We found a large number of genes significantly up- and downregulated in the BLM KO cells in comparison to WT cells as demonstrated by a Venn diagram (Fig. 9A) and volcano plots (Fig. 9B,C). LN229 BLM KO cells underwent stronger transcriptomic changes with 2,975 genes up- and 3,050 genes downregulated. Lesser numbers of genes (1,314 genes up- and 1,534 genes downregulated) were significantly changed in LN18 BLM KO cells. Notably, 1,224 up- and 847 downregulated genes were similarly regulated in BLM KO LN18 and LN229 cells indicating a common genetic network.

We analysed common DEGs using Kyoto Encyclopedia of Genes and Genomes (KEGG) and found numerous pathways and processes modified in BLM KO cells (Fig. 9D), with many genes implicated in focal adhesion, apoptosis, MAPK- and PI3K-Akt signalling pathways. Notably, a majority of DEGs were upregulated. We presented the selected upregulated KEGG pathways (cellular senescence, focal adhesion and axon guidance) identified in a cneplot gene network analysis (Fig. 9E).

**A**



**B**

LN18: KO vs WT



**C**

LN229: KO vs WT



**D**

LN18+LN229 KO vs WT
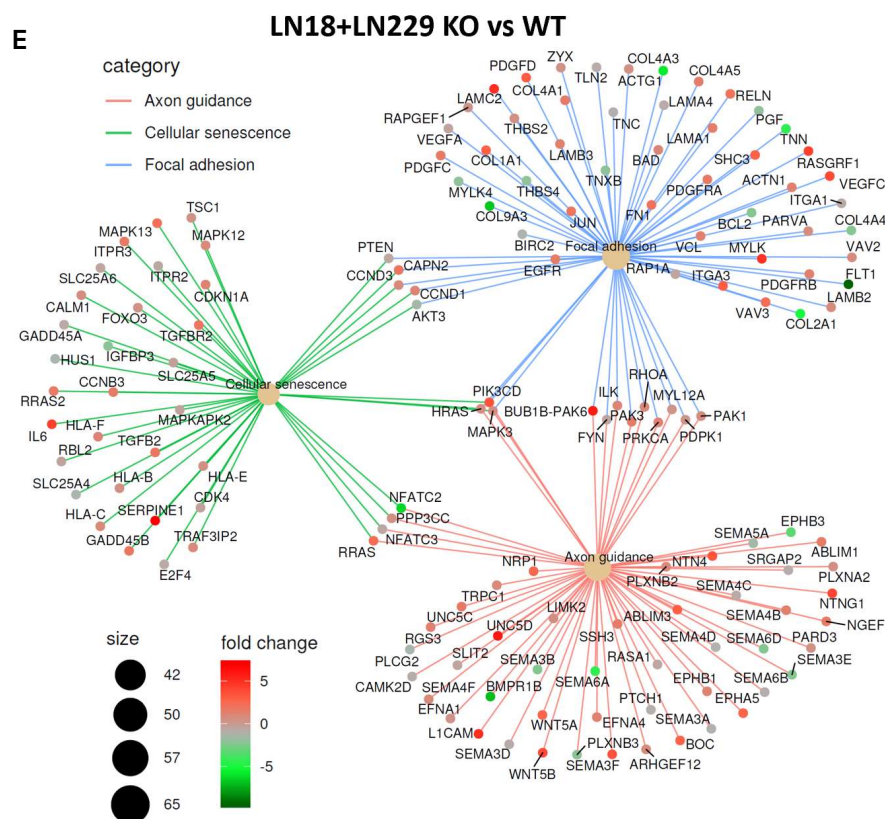
**Figure 9. Knock-down of BLM in glioma cells strongly affects gene expression in selected gene network.**
(**A**) Venn diagram representing several commonly down- and upregulated genes LN18 and LN229 BLM KO cells. Volcano plots representing down- and upregulated genes in LN18 (**B**) and LN229 (**C**) BLM KO cells versus appropriate controls (log$_2$ fold change<0 and log$_2$ fold change>0, respectively, and FDR-adjusted p<0.05). (**D**) Kyoto Encyclopedia of Genes and Genomes (KEGG) analysis of pathways commonly deregulated in LN18 and LN229 BLM KO cells when compared to WT cells. (**E**) Selected KEGG pathways are presented in a cnetplot gene network analysis. With the kind help of Bartosz Wojtaś, PhD.

## 4.3.   BLM affects response of glioma cells to chemotherapeutics

The transcriptomic analysis revealed changes of numerous pathways and processes modified in BLM KO, with many genes implicated in focal adhesion, apoptosis, MAPK- and PI3K-Akt signalling pathways that are important in regulating cell survival and tumour cell responses to chemotherapeutics. Therefore, we tested if BLM KO cells modified responses to the main anti-glioma therapeutic temozolomide (TMZ) that combined with radiotherapy after surgical resection represents the standard treatment for GBM patients (Strobel et al. 2019). We explored how BLM deficiency may affect sensitivity of human glioma cells to chemotherapeutics.

First, different concentrations of TMZ at various time points were tested, however the best response of glioma cells was noted for 72 h. A dose-response relationship was determined in BLM WT and KO, LN18 and LN229 cells exposed for TMZ at 50, 250 and 500 µM doses (Fig. 10A). In WT LN18 cells ($EC_{50}$=2,110 mM, $\eta^2$=0.01) TMZ had no effect, in contrast to BLM KO LN18 cells ($EC_{50}$=105 mM, $\eta^2$=0.71). Calculated $EC_{50}$ values (Fig. 10B) represent the vulnerability of glioma cells toward the drug and can be considered as a reliable indicator of the BLM KO impact. Moreover, the eta square ($\eta^2$) value shows directly the biological effect of the chemotherapeutics on the cells. A value closer to 1 indicates a higher effect size. More information about the $\eta^2$ and other effect size indicators is included in the Statistics subchapter in Materials and Methods.

Interestingly, LN229 cells responded differently to TMZ. WT cells were sensitive to the TMZ ($EC_{50}$=6.3 mM, $\eta^2$=0.82) and notably, a lack of BLM significantly sensitised the LN229 to the drug ($EC_{50}$=1.5 mM, $\eta^2$=0.98).

Moreover, another, Hedge's 'g' parameter was calculated, which indicated the effect size. The effect size between WT and BLM KO LN18 cells (g=0.53), and WT and BLM KO LN229 cells (g=3.5) displays more profound response of LN229 cells to the TMZ treatment.

Recent clinical trials for GBM patients attempt to increase cytotoxicity by combining TMZ with PARP-1 inhibitors (PARPi) such as olaparib (OLA) (Fulton et al. 2017; Lesueur et al. 2019). Combining PARP inhibitors with homologous recombination deficiency (exemplified by the BRCA1/2 deficiency) facilitates killing malignant cells due to the occurrence of the synthetic lethality (Farmer et al. 2005). Therefore, a sensitivity of BLM KO and WT LN18 and LN229 cells to OLA was determined for 72 h by means of MTT metabolism assay (Fig. 10C). In WT and BLM KO LN18 cells the dose-response dependency to OLA was not found ($EC_{50}$=undet, $\eta^2$=0.35; $EC_{50}$=105 µM, $\eta^2$=0.48, respectively). Nevertheless KO cells had significantly increased vulnerability to OLA when WT and KO groups were compared (g=1.6). Markedly, the WT LN229 cells did not display a dose-depended response to OLA ($EC_{50}$=1138 µM, $\eta^2$=0.09), contrary to BLM KO cells ($EC_{50}$=86 µM, $\eta^2$=0.92), with similar effect between the WT and KO groups (g=1.1) (Fig. 10D).

**B**

| cell line | | $EC_{50}$ [mM] | $\eta^2$ |
|---|---|---|---|
| LN18 | WT | 2110 | 0.01 |
| | KO | 105 | 0.71 |
| LN229 | WT | 6.3 | 0.82 |
| | KO | 1.5 | 0.98 |

**D**

| cell line | | $EC_{50}$ [µM] | $\eta^2$ |
|---|---|---|---|
| LN18 | WT | undet. | 0.35 |
| | KO | 105 | 0.48 |
| LN229 | WT | 1138 | 0.09 |
| | KO | 86 | 0.92 |
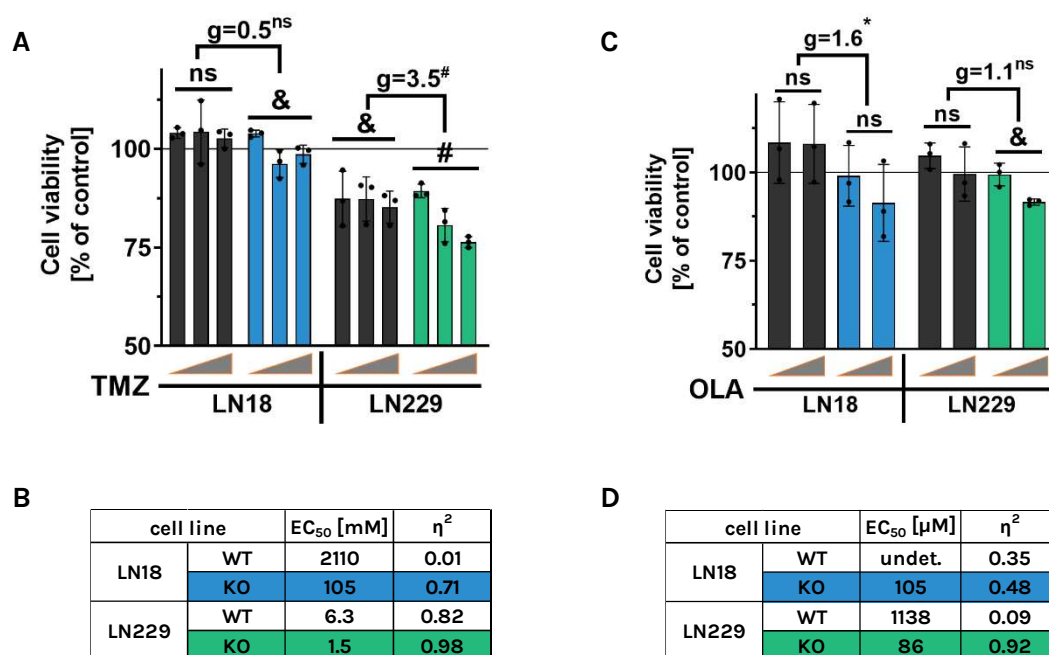
**Figure 10. The effects of chemotherapeutics on viability of WT and BLM KO glioma cells.** (**A,C**) Cell viability of WT or BLM KO LN18 and LN229 after (**A**) temozolomide (TMZ) and (**C**) olaparib (OLA) treatment for 72 h. Cell viability of control cells was set to 100% and is represented by a black solid line. (**B,D**) $EC_{50}$ values were calculated from linear regression from dose-response relationship. $\eta^2$ and Hedge's 'g' stand for effect size. Grey triangles represent the increased doses of TMZ (50, 250 and 500 µM) or OLA (1 and 5 µM). Statistical analysis was performed using linear contrast ANOVA analysis (*p<0.05, & p<0.01, # p<0.001), mean ± SD, n=3.

Interestingly, when TMZ was combined with OLA, the response of glioma cells strongly changed. Both BLM KO cells became more resistant to the treatment, when compared to WT group (Fig. 11A). Calculated $EC_{50}$ values for WT LN18 cells increased from 1.6 µM to 14.5 µM for BLM KO cells (Fig. 11B). LN229 behaved is a similar way, however $EC_{50}$ value for BLM KO cells could not be determined as cells were resistant and the dose-response relationship was no longer observed. Strikingly, the effect size between BLM WT and KO in case of LN18 cells was much higher (g=9.8) than in LN229 cells (g=4.9).



**B**

| cell line | | $EC_{50}$ [µM] | $\eta^2$ |
|---|---|---|---|
| LN18 | WT | 1.6 | 0.97 |
| | KO | 14.5 | 0.88 |
| LN229 | WT | 3.6 | 0.93 |
| | KO | undet. | 0.38 |
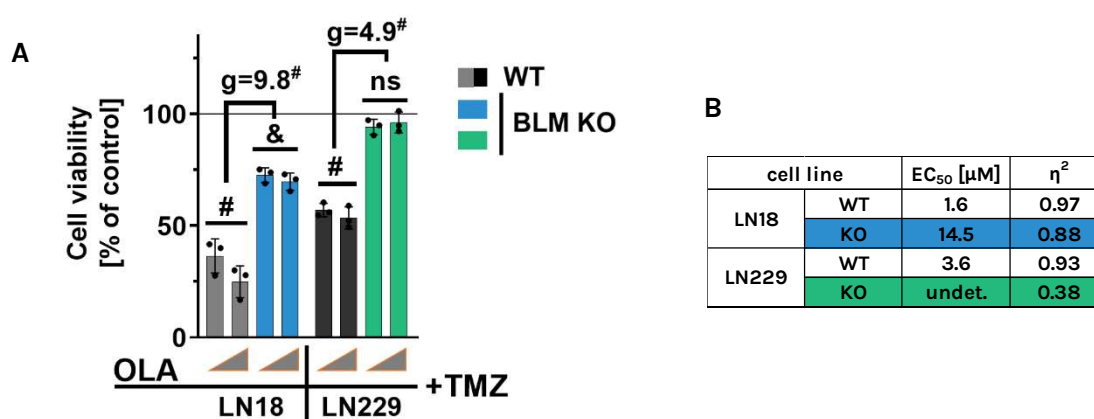
**Figure 11. Differential effects of the combined TMZ+OLA treatment on WT and BLM KO cells.** (**A**) Viability of WT or BLM KO LN18 and LN229 cells after the combined, temozolomide (TMZ) and olaparib (OLA), treatment for 72 h. Cell viability of control cells was set to 100% and is represented by a black solid line. (**B**) EC$_{50}$ values were calculated from linear regression from dose-response relationship. η$^2$ and Hedge's 'g' stand for effect size. Grey triangles represent the increased doses for OLA (1 and 5 μM) with constant 500 μM dose of TMZ. Statistical analysis was performed using linear contrast ANOVA analysis (& $p<0.01$, # $p<0.001$), mean ± SD, n=3.

The observed differences in the response of BLM WT and KO glioma cells to TMZ+OLA (T+O) were corroborated by changes in the levels of apoptosis markers: cleaved PARP [c-PARP], cleaved caspase 3 [c-casp3] and cleaved caspase 7 [c-casp7]. In LN18 cells, higher levels of cell death markers after TMZ or T+O treatment were detected in WT cells (Fig. 12A,B). In contrast, the levels of apoptotic markers were elevated in BLM KO LN229 cells after TMZ, and to a lesser extent, after the T+O treatment (Fig. 12C,D). OLA had no substantial impact on cell death in most analysed cases. Noteworthy, BLM KO LN229 cells displayed the elevated levels of c-PARP.
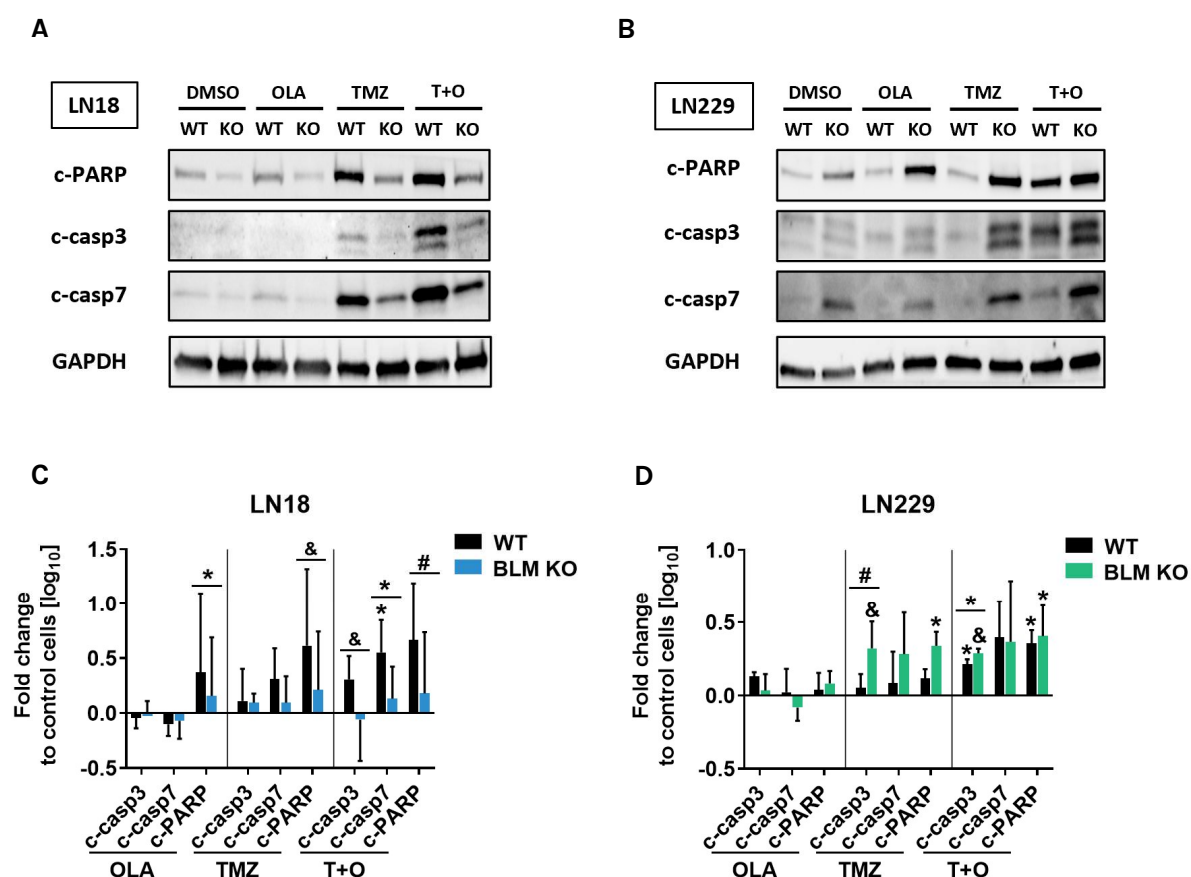
**Figure 12. Levels of apoptotic markers in various cells after specific treatments.**
Glioma cells were collected after treatments with 500 µM TMZ, 1 µM OLA or 500 µM + 1 µM T+O for 72 h. Total proteins were resolved by SDS-PAGE, transferred to nitrocellulose membranes and immunoblotted with indicated antibodies. (**A,B**) Representative immunoblots showing the apoptosis markers: cleaved PARP, cleaved caspase 3 and cleaved caspase 7 (c-PARP, c-casp3, c-casp7, respectively) in BLM KO and WT LN18 (**A**) and LN229 cells (**B**). Corresponding amounts of DMSO (a solvent for TMZ) were added to control cells. (**C,D**) Densitometry of immunoblots showing levels of the apoptotic proteins in BLM KO and WT LN18 (**C**) and LN229 (**D**) cells. GAPDH was used as a loading control. Statistical significance was determined by one-way ANOVA on logarithmic raw data followed by Dunnett's post hoc test in comparison to control cells (characters above the bars) or between the BLM KO and WT groups (characters above the lines). $*p<0.05$, & $p<0.01$, # $p<0.001$, n=3, ± SD.

To decipher, whether the observed resistance is strictly related to PARP-1 inhibitors, BLM KO and WT LN18 cells were treated with TMZ in a combination with either PARP-1 (Fig. 13A-C) or non-PARP-1 inhibitors (Fig. 13D-E). Cell viability was measured and $EC_{50}$ values were calculated. The resistance of BLM KO LN18 cells to the combined treatments was observed when cells were exposed to the combination of TMZ with other PARP-1 inhibitors: iniparib (INI, Fig. 13A), 3-aminobenzamide (3-ABA, Fig. 13B) and rucaparib (RUCA, Fig. 13C). Most cells in the treated groups responded to the drugs in a dose-response manner (designated by significance above the lines), especially in cells treated with the drug combination. In each case, the $EC_{50}$ value was higher in BLM KO group in comparison to WT group: $EC_{50}$ higher: 7.8 x for INI, 61.4 x for 3-ABA, and 6.5 x for RUCA. The effect size (g) between BLM KO and WT groups treated with PARPi and TMZ were calculated. Interestingly, the highest effect exhibited TMZ+RUCA with significant differences between BLM KO and WT groups in the response to the combined TMZ+RUCA treatment. Notably, the response of BLM KO and WT LN18 cells to PARPi alone was at similar levels. The viability of BLM KO LN18 and WT cells was comparable when TMZ was combined with non-PARPi: thioguanine (TG, Fig. 13D), etoposide (ETO, Fig. 13E) and doxorubicin (DOX, Fig. 13F). The ratio of calculated $EC_{50}$ values for BLM KO to WT cells were close to 1 (1.4 for 6-TG, 1.5 for ETO and 0.96 for DOX) indicating negligible differences in responses to the treatments. In contrast to PARPi, the effect size between BLM KO ant WT cells treated with non-PARPi+TMZ were much lower (g=0.09 for 6-TG and g=0.45 for ETO) with the exception of DOX (g=4.53). These results demonstrate that BLM deficiency

affects responses of glioma cells towards the clinically used chemotherapeutics targeting PARP-1 dependent pathways.
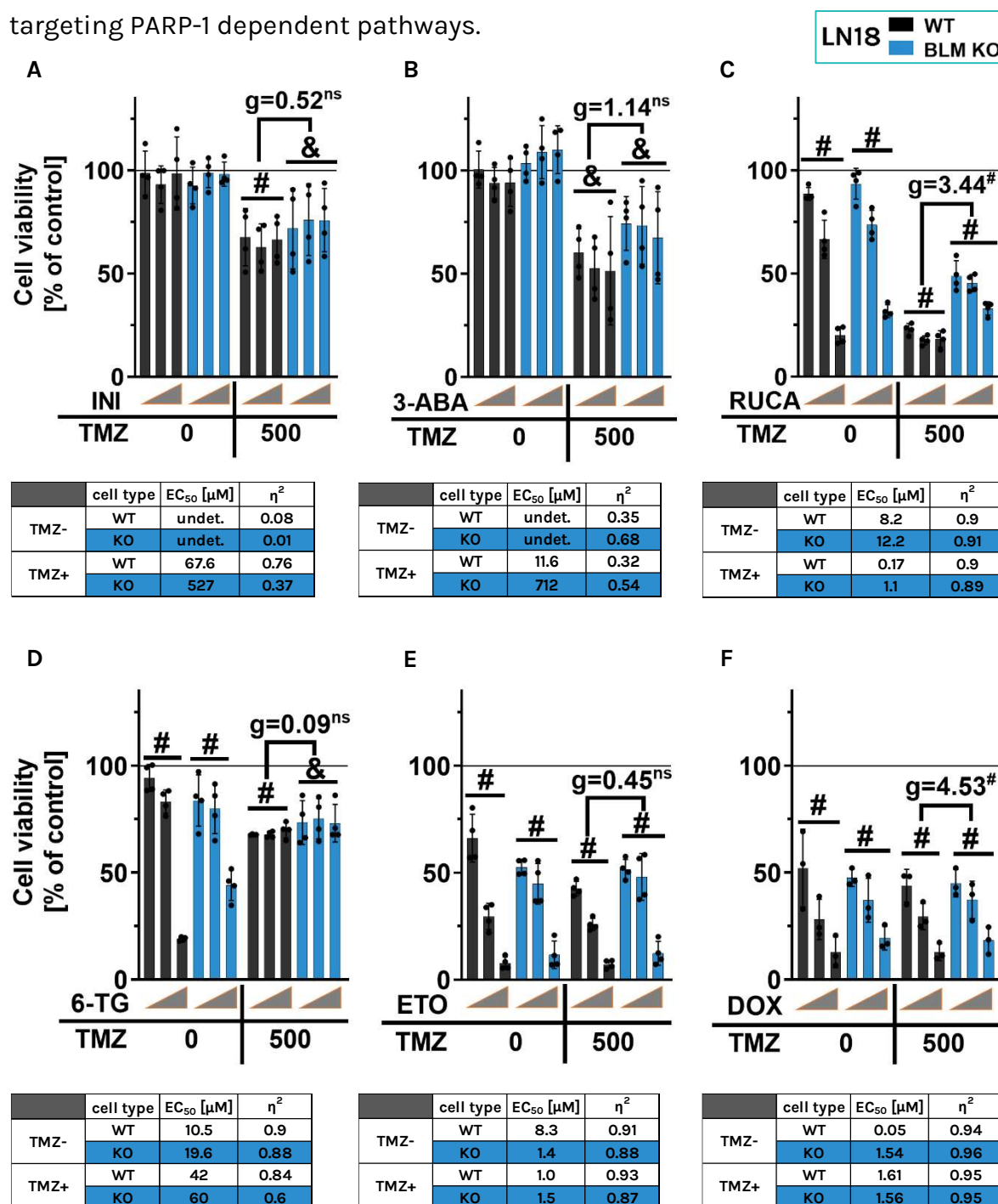


**Figure 13. Reduced vulnerability of BLM KO cells to the combined treatment is restricted specifically to TMZ with PARP inhibitors.**

Cell viability of WT or BLM KO LN18 cells after combined, temozolomide (TMZ) with (**A-C**) PARP1 inhibitors: (**A**) iniparib (INI), (**B**) 3-aminobenzamide (3-ABA) and (**C**) rucaparib (RUCA), as well as with (**D-F**) non-PARP-1 inhibitors: (**D**) 6-thioguanine (6-TG), (**E**) etoposide (ETO) and (**F**) doxorubicin (DOX), treatments. Cell viability of control cells was set to 100% and is represented by a black solid line. EC$_{50}$ values were calculated from linear regression from dose-response relationship. $\eta^2$ and Hedge's 'g' stand for effect size. Grey triangles represent increasing doses of compounds: (**A-E**) 1, 5 and 25 µM, and (**F**) 0.01, 0.2 and 1 µM, with constant 500 µM dose of TMZ. Statistical analysis was performed using linear contrast ANOVA analysis (*p<0.05, & p<0.01, # p<0.001), mean ± SD, n=4 (**A-E**) or n=3 (**F**).

Next, the intercellular changes after single and combined, TMZ and OLA, treatments of WT and BLM KO LN18 (Fig. 14A) and LN229 (Fig. 14B) cells were determined using the flow cytometry approach. The parameter of cell granularity reflects ongoing changes in the cell, measured the density of protein and organelles (like lysosomes, mitochondria) in the cytoplasm. The BLM KO displayed effect on untreated cells, increasing approximately 10x fraction of high granular cells (CTRL). For LN18 cells the single treatments of TMZ and OLA did not change the percentage of high granular cells in comparison to control, whereas for LN229 cells the OLA treatment increased 2x the number of cells with granularity. For WT cells in both groups the aforementioned treatment did not display differences. Notably, T+O treatment evoked the biggest changes in cell granularity for WT and BLM KO groups. Notably, the lack of BLM in LN229 cells increased the percentage of high-granular cells for 24% (Fig. 14B), whereas for LN18 cells the effect was not seen (Fig. 14A).
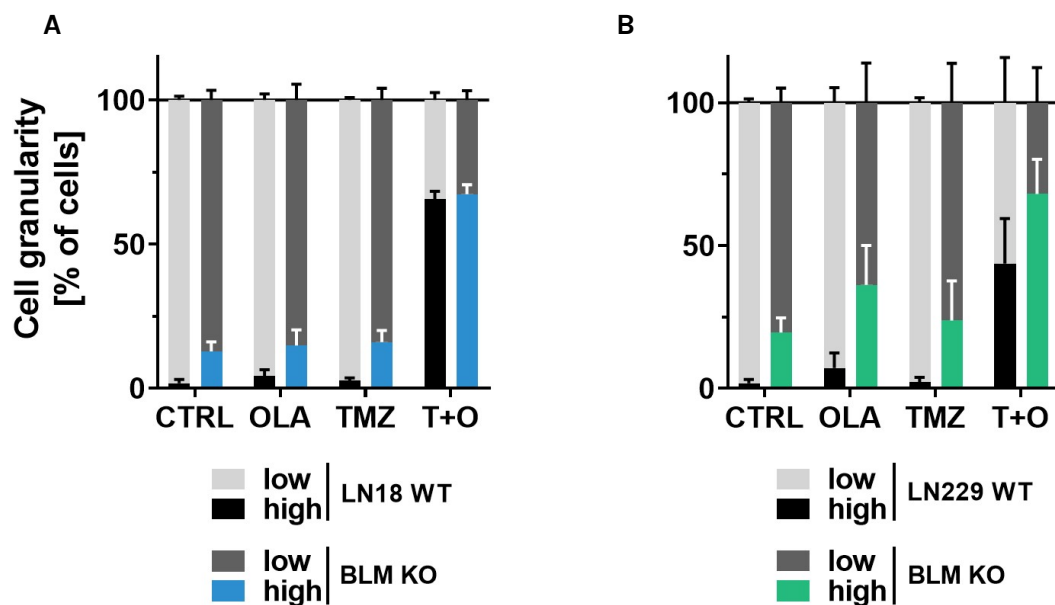


**Figure 14. Intercellular changes in WT and BLM KO glioma treated cells.**
(**A,B**) Percentages of high- and low-granular (**A**) LN18 (**B**) LN229 glioma cells after various treatments for 72h: 1 µM olaparib (OLA), 500 µM TMZ, 500 µM TMZ + 1 µM OLA (T+O). Cells were stained with propidium iodide and subjected to flow cytometry analysis, n=3, ≥10,000 events/sample.

### 4.4. The combined temozolomide and olaparib treatment has a strong impact on gene expression patterns in BLM deficient cells

To better understand the potential mechanisms of drug resistance in BLM KO glioma cells, we analysed transcriptomic changes undergoing in these cells after treatment with the T+O combination. We identified a set of common genes that were upregulated (431) and downregulated (315) in the drug-treated BLM KO glioma cells (Fig. 15A). KEGG analysis of DEGs in T+O-treated glioma cells showed many dysregulated functional pathways, when compared to untreated BLM KO glioma cells (Fig. 15B). The selected KEGG pathways detected in a cneplot gene network analysis are shown (Fig. 15C). Heatmaps for genes implicated in the cell cycle, cellular senescence and homologous recombination (Fig. 15D) pathways are demonstrated. Many genes from those pathways were upregulated in T+O-treated BLM KO cells, which indicates that the treatment stimulates processes related to the cell cycle regulation, DNA repair and senescence.

D
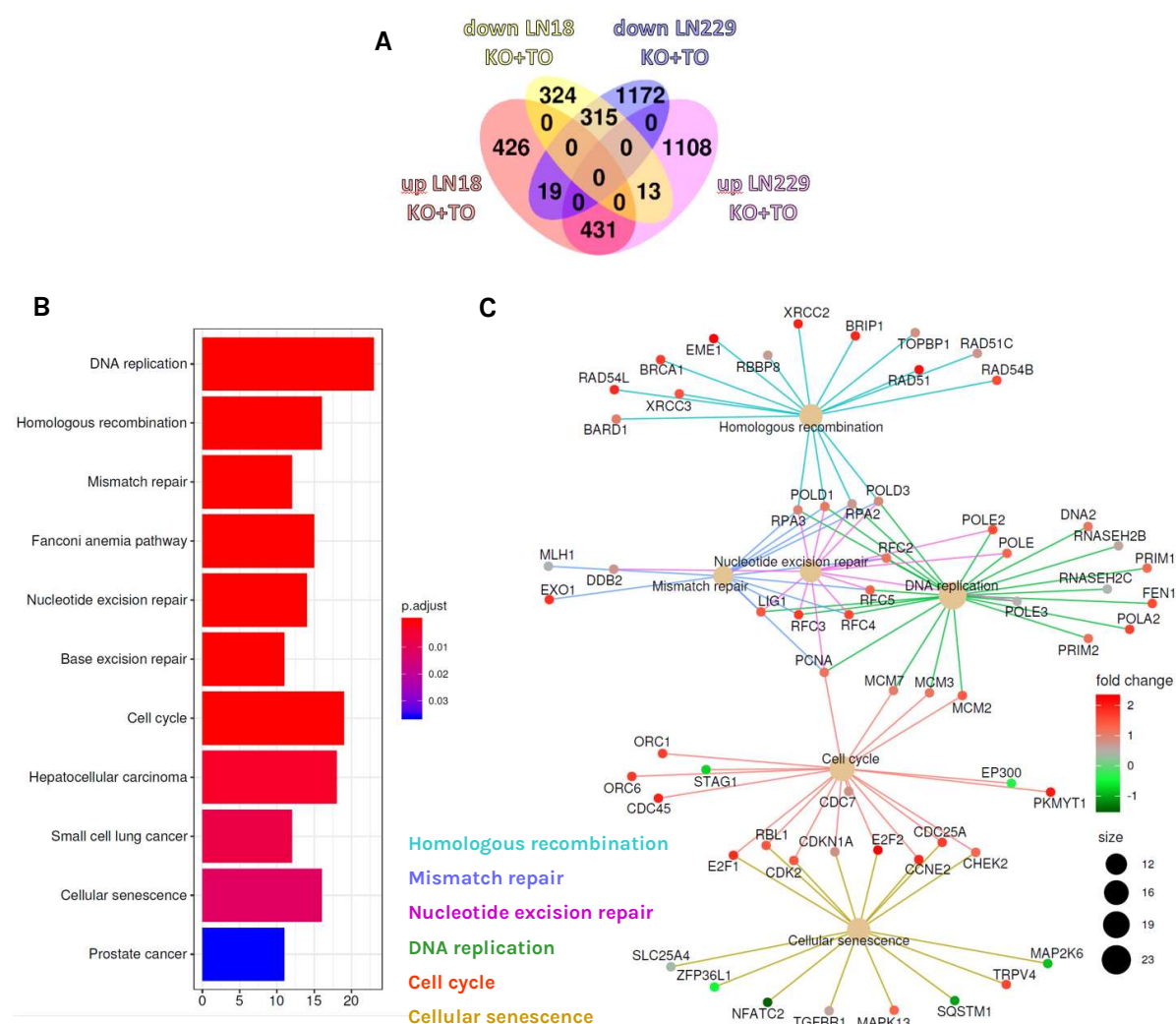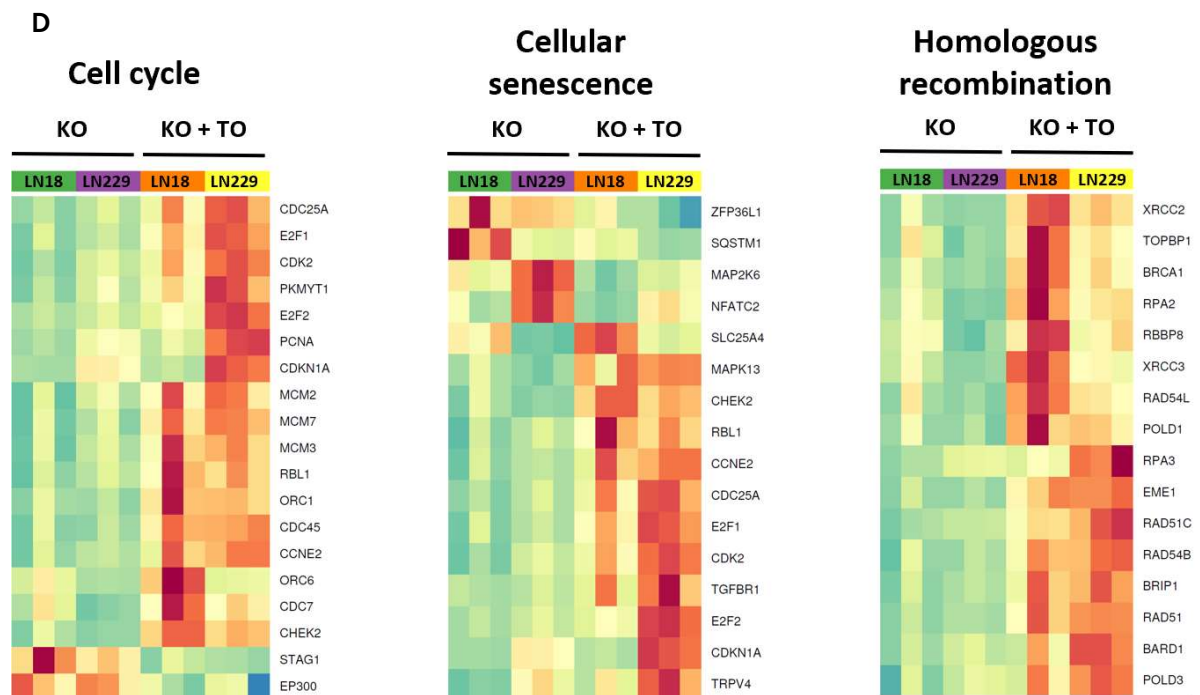


**Figure 15. Differentially expressed genes and pathways affected in T+O treated WT and BLM KO cells**.

(**A**) Venn diagram showing several significantly (FDR-corrected p<0.05) down- and upregulated genes in LN18 and LN229 BLM KO cells after the T+O treatment when compared to the control cells. (**B**) KEGG analysis of differentially expressed genes (FDR corrected p<0.05) displays commonly deregulated pathways in T+O-treated LN18 and LN229 BLM KO cells when compared to controls. (**C**) Predominantly affected KEGG pathways were revealed by a cnetplot gene network analysis. (**D**) Heatmaps showing selected, commonly deregulated KEGG pathways implicated in the Cell cycle, Cellular senescence and Homologous recombination represented as Zscore heatmaps. With the kind help of Bartosz Wojtaś, PhD.

## 4.5. BLM deficiency alters the cell cycle in untreated glioma cells or treated with T+O

The effects of chemotherapeutics on the cell cycle progression in WT and BLM deficient glioma cells were examined. Under basal conditions a large fraction of BLM KO LN18 cells was blocked in the G2/M phase (38%) in contrast to 5% of WT LN18 cells (Fig. 16A,B). This effect was not observed in BLM KO LN229 cells (Fig. 16C,D). The combined T+O treatment caused the cycle arrest in the G2/M phase in LN18 and LN229 cells (Fig. 16A-D) but in LN18 cells there were a striking differences between WT and BLM KO cells, while LN229 cells reacted similarly well to the combined treatment (Fig. 16C). In BLM KO LN18 cells TMZ or OLA alone did not induce the cell cycle arrest, however the combined treatment T+O resulted in significant polyploidisation in these cells (Fig. 16B).

Notably, BLM KO and WT LN229 cells responded well to the treatment with the G2/M arrest and there was not significant induction of polyploid cells (Fig. 16D).
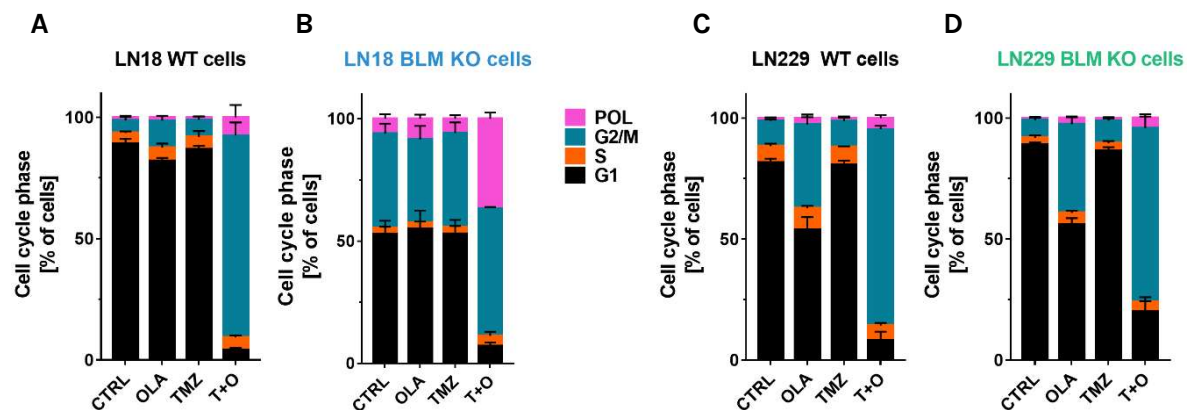


**Figure 16. Distinct responses of BLM KO LN18 glioma cells to the combined T+O treatment.** (**A-D**) Percentages of cells in the cell cycle phases and polyploidy in (**A**) LN18 WT, (**B**) LN18 BLM KO, (**C**) LN229 WT and (**D**) LN229 BLM KO glioma cells after various treatments for 72h: 1 µM olaparib (OLA), 500 µM TMZ, 500 µM TMZ + 1 µM OLA (T+O). Cells were stained with propidium iodide and subjected to flow cytometry analysis, n=3, ≥10,000 events/sample, mean ± SD.

### 4.6. The effects of restoring p53 activity in LN18 glioma cells

LN18 and LN229 cells differ in the TP53 activity, despite carrying the mutations in the *TP53* gene, the protein active in LN229 cells (Ellert-Miklaszewska et al. 2021). To find out if the drug-induced polyploidy is linked to the induction of TP53 activity after the T+O treatment, LN18 BLM KO cells were transfected with the plasmids carrying a functional *TP53* (pP53) or a control plasmid (pcDNA). Cells were co-transfected with a plasmid coding for enhanced green fluorescence protein EGFP (pEGFP) to study only transfected cells. The cells were subjected to the T+O treatment and analysed by flow cytometry (Fig. 17A-C) BLM KO LN18 cells transfected with pP53 exhibited significant reduction in the polyploidy after T+O (Fig. 17D,E). Quantification of the cell cycle distribution revealed the significant increase of the G2/M cells (Fig. 17D) and decrease of polyploid cells (Fig. 17E) after the T+O treatment, with the odds ratio (OR)=1.49.
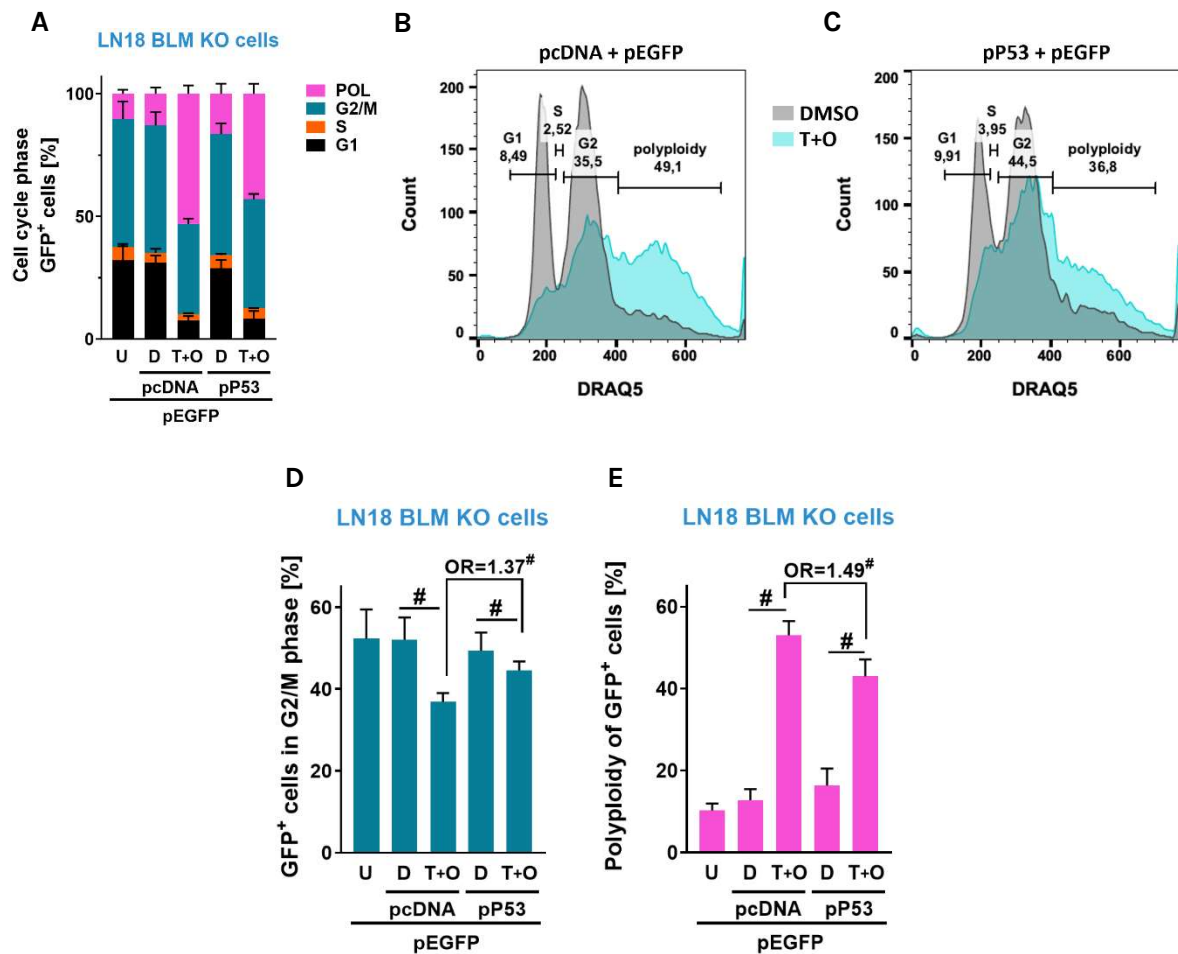
**Figure 17. Restoration of active p53 partly changes the responses of transfected cells to chemotherapeutics.**

(**A**) Quantification of the cell cycle and polyploidy in LN18 BLM KO cells transfected with control (pcDNA), carrying wildtype p53 (pP53) or EGFP (pEGFP) plasmids and subjected to the T+O treatment 24 h after transfection. Cells were stained with DRAQ5 dye and analysed using flow cytometry, n=5, ≥10,000 GFP+ events/sample, mean ± SD. The pEGFP expressing cells (U) served as controls. The representative histograms of GFP-expressing LN18 BLM KO cells transfected with (**B**) pP53 or (**C**) pcDNA and treated with T+O, stained with DRAQ5 and analysed by flow cytometry. Numbers represent percentages of cells in each phase. Quantification of (**D**) G2/M and (**E**) polyploidy in LN18 BLM KO cells transfected with a given plasmid and treated with T+O. Statistical analysis was performed using chi-square test comparing each condition versus the controls (# p<0.001) or between pcDNA and p53, analysing T+O groups (# p<0.001), n=5, ≥10,000 GFP+ events/sample, mean ± SD. OR stands for odds ratio. OR=1.37 CI95(1.33;1.40), OR=1.49 CI95(1.46;1.53).

To further confirm these results – centrosomes - the major microtubule organising centre of animal cells (Goundiam and Basto 2021) were visualised with γ-tubulin immunostaining in T+O treated BLM KO cells (Fig. 18A). Quantification of γ-tubulin signals confirmed the cell cycle changes (Fig. 18B). The treatment induced the appearance of polyploid cells (4 γ-tubulin foci or more) with single or multiple nuclei. Altogether, BLM knock-out in TP53-deficient LN18 glioma cells changes cell responses to the combined TMZ and OLA treatment and results in polyploidy of glioma cells.
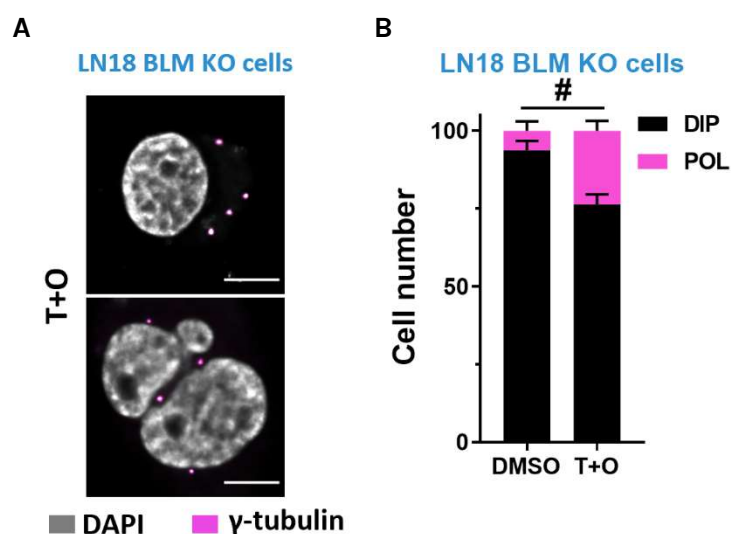


**Figure 18. Increased appearance of polyploid cells in BLM KO cells after the T+O treatment.** (**A**) Representative staining for γ-tubulin (a centrosome marker) in LN18 BLM KO cell after the combined T+O treatment. The pink dots depict the γ-tubulin foci in a single cell. Nuclei were visualised using DAPI staining. Scale bars: 10 µm. (**B**) Quantification of γ-tubulin foci in nuclei of LN18 BLM KO cells after T+O. Cells with 2 foci were considered as diploid (DIP), and with 4 or more, as polyploid (POL). Statistical analysis was performed using chi-square test (# $p<0.001$), n=3, 100 cells, mean ± SD.

### 4.7.    T+O treatment evokes cellular senescence in BLM KO LN229 cells

Striking changes in morphology of drug-treated BLM WT and KO cells were noted. Light microscopy showed that glioma cells exposed to T+O undergo morphological changes visible as increased cell size and flattened cell body. A number of cells with the oversized nuclei increased in BLM deficient glioma cells after the T+O treatment (Fig. 19A,B). F-actin staining visualised the cellular cytoskeleton and showed bigger cellular bodies in drug-treated cells in comparison to control groups (Fig. 20A,B). Interestingly, the fragmented nuclei

(Fig. 19A, yellow arrows), which indicate an onset of apoptosis, were found only in LN18 WT cells.
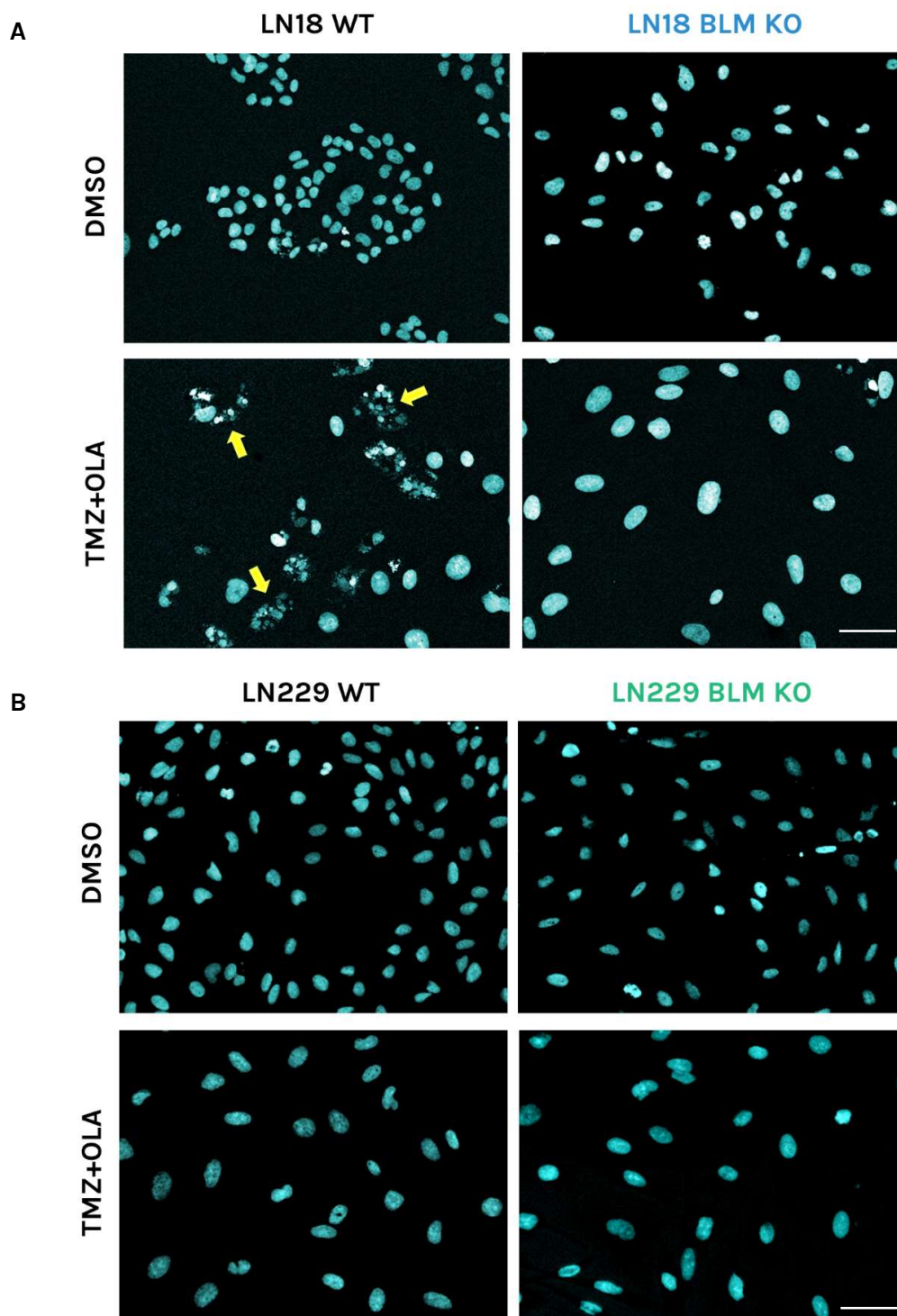


**Figure 19. Differences in apoptotic DNA fragmentation in T+O treated WT and BLM KO cells.** (**A,B**) Representative images of nuclei of BLM KO and WT (**A**) LN18 and (**B**) LN229 cells treated with 500 μM TMZ and 1 μM OLA (TMZ+OLA) for 48 h; DMSO served as a control. Yellow arrows indicate cells with apoptotic, fragmented nuclei. Nuclei were visualised using DAPI staining. Scale bars: 100 μm.

Moreover, in the T+O-treated BLM WT and KO LN18 cells, the stress fibres, indicated by orange arrows, were observed (Fig. 20A). The fibres were present as well in the untreated BLM KO cells. To lesser extent, the fibres were seen in LN229 cells (Fig. 20B).
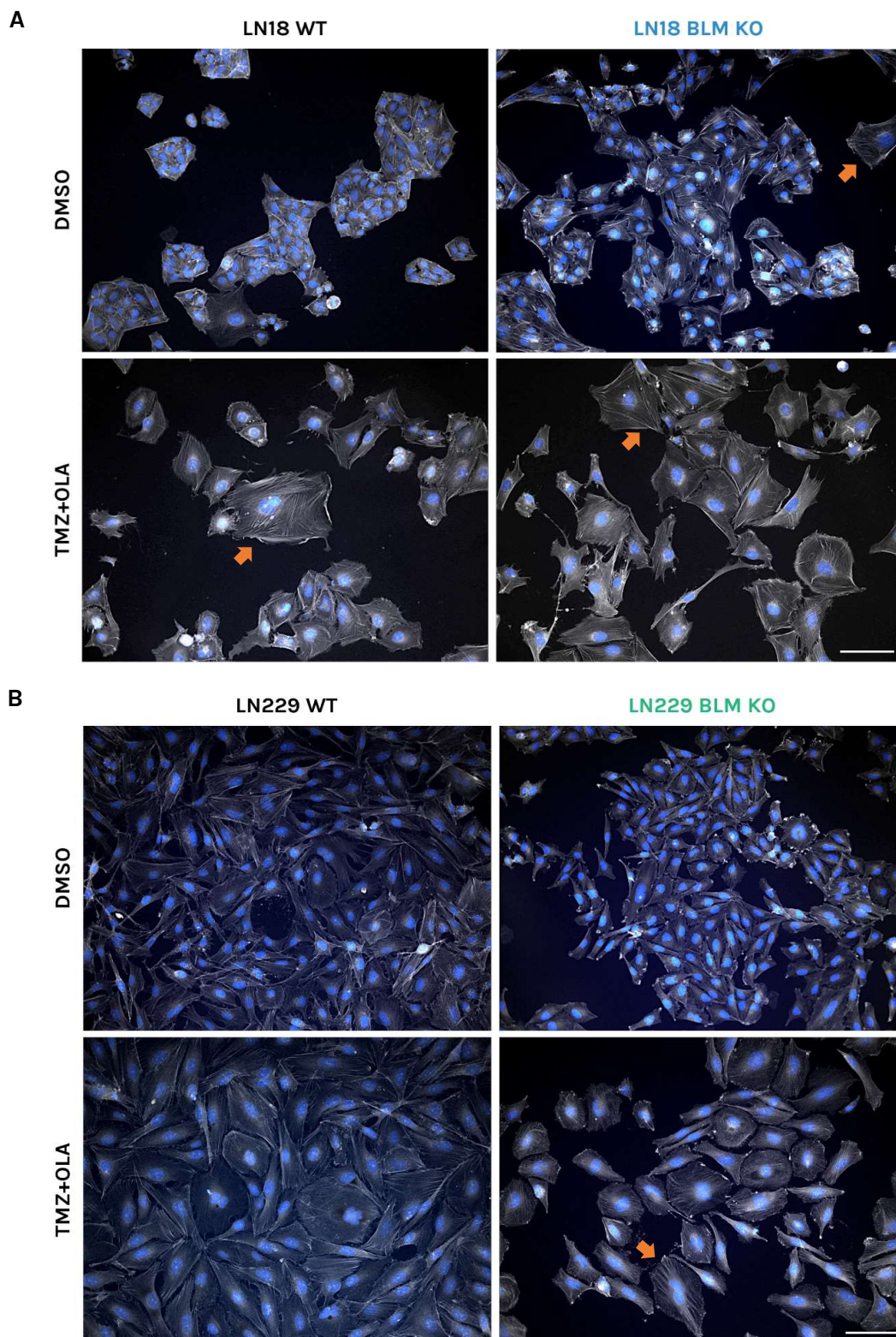
> **Figure 20. Visualisation of stress fibres in T+O treated glioma cells reveals differences in cell morphology.**
> (**A,B**) Representative images of F-actin staining of BLM KO and WT (**A**) LN18 and (**B**) LN229 cells treated with 500 µM TMZ and 1 µM OLA (TMZ+OLA) for 48h; DMSO served as a control. Nuclei were visualised using DAPI staining. Orange arrows indicate stress fibres. Scale bars: 100 µm.

An enlarged size of growth arrested cells is a marker of cellular senescence (Bojko et al. 2019), thus activity of the β-galactosidase (β-gal), a lysosomal enzyme upregulated in senescent cells, was measured in glioma cells after the T+O treatment. While in T+O treated WT and BLM KO LN18 cells rare β-gal positive cells were detected (Fig. 21A), a number of such cells appeared amongst BLM KO LN229 cells (Fig. 21A). Quantification of β-gal positive cells showed that several β-gal positive cells increased after the treatment, but there was no significant difference between WT and BLM KO LN18 cells (OR=2.1) (Fig. 21B). Markedly, there were fewer β-gal$^+$ cells in treated BLM KO cells. In contrast, a number of β-gal$^+$ cells significantly increased among T+O treated WT LN229 cells, in particular in BLM KO cells (OR=2.9) (Fig. 21B). Cell granularity is another marker of cellular senescence that can be determined using flow cytometry. The T+O treatment increased cellular granularity in LN18 cells independently of the BLM status (OR=1.1) (Fig. 21C). However, a percentage of highly granular LN229 cells was significantly higher in BLM KO cells (OR=3.3) (Fig. 21C).

These results show that the T+O treatment induces the cellular senescence mostly in BLM KO L229 cells and to a lesser extent in BLM KO LN18 cells.
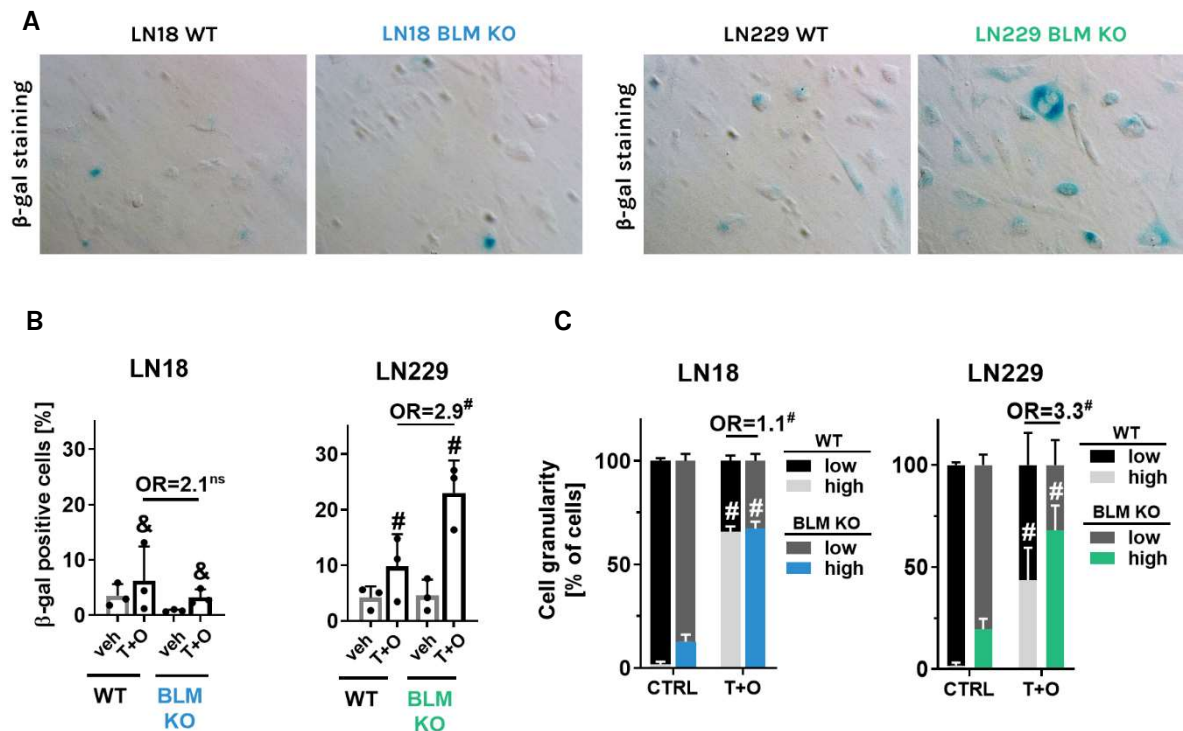
**Figure 21. The appearance of senescent cells in T+O treated BLM KO LN229 cells.**
(**A**) Representative images of β-galactosidase (β-gal) enzyme staining of BLM KO and WT LN18 and LN229 cells after T+O. Blue colour indicates cells with the increased β-gal activity. (**B**) Quantification of β-gal positive cells amongst T+O-treated BLM KO and WT LN18 and LN229 cells. Statistical analysis was performed using chi-square test and compared treated to control cells (DMSO) (above the bars, & p<0.01, # p<0.001) or between WT and BLM KO cells (above the line, # p<0.001), n=3 in duplicates, mean ± SD. OR stands for odds ratio. OR=2.1 CI95(1.1; 3.9), OR=2.9 CI95(2.0;4.2). (**C**) Cell granularity of T+O-treated BLM KO and WT LN18 and LN229 cells determined by flow cytometry. Statistical analysis was performed using chi-square test comparing treated to control cells (CTRL) (above the bars, # p<0.001) or the WT versus BLM KO cells (above the lines, # p<0.001), n=3, ≥10,000 events/sample, ± SD. OR stands for odds ratio. OR=1.1 CI95(1.0;1.1), OR=3.3 CI95(3.2;3.4).

RNAseq data were analysed with a focus on senescence-related genes. In line with the presented findings, the expression of genes belonging coding for proteins typical for the Senescence-Associated Secretory Phenotype (SASP) was upregulated in WT and BLM KO LN229 cells in comparison to LN18 cells. The T+O treatment augmented the expression of SASP related genes in BLM KO LN229 glioma cells (Fig. 22).
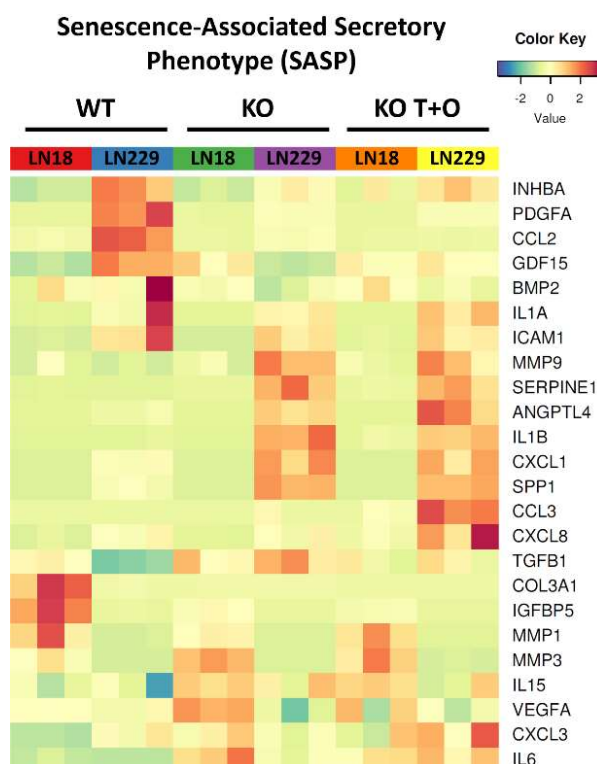
**Figure 22. Expression of SASP related genes is upregulated in BLM KO LN229 cells and the T+O treatment augments their expression.**

Heatmap showing expression of genes belonging to Senescence-Associated Secretory Phenotype (SASP) related genes in WT, KO, and T+O treated KO glioma cells, represented as Zscore. With the kind help of Bartosz Wojtaś, PhD.

## 4.8. RecQL4 is overexpressed in malignant gliomas

The RecQL4 helicase belongs to the same RecQ-helicase family as BLM and interacts with PARP-1 in DNA replication and repair processes (Bohr 2008). We studied if the observed effects of BLM deficiency on cell responses to drugs are similar after the knock-out of RecQL4.

Expression of RecQL4 in gliomas was evaluated by immunohistochemical staining of tissue microarrays containing multiple sections of gliomas along with normal brains (Fig. 23). We found that RecQL4 was present in the nucleus and in the cytoplasm of the cells. We divided the presence of RecQL4 into 3 groups: 'mostly nuclear', 'mostly cytoplasmic' and 'both'. The percentage of specimens marked as 'both' was higher in high-grade gliomas. Specimens marked as 'mostly nuclear' decreased in high-grade gliomas. In the majority of 'normal brain' specimens RecQ4 was present mainly in the cytoplasm, with the minor nuclear staining in the cells.
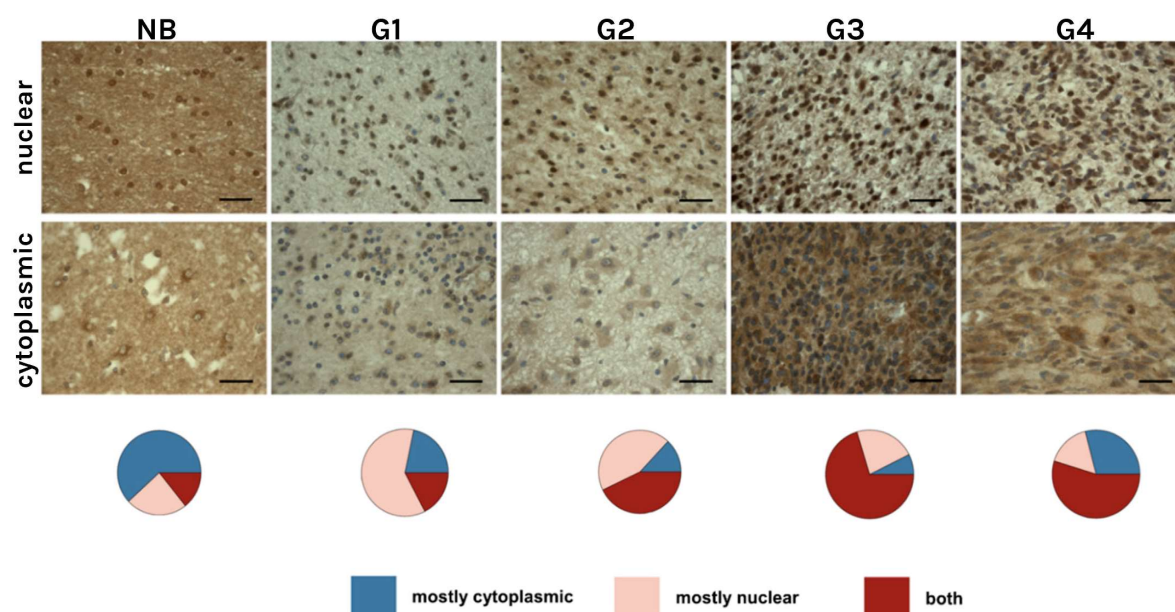
**Figure 23. Representative immunostaining showing expression of the RecQL4 protein in the glioma tissue microarrays.**

TMAs included astrocytomas (n=132), glioblastomas (n=31), oligoastrocytomas (n=7), oligodendrogliomas (n=9), ependymomas (n=11), ganglioglioma (n=1) and gliosarcoma (n=1), plus tumour adjacent and normal brain (NB) tissues (n=8). RecQL4 expression was visible as high nuclear and low cytoplasmic signal (upper panel) and low nuclear and high cytoplasmic signal (bottom panel). Quantification of RecQL4 immunoreactivity is presented in a form of pie charts. Statistical significance was determined by chi-squared test. p-values of NB p = 1.0, G1 p = 0.019, G2 p = $1.1 \times 10^{-5}$, G3 p = $6.3 \times 10^{-5}$, G4 p = 0.011. Pie charts calculated with the kind help of Jakub Mieczkowski, PhD. Scale bars: 100 μm.

## 4.9.   RecQL4 deficiency does not affect the responses of glioma cells to the combined T+O treatment

We wondered whether the observed resistance to TMZ+OLA is specific to BLM KO cells or is shared with RecQL4 KO cells. Therefore, we used LN18 and LN229 cells with RecQL4 knock-out (RQ4 KO), previously generated and characterised in the Laboratory of Molecular Neurobiology (Król et al. 2020). Cell viability of RecQL4 KO LN18 and LN229 cells (Fig. 24A) was similarly affected by the T+O treatment (mean viability≈45% in each RQ4 KO group). The comparison of treated RecQL4 KO LN18 to WT cells showed the high effect size (g=6.6). No significant changes between T+O treated WT and KO LN229 cells were noted and the effect size was low (g=0.3). Moreover, $EC_{50}$ values were calculated (Fig. 24B).

**A**



**B**

| cell line | | EC$_{50}$ [μM] | η$^2$ |
|---|---|---|---|
| LN18 | WT | 0.35 | 0.98 |
| | KO | 2.18 | 0.98 |
| LN229 | WT | 1.88 | 0.98 |
| | KO | 1.48 | 0.9 |
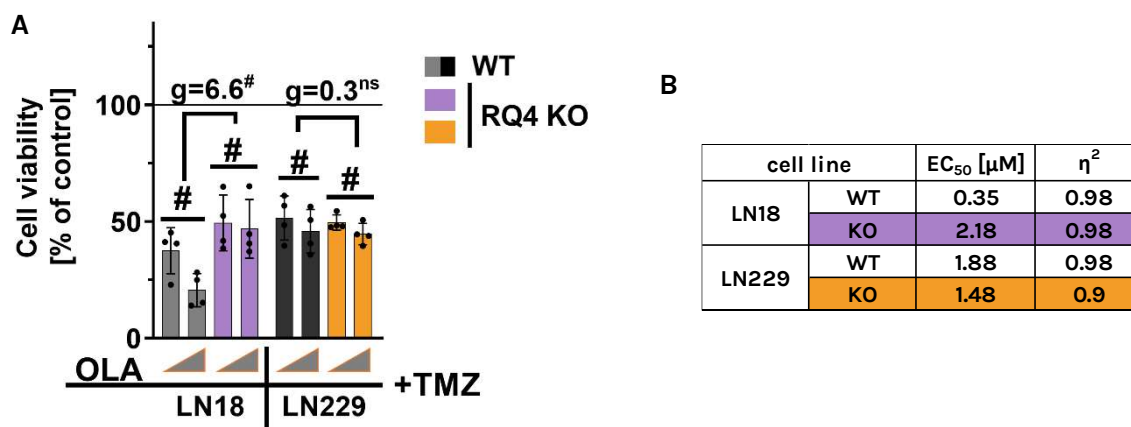
**Figure 24. RecQL4 deficiency does not affect cell responses to the combined T+O treatment.** (**A**) Cell viability of WT and two RQ4 KO clones of LN18 and LN229 cells after exposure to 500 μM TMZ and 1- or 5 μM olaparib (T+O) for 72 h was determined using a MTT metabolism test. Cell viability of control cells was set to 100% and is represented by the black solid line. (**B**) EC$_{50}$ values were calculated from linear regression from dose-response relationship. η$^2$ and Hedge's 'g' stand for effect size. Grey triangles represent increasing doses of compounds. Statistical analysis was performed using linear contrast ANOVA analysis (*p<0.05, & p<0.01, # p<0.001) n=4, mean ± SD.

The levels of cell death markers in treated cells were assessed using Western blotting. The upregulation of c-PARP, c-casp7 levels in RecQL4 KO glioma cells indicated induction of apoptosis in treated cells, independently of their TP53 status (Fig. 25A). Quantification of the densitometric analysis on immunoblots corroborated those results (Fig. 25B).

**A**



**B**
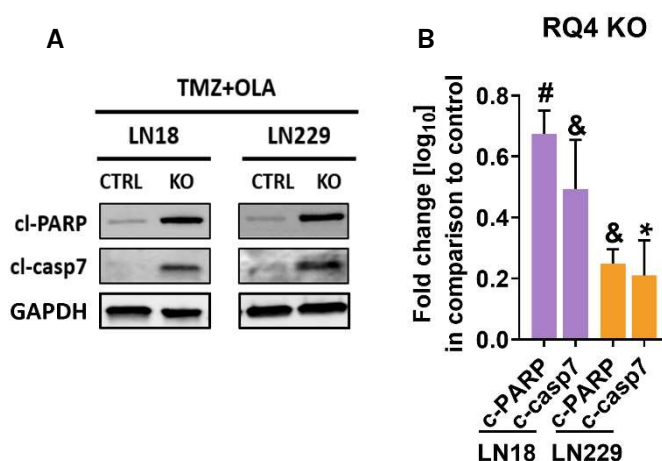
**Figure 25. RecQL4 deficiency does not affect apoptotic cell responses T+O treatment.** (**A**) Representative immunoblots showing the levels of the cleaved, apoptotic proteins (c-PARP, c-casp7) in RecQL4 KO and WT LN18 and LN229 cells after T+O. (**B**) Densitometric analysis of immunoblots. GAPDH was used as a loading control. Statistical significance was determined by one sample t-test on logarithmic raw data (*p<0.05, & p<0.01, # p<0.001), n=3, mean ± SD.

Cell cycle analyses performed by flow cytometry demonstrated the accumulation of the G2/M arrested cells following the combined treatment in tested glioma cells (Fig. 26). The percentage of the G2/M arrested cells in both treated RecQL4 WT and KO cells was similar, approximately 90%. Markedly, similar percentages of polyploid cells were detected in treated RecQL4 KO LN18 cells, and blocked in the G2/M phase after RecQL4 WT or KO cells.
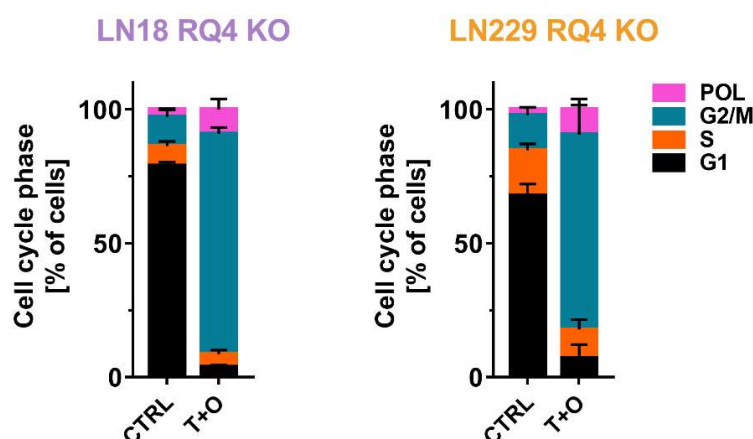


**Figure 26. Cell cycle analyses of T+O treated cells with RecQL4 deficiency.**
Percentages cells in the cell cycle phases in cultures of RecQL4 KO and WT LN18 and LN229 cells after the T+O treatment, determined using the propidium iodide staining and flow cytometry, n=3, ≥10,000 events/sample, mean ± SD.

F-actin staining revealed the increased size of LN18 and LN229 RecQL4 WT and KO treated glioma cells and more flattened cell morphology (Fig. 27). In the majority of LN18 cells the stress fibres are present, as indicated by the orange arrow, whereas in flat, enlarged LN229 cells, the ongoing DNA fragmentation is indicated by green arrows.
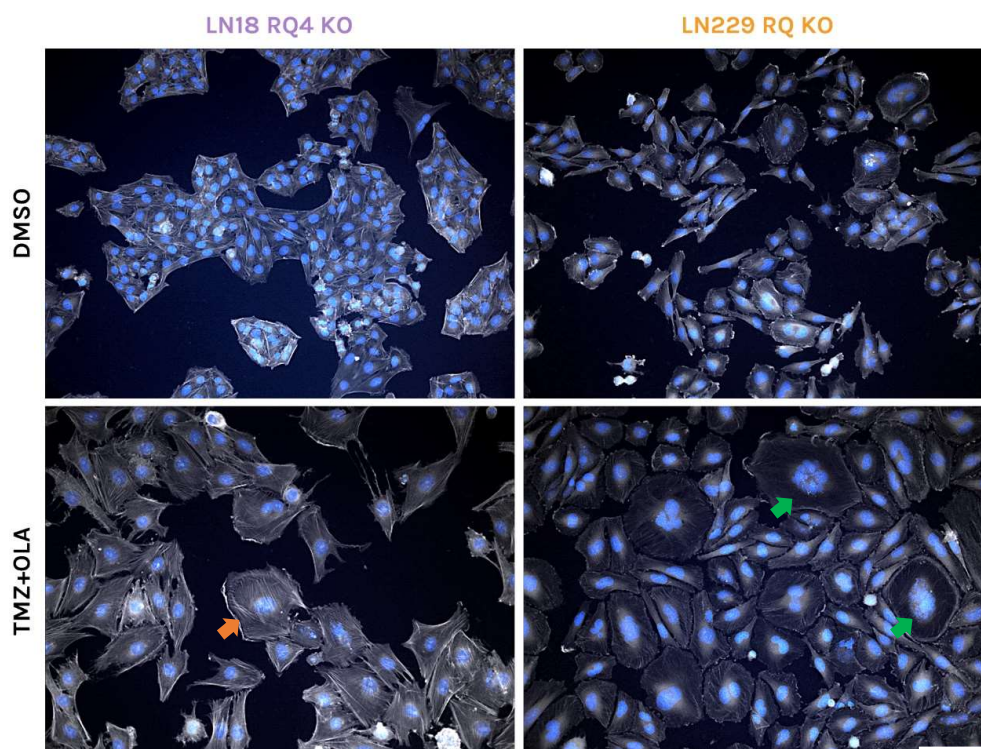
**Figure 27. Morphological changes induced in drug-treated REQCL4 deficient cell cultures.** Representative images of F-actin staining of RecQL4 KO and WT LN18 and LN229 cells exposed to 500 µM TMZ and 1 µM OLA (TMZ+OLA) for 48h; DMSO served as a control. Nuclei were visualised using DAPI staining. Orange arrow indicates stress fibres, whereas green arrows indicate fragmented nuclei. Scale bar: 100 µm.

The assessment of β-gal activity in RecQL4 KO LN18 (Fig. 28A) and LN229 cells (Fig. 28B), and counting β-gal positive cells cultures after T+O treatment (Fig. 28C,D) showed the elevated level of β-gal in most tested cells. Only in RecQL4 KO LN18 cells accumulation of β-gal positive cells was not observed (Fig. 28C) and was significantly lower in comparison to drug-treated LN18 WT cells (OR=1.8). In contrast, the RecQL4 KO LN229 cells exhibited the increased percentage of β-gal⁺ cells, however in comparison to RecQL4 WT LN229 cells, the response was not significant and calculated odds ratio was negligible (OR=1.2) (Fig. 28D). Moreover, cell granularity analysis performed by flow cytometry indicated no significant differences between T+O treated RecQL4 WT and KO cells (OR=1.1) (Fig. 28E) and more interestingly, a percentage of high-granular cells in RecQL4 KO LN229 cells was lower when compared to WT cells (OR=3.5) (Fig. 28F). These results show that a deficiency of specific helicases has a different impacts on glioma cells and their response to the T+O treatment.
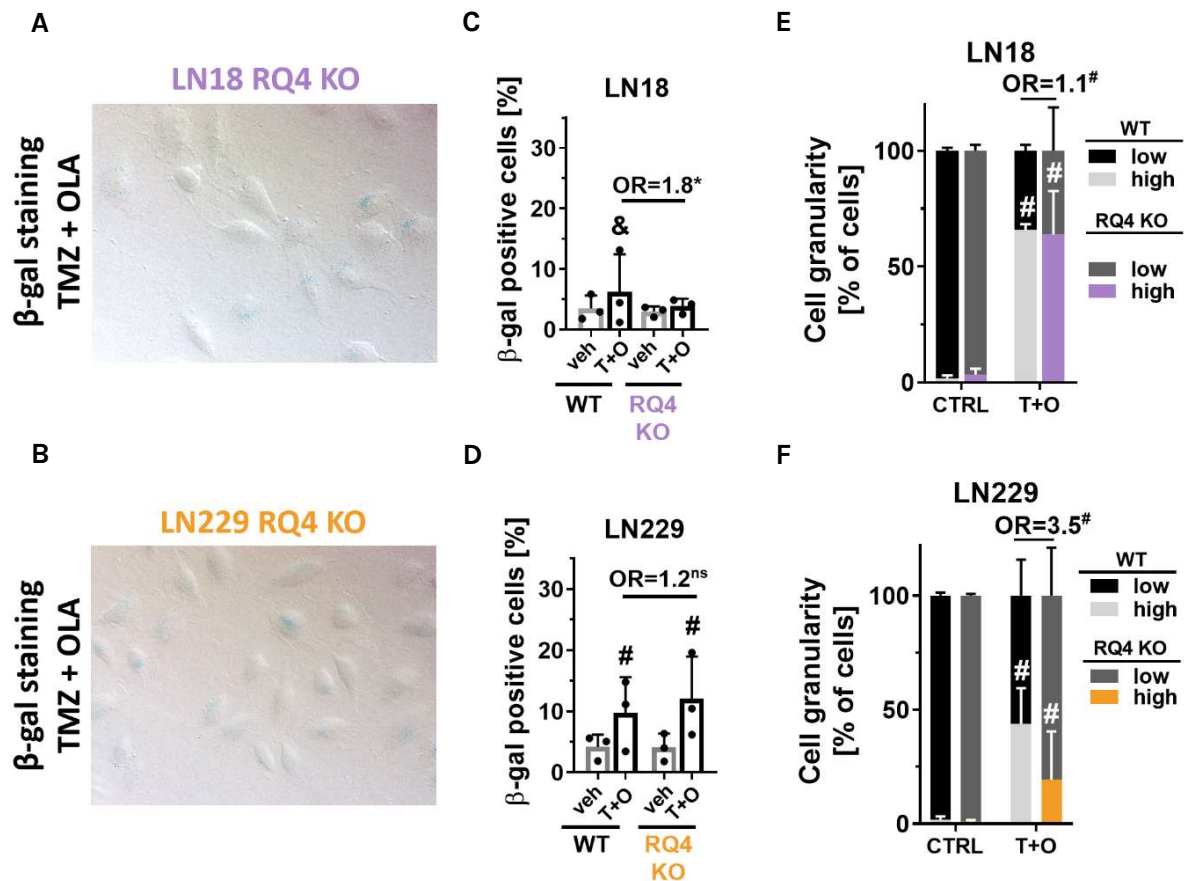
**Figure 28. RecQL4 deficiency does not affect drug induced cellular senescence in glioma cells.**

(**A,B**) Representative images of β-gal staining of RecQL4 KO LN18 (**A**) and LN229 (**B**) cells after the T+O treatment. Blue colour indicates the increased activity of β-galactosidase. (**C,D**) Quantification of β-gal positive cells amongst control and treated RecQL4 KO (**C**) LN18 and (**D**) LN229 cells. Statistical analysis was performed using a chi-squared test in comparison of treated versus control cells (above the bars, & p<0.01, # p<0.001), or between the WT and RecQL4 KO cells (above the lines, *p<0.05), n=3, in duplicates, ± SD. OR stands for odds ratio. OR=1.8 CI95(1.0;3.2), OR=1.2 CI95(0.51-1.33). (**E,F**) Cell granularity of T+O-treated BLM KO and WT (**E**) LN18 and (**F**) LN229 cells determined by flow cytometry. Statistical analysis was performed using chi-square test in comparison of treated to control cells (CTRL) (above the bars, # p<0.001) or between the WT and RecQL4 KO cells (above the lines, # p<0.001), n=3, ≥10,000 events/sample, ± SD. OR stands for odds ratio. OR=1.1 CI95(1.05;1.13), OR=3.5 CI95(3.36;3.64).

## 4.10. The effects of deficiency of BLM and RecQL4 helicases on development of *Xenopus* tadpoles

The presented results revealed differences in the roles of specific helicases from the RecQ family. We explored how specific helicase deficiency would affect organism development. Thanks to the collaboration with Prof. Matthew Guille from the European Xenopus Resource laboratory in Portsmouth, UK, the engineered animals were created using CRISPR/Cas9 technology. We assessed the effect of depletion of *blm* and *recql4* (rq4) in a *Xenopus* model.

The experiments were conducted together with Ms Gemma Bavister and Prof. Matthew Guille at the Portsmouth University. The efficacy of genome editing was determined with a T7 Endonuclease assay. Embryos injected with a specific sgRNA were assessed for mismatch repair errors with this assay. TIDE analysis confirmed that the targeting efficiency as ~30%. The preliminary data indicated some developmental abnormalities in the *blm* and *rq4*-deficient tadpoles. The effects were visualised with microCT (Fig. 29A). After injections of gRNA/Cas9 targeting both helicases, around 50% of tadpoles died in a couple of days (Fig. 29B).

Further, we analysed morphology and behaviour of surviving tadpoles. The morphological differences between un-injected and crispant embryos were identified using a stereomicroscope. The morphology of the *blm* and *rq4*-deficient tadpoles was abnormal when compared to WT tadpoles (Fig. 29C). The representative microtomography images (Fig. 29A) show the normal tadpole (WT) and the *blm* and *rq4*-deficient tadpoles with oedema (blue arrows) and reduced eye size (white arrows). Moreover, the helicase-deficient tadpoles were either unresponsive to stimuli or swam abnormally (Fig. 29D).
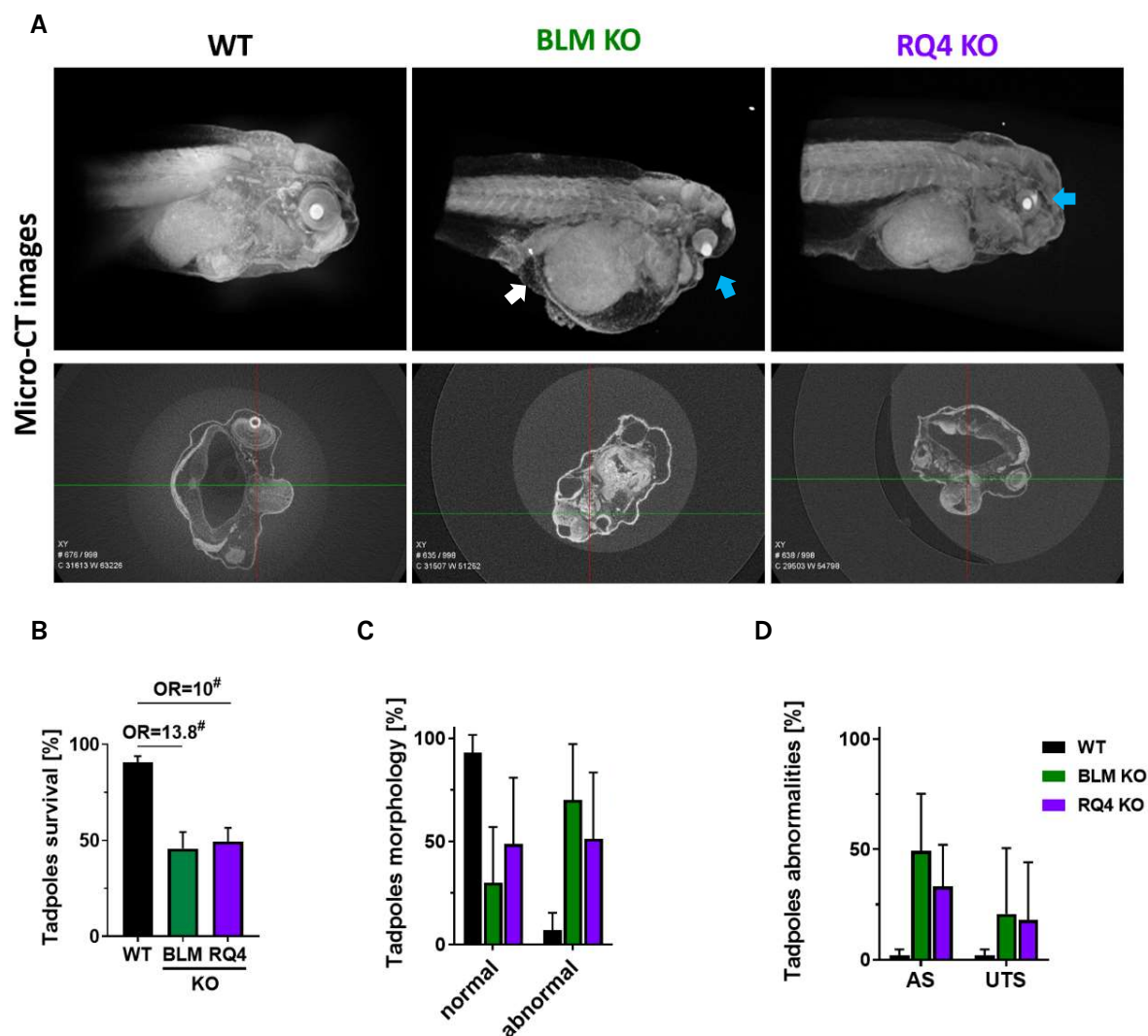
**Figure 29. The abnormalities detected in development of the *blm* and *rq4*-deficient *Xenopus* tadpoles.**

(**A**) Microtomography images of Wild type (WT) and knock-out (KO) tadpoles at a stage 44 showing developmental abnormalities in the *blm* and *rq4*-deficient tadpoles. (**B**) Total survival of tadpoles after injections of Cas9 alone (WT) and together with *blm* and *rq4* sgRNA (KO). (**C**) The percentage of tadpoles with normal and abnormal morphology 4 days after injections. (**D**) The abnormalities of tadpoles after injections. AS stands for 'abnormal swimming', and UTS for 'unresponsive to stimuli'. Statistical analysis was performed using chi-square test (# $p < 0.001$, n=4, 40 tadpoles per group). OR stands for odds ratio. OR=13.8 CI95(7;27.3), OR=10 CI95(5.3-18.8). With the kind help of Ms Gemma Bavister and Prof. Matthew Guille.

# 5. DISCUSSION

## 5.1. Elevated expression of BLM in malignant gliomas

In this study we demonstrated that mRNA and protein levels of BLM, a member of RecQ helicase family, are upregulated in malignant gliomas. Exploring of TCGA datasets shows high expression of BLM has an impact on GBM patient survival as survival of glioma patients with high *BLM* expression was shorter. RecQ helicases participate in important cellular events including replication, transcription, recombination and DNA repair cooperating with many enzymes including PARP1 or with other members of RecQ family (Croteau et al. 2014). The increased expression of BLM in fast proliferating tumour cells may be related to increased proliferation of tumour cells and the enzyme involvement in separating DNA strands during replication.

Our results are consistent with a couple of previous studies reporting augmented expression of BLM in tumours cells. Tong Ong *et al.* reported the significantly higher *BLM* expression in GMBs in comparison to lower-grade gliomas (Ong et al. 2017). Increased levels of *BLM* mRNA were found in other tumours and the high *BLM* expression inversely correlated with survival of breast cancer (Arora et al. 2015), cholangiocarcinoma (Du et al. 2021) or pancreatic adenocarcinoma patients (Li et al. 2022). Up to date, findings of increased BLM expression in different cancers support the importance of BLM in tumour progression. Zhu *et al.* had performed the meta-analysis of expression of all the RecQ helicases and assessed the prognosis based on their expression in breast cancer patients. Overexpression of *BLM* was associated with reduced distant metastasis-free survival (DMFS) in all patients, whereas high level of *RecQL4* was inversely correlated with patient overall survival, DMFS and relapse-free survival (Zhu et al. 2018). Moreover, in breast cancer patients the risk factors are often linked to oestrogen-related pathways and oestrogen (ER) has been shown to modulate mRNA levels of homologous repair genes, including *BLM*. Zach *et al.* found the impairments of double-strand breaks repair in ER-positive breast cancer cells deprived of oestrogens and hypersensitisation to DNA damage in those cells (Zach et al. 2022). An integrative analysis of therapy resistance and transcriptomic profiling of glioblastoma cells performed by Schnöller *et al.* revealed that the expression of *BLM* positively correlates with radio-resistance either applied as a single shot or fractionated (Schnöller et al. 2022).

Furthermore, *BLM* was identified as a gene involved in radio-resistance and self-renewal of neural stem/progenitor cells (NSPC). BLM takes part in DNA translesion synthesis, a process of bypassing of unrepaired DNA lesions during DNA replication, especially needed for glioma stem cells to maintain malignancy (Ong et al. 2017). The presented studies highlighted a multifunctional role of BLM in many types of cancers, connecting overexpression of BLM with unfavourable outcomes. For this reason, BLM might be considered as a potential target in cancer.

The levels of BLM mRNA and protein were elevated in numerous glioma cell cultures in comparison with non-transformed astrocytes. Markedly, GBM patient-derived WG4 cells showed the highest level of *BLM* mRNAs, which did not reflect at the protein level when compared to other glioma cells. BLM protein levels were higher in established glioma cells in comparison to patients-derived primary cell cultures (WG4 and WG9). The discrepancies between mRNA and protein levels occur frequently (Ochocka et al. 2023). Genome-wide correlation between protein level and corresponding mRNA expression shows 40% overlap (Koussounadis et al. 2015), thus such discrepancies are understandable.

BLM expression was particularly high in established LN18, LN229 and T98 glioma cells, characterised by high proliferation rate. The results are consistent with the BLM involvement in cell replication and proliferation (Kaneko et al. 1997). While patient-derived cultures better reflect the tumour heterogeneity, some of them grow slowly and during the multiple subculture steps, the clonal selection or genetic drift can appear (Sottoriva et al. 2013; Ciechomska and Wojnicki et al. 2023). Nevertheless, the high BLM expression in numerous glioma cell cultures including primary cultures as well as BLM abundance in malignant gliomas confirm that upregulation of its expression is a part of tumorigenesis.

## 5.2. BLM and RecQL4 (mis)localisation in tumours

Evaluation of BLM expression and localisation of the protein in human glioma tissue microarrays brought interesting results. In malignant gliomas (WHO grades 3 and 4) BLM was found mostly in the cytoplasm while in normal brain and low-grade gliomas BLM was located primarily in the nuclei. As know functions of BLM point to its role in events occurring in the nucleus, such altered localisation indicates distinct functions of BLM in malignant tumours. Such mis-localisation

of BLM has been detected in other tumours. The cytosolic BLM was found in breast cancers, where its abundance correlated with increased aggressiveness (Arora et al. 2015). The aberrant overexpression of BLM in the cytoplasm in colorectal cancers was associated the CpG island promoter hypomethylation and increased DNA damage responses (Votino et al. 2017).

There are several potential explanations for the distinct BLM localisation in a cytoplasm of tumours cells. The reported *BLM* mutations resulting in alterations in the nuclear targeting signal (NLS) domain (Kaneko et al. 1997) or dysregulation of mechanisms responsible for nuclear targeting might change localization of BLM in glioma cells. Altogether, 64 mutations have been identified and within the *BLM* gene in Bloom Syndrome patients (based on Bloom's Syndrome Registry). Strikingly, 54 mutations caused premature termination of protein translation and 10 mutations were classified as missense ones (German et al. 2007). Studies by Hayakawa *et al.* shed light upon the specific mutations causing changes in localisation of BLM protein by using plasmid constructs expressing EGFP and various BLM protein variants focused on the C-terminal region. The lack of $Arg^{1344}$, $Lys^{1346}$ or $Arg^{1347}$ resulted in equal distribution between nucleus and cytoplasm, whereas substitution of $Arg^{1344}$, $Lys^{1346}$, $Arg^{1347}$ or $Arg^{1348}$ with non-basic amino acids impaired the nuclear localization of the BLM protein (Hayakawa et al. 2000). Markedly, all nonsense mutations are deleterious for Bloom Syndrome patients (Bythell-Douglas and Deans 2021). Recently, new non-synonymous single nucleotide polymorphisms (nsSNP) in the *BLM* gene have been discovered. This "28 'stop gained'- and 1 'start lost'" mutations can cause expression of the truncated forms of BLM lacking the nuclear signal or important domains responsible for nuclear localisation (Alzahrani et al. 2020). However, the aforementioned computational analysis should be validated experimentally to ultimately decipher this phenomenon.

Our group had previously reported that a different helicase from the same family RecQL4 was localised mostly in the nucleus and cytoplasm in lower-grade gliomas and control tissues, whereas cytoplasmic accumulation was observed in WHO grade 4 gliomas (Król et al. 2020). RecQL4 is the only RecQ helicase performing a role in maintaining the mitochondrial genome integrity and its cytoplasmic localisation in glioma cells has been documented (Croteau et al. 2012). In this study, we did not perform staining for mitochondrial markers in cells,

thus we cannot fully explain functions of RecQL4 in the cytoplasm. Intracellular trafficking of RecQL4 can be affected by deletion of one of the NES (nuclear exporting signal), pNES2 (putative nuclear exporting signal 2, aa1187–1198) which results in reduction of the cytoplasmic localisation or posttranslational modifications. The RecQL4 C-tail polyubiquitination in the NES intact region enriches its protein level in cytoplasm (Chi et al. 2012), whereas acetylation of lysine residues by p300 histone acetyltransferase within the NLS (nuclear localization signal) significantly diminishes the nuclear localisation of RecQL4 (Dietschy et al. 2009). Moreover, interactions with other proteins can locally affect subcellular localisation of helicases, as RecQL4 modulates p53 transport to mitochondria in normal human cells in the absence of exogenous stress (De et al. 2012). The presented results show that both helicases are present in both cytosolic and nuclear compartments. For BLM there is no clear evidence about its role in the cytoplasm and whether this cytoplasmic confinement reflects protein malfunction related to tumorigenesis.

### 5.3. BLM functions in glioma cells: replication, DNA repair and beyond

Immunocytochemistry staining showed accumulation of BLM at the DNA damage loci marked by the assembly of γH2AX after UVC. γH2AX accumulates at double strand breaks that is independent of the repair pathway used by the cell. H2AX phosphorylation triggers a chain of events and post-translational modifications enabling an increase in DNA accessibility and the recruitment and accumulation of a multitude of DDR proteins at the site of the DNA lesion (Bouquet et al. 2006). While BLM involvement has been well studied, we focused on the role of this protein in responses to chemotherapeutics used in glioma therapy.

In this study we used the CRISPR/Cas9 genome editing to delete *BLM* in LN18 and LN229 glioma cells to better define its functions. BLM deficiency in glioma cells reduced proliferation of LN18 and LN229 cells and the cell cycle analysis showed that more BLM KO LN18 cells than WT cells were arrested in the G2/M phase. The differences between WT and BLM KO were further highlighted by the transcriptomic analysis that demonstrated downregulation of minichromosome maintenance genes (MCM2,3,4,5,6,7) and essential factors for transcription initiation in BLM KO LN18 cells. Interestingly, such changes were not detected in BLM KO LN229 cells. The distinct transcriptomic profiles in different glioma cells

suggest that either a role of BLM or its interacting proteins are cell-specific. Arkaitz *et al.* reported that knock-down of MCM2 and MCM3 induced the accumulation of cells in the G2 phase, most likely due to accumulation of DNA damage in dividing cells (Arkaitz et al. 2008).

BLM knock-out in LN18 and LN229 cells resulted in immense transcriptomic changes, illustrating how the tumour cells adapt to the loss of one the crucial genome maintenance proteins. When we focused on common differentially regulated genes, BLM KO cells showed dysregulation of functional pathways implicated in focal adhesion or tight junctions. This was consistent with the observed slight changes in cell morphology. Moreover, the observed changes in expression of genes in BLM KO cells were associated with apoptosis and cellular senescence pathways. These observations suggested that BLM-deficient cells might differently respond to chemotherapeutics than WT cells.

TMZ is a commonly used alkylating drug in the clinic for glioma treatment. Since 2005 TMZ is included together with surgical resection and radiotherapy as the Stupp protocol for GBM treatment (Stupp et al. 2005). After 18 years, GBM treatment remains the same and GBM patient survival rate did not change significantly. Due to tumour heterogeneity, MGMT mediated repair mechanisms, increased p53 activity, epigenetic alterations and other factors, GBMs are hard to treat and acquire the TMZ resistance (Oliver et al. 2020). More recently, olaparib that targets PARP1, one of the proteins cooperating with RecQ helicases in DNA repair and genome maintenance (Veith and Mangerich 2015), has been introduced as an anti-glioma chemotherapeutic. PARPi were successfully used in breast and ovarian cancers with the BRCA1/2 deficiency (Rose et al. 2020). The recent clinical trials combined the Stupp protocol with OLA or other PARPi exploring a potential of synthetic lethality in GBMs (Fulton et al. 2017; Lesueur et al. 2019) and the application of PARPi in certain groups of GBMs is recommended in basket trials (NCT01390571, NCT04166435) (Bisht et al. 2022). Recently, there are two recruitments for clinical trials of patients with recurrent glioma (NCT04910022) or glioma with *IDH1/2* mutations (NCT03749187). The treatment involves TMZ combined with PARPi: NMS-03305293, and BGB-290, respectively. PARP1 is one of the proteins cooperating with RecQ helicases in DNA repair and genome maintenance (Veith and Mangerich 2015) and its inhibitors (such as OLA) are supposed to enhance cytotoxicity of DNA damaging drugs.

Moreover, the combination of TMZ and PARPi (OLA) has been explored in a clinical trial of GBMs and restoration of chemosensitivity to TMZ by PARPi in MSH6-inactivated gliomas and overcoming acquired chemoresistance caused by MMR deficiency has been reported (Higuchi et al. 2020).

For detailed studies of the effects of TMZ, OLA and the combined treatment on glioma cells, we selected two glioma cell lines having similarly high expression of BLM, but differing in other proteins crucial of response to chemotherapy. LN18 cells are TP53-deficient and have the active MGMT enzyme, so the cells do not respond to most chemotherapeutics (Happold et al. 2012). LN229 cells (having a partly active TP53 and low MGMT protein expression) respond relatively well to chemotherapy (Ellert-Miklaszewska et al. 2021). BLM depletion had the strongest effect on LN229 cells after TMZ treatment augmenting drug toxicity. The effect of OLA on BLM deficient cells was negligible even at high OLA concentrations and when combined with TMZ reduced its effectiveness. This finding is in contrast to the expectations as according to a concept of the synthetic lethality, homological recombination (HR)-deficient cells should display increased susceptibility to PARPi (Farmer et al. 2005). For example, Kong *et. al* reported synergistic effect of BLM inhibition by the ML216 compound when combined with PARP inhibition in olaparib resistant non-small lung cancer cells (Kong et al. 2021). Studies by Wang *et al.* presented a beneficial role of a new BLM inhibitor - quinazolinone derivate '9h' - in HCT116 colon cancer cells, where DNA damage at the telomere region and induction of apoptosis were observed. The therapeutic effect was augmented by combination with PARPi (Wang et al. 2020b). Up to now, ML216 remains the only, commercially available BLM helicase inhibitor (Rosenthal et al. 2010), despite of the fact that other more potent inhibitors were reported (Wang et al. 2020b; Chen et al. 2021). Notably, ML216 has not appeared in any clinical trials.

The explanation for the lack of a synergistic effect of PARPi on BLM deficient glioma cells could be that other BLM interacting partners (i.e. RecQL4, WRN) replace BLM functionally or in BLM lacking cells PARP pathway is already disabled and cannot be further inhibited. We can rather exclude the first mechanism as we did not observe the increase of RecQL4 in BLM-KO cells by Western blotting. A deeper analysis of genetic background of these tumour cells is needed to fully explain a lack of PARPi synergistic effect in BLM KO glioma cells. GBM cells rarely

have *BRCA1/2* mutations and therefore are HR proficient, so PARPi alone do not show anti-tumour efficacy (Parsons et al. 2008). We found distinct responses of BLM deficient glioma cells treated with TMZ alone in comparison to TMZ+OLA. WT glioma cells were more vulnerable to the TMZ+OLA treatment, whereas BLM KO cells were resistant and induced different mechanisms to escape cell death. We performed RNA sequencing of control and drug-treated cells and found some transcriptomic responses that could guide us regarding molecular underpinning of this drug-resistance. Transcriptomic changes induced in LN18 and LN229 BLM KO cells by the T+O treatment involved upregulation of genes implicated in DNA replication, DNA repair and cellular senescence pathways.

Differences in WT and BLM KO cells response to TMZ+PARPi led to the query if the effect is exclusive for PARPi. TMZ was tested in combination with other PARPi (iniparib [INI], 3-aminobenzamide [3-ABA], rucaparib [RUCA]) and unrelated drugs (6-thioguanine [6-TG], etoposide [ETO], doxorubicin [DOX]) to explore which drugs would act synergistically with TMZ on WT and BLM KO cells. Similarly to OLA, other PARPi combined with TMZ did not show additive effects on BLM KO cells. This was confirmed by calculated Hedge's 'g' values. The non-significant difference and smallest 'g' value was noted for TMZ+INI. Rucaparib showed favourable outcome in randomised phase II trials in patients with triple-negative breast cancer, however the results of phase III were negative. *In vitro* experiments displayed poor inhibition of PARP and the drug has a distinct structure from other PARP inhibitors (Patel et al. 2012; Mateo et al. 2013). INI was shown as a non-selective modifier of cysteine-containing proteins in tumour cells and the primary mechanism of action is likely not *via* PARP inhibition (Liu et al. 2012). 3-ABA (a first generation of PARPi) was efficient in elimination of WT LN18 cells when combined with TMZ (Pandya et al. 2010). The most potent RUCA, a second generation PARPi, displayed dose-dependent toxicity in BLM KO and WT LN18 cells, irrespectively of TMZ co-treatment. Nevertheless, the resistance to the combined TMZ+RUCA treatment was still observed in BLM KO cells. RUCA is a FDA approved drug or treatment of ovarian cancer regardless of the *BRCA1/2* status and for *BRCA1/2* mutated ovarian cancer patients (Nientiedt et al. 2021). Recent study showed a high activity of RUCA in castration-resistant prostate metastatic cancers associated with BRCA deficiency (Fizazi et al. 2023). Pan-PI3K inhibitor BKM120 combined with RUCA sensitised BRCA-proficient GBM tumours to PARPi,

which provides novel therapeutic opportunities (Zhang et al. 2021). Beneficial effects of TMZ+RUCA have been limited in orthotopic glioblastoma xenografts due to ineffective drug penetration into the central nervous system (Parrish et al. 2015).

To better understand the unexpected lack of TMZ+PARPi efficacy in BLM deficient glioma cells, we tested non-related chemotherapeutics in combination with TMZ. 6-TG, a purine analogue of guanine, was introduced to treat recurrent high-grade gliomas with TMZ, however the effect of combination was negligible in comparison to conventional alkylating agents. Nevertheless, TMZ+6-TG combination was promising in patients with recurrent anaplastic gliomas (Walbert et al. 2010). Etoposide, an inhibitor of DNA topoisomerase II, displayed the synergistic activity with TMZ in children with recurrent malignant brain tumours (Ruggiero et al. 2020). Doxorubicin also blocks the topoisomerase II activity and TMZ-DOX conjugates demonstrated a potential in glioblastoma chemotherapy (Du et al. 2020). Based on calculated $EC_{50}$ values from cell viability assay, most of those drugs when combined with TMZ were equally effective in WT and BLM KO LN18 cells. Moreover, Hedge's effect size 'g' is relatively small suggesting a lack of significant differences between WT and BLM KO cells. A strong effect size evident in the DOX+TMZ treated cells, despite clearly visible similar response to the treatments, could be explained as a result of only 4 doses with strong cell responses, resulting in a sharp slope of the calculated linear model. In this case, even little change in the cell viability, results in considerable changes of the global response. It should be also mentioned that in such studies testing more doses is needed to obtain the most accurate results and using 4 doses to determine the $EC_{50}$ represents a slight limitation of this study. Nonetheless, based on obtained $EC_{50}$ values for PARPi and other chemotherapeutics combined with TMZ, we conclude the resistance displayed by BLM KO cells occurs only in case of TMZ+PARPi. This evidence indicate the role of BLM in modulating the cell response to drug-induced stress connected with a predominant impairment of the BER repair pathway.

### 5.4. Role of BLM in decision making between various cellular responses to chemotherapeutics

Severe DNA damage typically leads to the growth arrest and initiation of various cellular responses that will drive cells into cell death. However, tumours cells that are deficient in tumour suppressors, cell cycle inhibitors or apoptotic proteins developed many mechanisms of cell death evasion (Bedoui et al. 2020). BLM KO cells exposed to TMZ+OLA were arrested in the G2/M phase of the cell cycle and underwent polyploidisation or cellular senescence. Both processes are considered as therapy-induced mechanisms of cell death escape and senescent cells are frequently polyploid (Saleh et al. 2022). Tetraploid cells can arise due to the mitotic slippage from the prolonged mitotic arrest or cytokinesis failure (Kuffer et al. 2013). As BLM participates in the correct chromosome segregation and resolving anaphase bridges (Chan et al. 2007), its deficiency in TMZ+OLA -treated glioma cells may lead to the cytokinesis failure under stress conditions. However this effect was not observed in treated BLM KO LN229 cells, pointing out to other mechanisms involved. Notably, the increase of polyploidy was TP53 dependent, as restoration of the functional p53 in LN18 BLM KO cells reduced percentages of polyploid cells. LN229 cells responded differently to the drug combination. After TMZ+OLA treatment, percentages of cells undergoing the cell cycle arrest and having increased number of β-gal$^+$ senescent cells were significantly higher among BLM KO LN229 cells than WT cells. Interestingly, Schwarzenbach *et al.* have reported the appearance of polyploid LN229 cells after TMZ (50 μM) alone and TMZ combined with pamiparib (PARPi) (Schwarzenbach et al. 2021). The results presented here show that TMZ+OLA induced cellular senescence in BLM deficient LN229 glioma cells, which is evidenced by the appearance of enlarged, β-gal$^+$ cells and increased granularity.

Inducing drug-triggered senescence is explored in cancer treatment as such action results in the cycle arrest and senescence cells can be selectively removed with senolytic drugs (Zhang et al. 2022b). As neoplastic cells can emerge from senescent cells after cessation of chemotherapy (Was et al. 2017), the removal of senescent tumour cells is recommended.

Interestingly, while RecQL4 helicase is assumed to perform similar functions as BLM in DNA replication and repair, RecQL4 deficient LN18 and LN229 glioma cells responded similarly as WT cells and TMZ+OLA induced their

apoptosis. These cells did not undergo polyploidy when exposed to the drug combination and a similar, low fraction of senescent cells emerged after the treatment. These findings emphasise the distinct role of the BLM helicase in the response to chemotherapeutics.

There is a growing evidence that chemotherapeutics trigger cell death *via* apoptosis pathway and/or cellular senescence. In many studies the increased activity of β-gal is indicated as a sign of senescence while the increase of β-gal might be also due to overgrowth of the cells or cell starvation. Both processes are associated with the increased lysosomal activity (Lee et al. 2006; Leontieva et al. 2014). It has to be pointed out that cellular senescence is a complex process and many different parameters such as flatten cell morphology, cell granularity, γH2AX-foci, SASP, *etc*) should be measured simultaneously to carefully assess this process. TMZ was shown to induce not only the apoptotic cell death. This alkylating agent at low doses and after prolonged treatment induces cellular senescence (Beltzig et al. 2022a). Both effects involve $O^6$-methylguanine ($O^6$MeG) and are inhibited in the presence of MGMT and MMR deficiency, suggesting the similarity of upstream DNA damage response pathways. Markedly, $O^6$MeG-triggered senescence was shown to be mediated by autophagy in LN229 cells (Knizhnik et al. 2013). The DNA repair pathway of TMZ-induced senescence requires functional p53 and sustained p21 induction, whereas p53-deficient cells not expressing p21 did not undergo the cellular senescence, but could be blocked in the G2/M cell cycle phase. TMZ-induced senescence was accompanied by induction of the SASP and activation of NF-κB pathway (Aasland et al. 2019).

Altogether, aforementioned findings are generally in agreement with our studies, although in our hands TMZ treatment alone did not induced cellular senescence. This discrepancy might be due to a use of TMZ at high concentrations in short time experiments, that induced rather apoptotic cell death than senescence. This conclusion is based on detecting of apoptotic proteins by Western blotting and cell granularity analyses.

### 5.5. Senotherapies in cancer

Malignant tumours have an ability to evade senescence, nonetheless tumour cells may be forced to enter the senescence state *via* the pathway of therapy-induced senescence (TIS) (Collado and Serrano 2010). The preclinical

evidence of aggressive relapses, chronic treatment-related toxicity and increased secondary tumour incidence might be consequences of persisting TIS cells, thus implementation of senotherapies is a reasonable solution. Elimination of senescent cells can be achieved through the application of senolytic drugs and targeting secretion of SASP factors using senomorphic agents (Schmitt et al. 2022). Navitoclax, a senolytic drug, and a BCL-2 family inhibitor, targeting BCL-2, BCL-XL and BCL-W, preferably kills the senescent cells in cell cultures (Chang et al. 2016). Moreover, enhanced effects of the drug were observed in A549 and MDA-MB-231 xenografts in mice (Saleh et al. 2020), and reduced tumour growth ovarian and breast cancer xenografts when co-treated with PARPi (Fleury et al. 2019). Interestingly, navitoclax attenuated COVID-19 lung pathology in SARS-CoV2-infected hamsters and ACE-2-transgenic mice, similarly to another senolytic drug, fisetin, a tyrosine kinases PI3K inhibitor (Lee et al. 2021). Navitoclax was enrolled in clinical trials with various chemotherapies such as etoposide in small cell lung cancer (NCT00878449) or paclitaxel (NCT00891605) in solid tumours (Paez-Ribes et al. 2019). As a single agent was used in phase II study in platinum resistant/refractory recurrent ovarian cancer (NCT02591095) (Brachet et al. 2017).

Fisetin inhibited proliferation, migration and metastasis of triple negative breast- and ovarian cancer cells, and pancreatic xenograft models (Li et al. 2018; Jia et al. 2019). Targeting SASP by senomorphic drugs was beneficial for mice treated by metformin or rapamycin, modulating NF-κB and mTOR pathways, respectively (Pollak 2012; Moiseeva et al. 2013; Laberge et al. 2015). Temsirolimus, a mTOR kinase inhibitor, was combined with rituximab in the phase II of diffuse large B cell lymphomas (NCT0165306) (Witzens-Harig et al. 2013).

CDD111 targeting p38 MAPKK prevented breast cancer metastases and chemotherapy-induced bone loss in mice (Murali et al. 2018). Anti-IL-1β antibody canakinumab was approved for the various pyrexia-featured inflammatory syndromes and displayed beneficial effects in several trials on non-small-cell lung cancer (Lau et al. 2019; Schenk et al. 2019).

The senescent state can be induced by targeting tumour suppressors or oncogenes. For example, the *PTEN* status determines the cell fate of glioma cells after ionizing radiation. Premature senescence was present when *PTEN* was mutated while tumour cells with the intact *PTEN* underwent apoptosis (Lee et al. 2011). There are several studies on the role of senolytic drugs in modulating

the vulnerability of glioma cells to chemotherapeutics. Schwarzenbach *et al.* indicated the role of targeting anti-apoptotic factors c-IAP1, c-IAP2 and Bcl-2 to eliminate senescent glioblastoma cells following TMZ treatment (Schwarzenbach et al. 2021). Rahman *et al.* reported that BCL-XL inhibition leads to selective vulnerability of glioblastoma cells (Rahman et al. 2022).

Distinctive features of senescent tumours cells might be exploited for the selective eradication of these cells (senolysis) (Wang et al. 2022). Beltzig *et al.* conducted comprehensive studies applying different senolytics on TMZ-induced senescent LN229 and A172 glioma cells. BCL-family inhibitors, ABT-737 and ABT-263 (navitoclax), and autophagy inhibitors, chloroquine and PX866 showed promising results in eradication of senescent cells and increasing apoptotic events in LN229 cells. Interestingly, natural compounds fisetin artesunate displayed the senolitic activity in LN229 and A172 cells. However, such approaches failed to remove senescent cells after treatment with irradiation and lomustine, DNA crosslinking chloroethylating agent used often 2$^{nd}$ line in glioma therapy (Beltzig et al. 2022b).

Recent findings by Salam *et al.* tackle an issue of tumour-promoting properties of senescent cells in glioblastoma patients and mice. Partial removal of p16$^{Ink4a}$-expressing malignant senescent cells modified the tumour microenvironment and improved the survival of GBM-bearing female mice. Notably, mouse senescent signature was conserved in GBM patients and its enrichment was a predictor of a worse survival. Moreover, combining immunohistochemistry, genetic knock-downs and single-cell and bulk RNA sequencing, the link between senescence and transcription factor NRF2 has been established, thus NRF2 might be a novel therapeutic target in senescent cells (Salam et al. 2023). Cellular senescence is a double edge sword, balancing between favourable features like the cell cycle arrest, and displaying SASP involved in a persistent inflammatory state. While senolytics are interesting agents for adjuvant therapies in cancer, till now none of senolytics entered clinical trials in glioma treatment.

The 'golden standard' markers for senescent cells are still missing (Beauséjour et al. 2003) and withdrawal from the cell cycle might be associated with other cell states such as drug-tolerant persistence, dormancy, terminal differentiation or quiescence (He and Sharpless 2017). Many drugs commonly used

in the clinic such as bleomycin, cisplatin, doxorubicin, etoposide *etc*, as well as the γ-irradiation, are able to evoke therapy induced senescence (Ewald et al. 2010).

### 5.6.    Therapeutical modalities against polyploid cells

Despite aggressive phenotype of polyploid giant cancer cells (PGCC) there are some therapeutic opportunities to eradicate these cells. Tamoxifen therapy reduced the colony formation of PGCC, interfering with ASAH1 (sphingolipid enzyme acid ceramidase) (White-Gilbertson et al. 2020) whereas inhibition on 2DG (2-deoxy-D-glucose) led to PGCC death by apoptosis and autophagy in chronic myelogenous leukaemia (Liu et al. 2013). Moreover some mTOR inhibitors (rapamycin, PP242, AZD8055) prevented formation of PGCC and decreased survival of PGCC by changing accumulation and localisation of survival-related proteins. The combination of mTOR and Aurora kinase inhibitors was used to increase drug sensitivity in breast cancer and acute myeloid leukaemia cells (Liu et al. 2013; Sharma et al. 2014).

Another complication of ineffective therapy is the appearance of polyploid cells. Wang *et al.* reported the aberrant Cdk1 expression that interferes with apoptosis and facilitates the formation of polyploid senescent cells in NCI-H1299 non-small cell lung carcinoma cells. These polyploid cells can escape from senescence and resume cell divisions. The cyclin-dependent kinase inhibitor p27[Kip1] was shown to inhibit Cdk1 and reduce polyploidy (Wang et al. 2013b). The polyploidy state results from DNA over-replication, abrogated mitosis and unsuccessful cytokinesis (Ivanov et al. 2003; Nakayama et al. 2009). Polyploid giant cells arise by endo-reduplication or asymmetrical genomic reduction (Erenpreisa et al. 2005). Depolyploidisation process involves telomere clustering, nuclei reconstruction and chromosome double-loops formation (Erenpreisa et al. 2000). Moreover, diploid and paradiploid daughter cells are produced by asymmetrical genomic reduction (Erenpreisa et al. 2005). According to Sundaram *et al.* polyploid cells can divide in the way of neosis, that resembles yeast budding, giving a rise to tiny Raju cells (Sundaram et al. 2004). Interestingly, Czarnecka-Herok *et al.* reported that the escape of cancer cells from senescence/polyploidy is connected with the presence of small descendants inside the giant polyploid MCF7 cells (Czarnecka-Herok et al. 2022).

Despite of very low frequency of polyploid cells division, even 1 to $1x10^6$ (Roberson et al. 2005), this phenomenon must not be neglected as malignant offsprings may rebuild the tumour. We observed the increased population of BLM KO LN18 cells in the polyploid state after TMZ+OLA treatment. The increased polyploidy was due to the p53 deficiency as ectopic expression of the functional p53 reduced the polyploid fraction of the glioma cells. We did not study if the cells are able to escape senescence with time. Altogether, we conclude that the observed polyploidy and induced cellular senescence are different or may be interconnected ways tumours cells employ to escape from the cell death under unfavourable environmental conditions.

### 5.7.    Developmental abnormalities in *blm* and *recql4*- depleted *Xenopus* tadpoles

To decipher the role of blm in animal studies, we employed a *Xenopus* model which was used in 1988 to isolate the DNA helicase from *Xenopus laevis* ovaries (Poll and Benbow 1988). We observed increased embryos lethality and the developmental abnormalities in *blm* and *recql4* depleted tadpoles. These results are in agreement with data form other organisms. blm has been shown to contribute to germ line development and longevity in zebrafish. Annus *et al.* reported that a lack of *blm* does not impair early somatic development of zebrafish embryos but the lifespan of the mutant was markedly shortened. Moreover, all *blm* mutant males had fertility defects, displaying spermatocytes block in the meiotic prophase I (Annus et al. 2022). Ruchert *et al.* noted that *Blm* facilitates replication through repetitive DNA sequences in *Drosophila* during the rapid syncytial cycles of the embryonic development (Ruchert et al. 2022). Furthermore, Blm impairment leads to meiotic abnormalities such as improper pairing of homologous chromosomes, thus Blm deficiency leads to apoptosis during spermatogenesis (Holloway et al. 2010). Notably, loss-of-function mutations in *BLM* orthologs in *Caenorhabditis elegans*, *Drosophila melanogaster*, *Danio rerio* and *Mus musculus* recapitulated the Bloom Syndrome symptoms (Cunniff et al. 2017). Similarly, *recql4* depletion in mice resulted in growth retardation, skin abnormalities and hypoplasia of several tissues (Hoki et al. 2003). In *Drosophila melanogaster* and *Mus musculus* the knock-out of recql4 helicase caused embryonic lethality (Ichikawa et al. 2002; Wu et al. 2008).

Interestingly, *Xenopus laevis* was critical in investigation of recql4 functions during replication (Sangrithi et al. 2005).

### 5.8. Distinct roles of RecQ family helicases in cell responses to chemotherapeutics

RecQ helicases belong to a highly conserved family and are considered a genome 'guardians' that maintain DNA and chromosome stability. The crystal structure of RecQ helicases shows several conserved functional domains. Some of these domains occur a given member of the RecQ helicases and may be important in defining functions of the specific helicase (Chu and Hickson 2009). We have previously reported that RecQL4 depletion in glioma cells did not affect basal cell viability, slightly impaired DNA replication, induced vast transcriptomic changes and increased chemosensitivity of glioma cells to TMZ. RecQL4 KO cells grown as sphere cultures had reduced sphere forming capacity, stronger responded to TMZ upregulating cell cycle inhibitors and pro-apoptotic proteins (Król et al. 2020).

As BLM deficiency in glioma cells had a strong effect on cell responses after TMZ+OLA, we replicated some studies using RecQL4 depleted LN18 and LN229 cells. Notably, the RecQL4 deficient glioma cells did not show the resistance to the TMZ+OLA treatment and RecQL4 KO cells were equally vulnerable to the drugs as RecQL4 WT cells. Both LN18 and LN229 RecQL4 KO cells underwent apoptosis after the combined treatment, and the polyploid cells were not detected among the treated LN18 cells. This set of results underlines the different functions of BLM and RecQL4 helicases in glioma cells in the therapy response. One of the reasons might be the fact that BLM levels increase in RecQL4 KO cells and likely exert the compensatory effect. We did not observe a compensatory increase of the RecQL4 level in BLM KO cells. Deeper studies are needed to understand the mechanisms of action of both helicases, particularly in polyploidisation process.

We propose that the BLM helicase, which is upregulated in malignant gliomas, is a new therapeutic target in tumour cells, which may pave way to the development of specific BLM inhibitors. As the TMZ+OLA treatment is already in the clinic, we propose that testing BLM expression, MGMT and TP53 status could help to better predict a patient response to such treatment.

While genetic alterations in the *BLM* gene have not yet been reported in gliomas, manipulation of the BLM level could be additional strategy to improve the option of patients with deadly brain tumours.

## 6. SUMMARY AND CONCLUSIONS

**In the present study we report the following findings:**

1. The levels of BLM mRNA and protein are upregulated in malignant glioma and high *BLM* expression negatively correlates with GBM patient survival.

2. A majority of BLM protein is localised in nuclei and cytoplasm in glioblastoma cells in contrast to normal brains and low-grade gliomas.

3. BLM deficiency changes the glioma cells respond to TMZ combined with PARPi suggesting that BLM cooperates with PARP1 in post-therapy DNA repair.

4. The BLM expression, MGMT activity and TP53 status in glioma cells define whether the cells exposed to chemotherapeutics would die by apoptosis or evade cell death by inducing senescence and polyploidy.

5. Our findings suggest that the BLM helicase, which is upregulated in malignant gliomas, might be a new target in tumour cells, which may pave way to the development of specific BLM inhibitors.

6. RecQL4 deficient cells respond similarly as WT cells to TMZ+OLA, underlining the distinct actions of helicases.
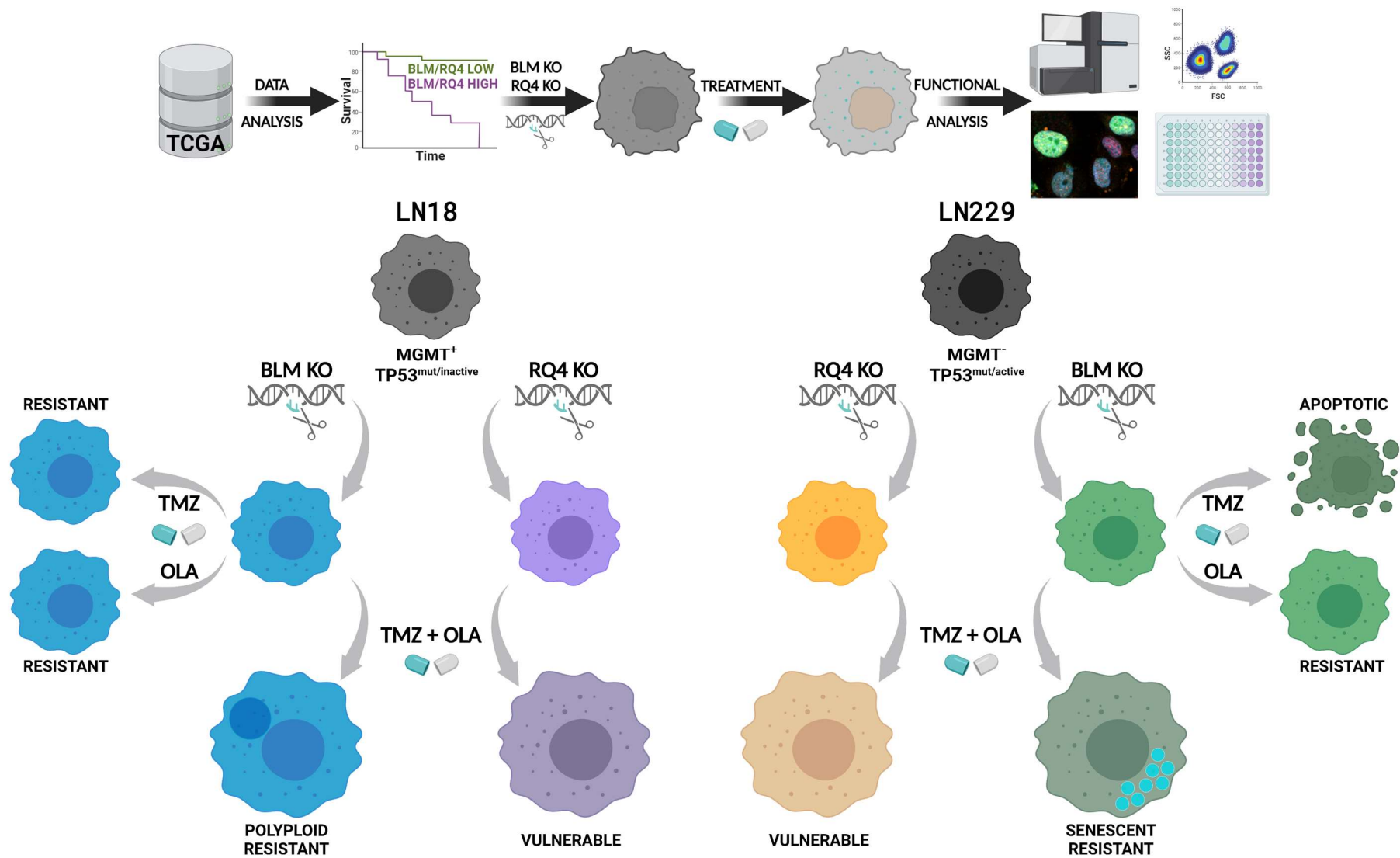
## 7. PUBLICATIONS (RELATED TO THE THESIS)

1.  **BLM helicase overexpressed in human gliomas contributes to diverse responses of human glioma cells to chemotherapy (*in revision* in Cell Death Discovery 2023, https://doi.org/10.21203/rs.3.rs-2621118/v1).**
    **Kamil Wojnicki**, Agnieszka Kaczmarczyk, Bartosz Wojtas, Bozena Kaminska.

2.  **Exploring Novel Therapeutic Opportunities for Glioblastoma Using Patient-Derived Cell Cultures (Cancers, 2023).**
    Iwona A. Ciechomska*, **Kamil Wojnicki***, Bartosz Wojtas, Paulina Szadkowska, Katarzyna Poleszak, Beata Kaza, Kinga Jaskula, Wiktoria Dawidczyk, Ryszard Czepko, Mariusz Banach, Bartosz Czapski, Pawel Nauman, Katarzyna Kotulska, Wieslawa Grajkowska, Marcin Roszkowski, Tomasz Czernicki, Andrzej Marchel and Bozena Kaminska.

3.  **Regulatory networks driving expression of genes critical for glioblastoma are controlled by the transcription factor c-Jun and the pre-existing epigenetic modifications (Clinical Epigenetics, 2023).**
    Adria-Jaume Roura, Paulina Szadkowska, Katarzyna Poleszak, Michal J. Dabrowski, Aleksandra Ellert-Miklaszewska, **Kamil Wojnicki**, Iwona A. Ciechomska, Karolina Stepniak, Bozena Kaminska, Bartosz Wojtas.

4.  **Specialized functions and sexual dimorphism explain the functional diversity of the myeloid populations during glioma progression (Cell Reports, 2023).**
    Natalia Ochocka, Pawel Segit, **Kamil Wojnicki**, Salwador Cyranowski, Julian Swatler, Karol Jacek, Wieslawa Grajkowska, Bozena Kaminska.

5.  **Improvements in Quality Control and Library Preparation for Targeted Sequencing Allowed Detection of Potentially Pathogenic Alterations in Circulating Cell-Free DNA Derived from Plasma of Brain Tumor Patients (Cancers, 2022).**
    Paulina Szadkowska, Adria-Jaume Roura, Bartosz Wojtas, **Kamil Wojnicki**, Sabina Licholai, Tomasz Waller, Tomasz Gubala, Kacper Zukowski, Michal Karpeta, Kinga Wilkus, Wojciech Kaspera, Sergiusz Nawrocki, Bozena Kaminska.

6.  **A novel oral arginase 1/2 inhibitor enhances the antitumor effect of PD-1 inhibition in murine experimental gliomas by altering the immunosuppressive environment (Frontiers in Oncology, 2021).**
    Paulina Pilanc, **Kamil Wojnicki**, Adria-Jaume Roura, Salwador Cyranowski, Aleksandra Ellert-Miklaszewska, Natalia Ochocka, Barłomiej Gielniewski, Marcin M Grzybowski, Roman Błaszczyk, Paulina S Stańczak, Paweł Dobrzański, Bozena Kaminska.

7.  **Single-cell RNA sequencing reveals functional heterogeneity of glioma-associated brain macrophages (Nature Communications, 2021).**

Natalia Ochocka\*, Pawel Segit\*, Kacper Adam Walentynowicz, **Kamil Wojnicki**, Salvador Cyranowski, Julian Swatler, Jakub Mieczkowski, Bozena Kaminska.

8. <span style="color:teal">**Aberrantly expressed RecQL4 helicase supports proliferation and drug resistance of human glioma cells and glioma stem cells**</span> **(Cancers, 2020).**
Sylwia K. Król, Agnieszka Kaczmarczyk, **Kamil Wojnicki**, Bartosz Wojtas, Bartłomiej Gielniewski, Wiesława Grajkowska, Katarzyna Kotulska-Jóźwiak, Cezary Szczylik, Ryszard Czepko, Mariusz Banach, Wojciech Kaspera, Wojciech Szopa, Andrzej Marchel, Tomasz Czernicki, Bozena Kaminska.

9. **Tumour-derived CSF2/granulocyte macrophage colony stimulating factor controls myeloid cell accumulation and progression of gliomas (British Journal of Cancer, 2020).**
Malgorzata Sielska, Piotr Przanowski, Maria Pasierbińska, **Kamil Wojnicki**, Katarzyna Poleszak, Bartosz Wojtas, Dominika Grzeganek, Aleksandra Ellert-Miklaszewska, Min-Chi Ku, Helmut Kettenmann, Bozena Kaminska.

10. **Gliosarcoma Is Driven by Alterations in PI3K/Akt, RAS/MAPK Pathways and Characterized by Collagen Gene Expression Signature (Cancers, 2019).**
Bartosz Wojtas, Bartlomiej Gielniewski, **Kamil Wojnicki**, Marta Maleszewska, Shamba S. Mondal, Pawel Nauman, Wieslawa Grajkowska, Rainer Glass, Ulrich Schüller, Christel Herold-Mende, Bozena Kaminska.

11. **In Search for Reliable Markers of Glioma-Induced Polarization of Microglia (Frontiers in Immunology, 2018).**
Kacper A. Walentynowicz, Natalia Ochocka, Maria Pasierbinska, **Kamil Wojnicki**, Karolina Stepniak, Jakub Mieczkowski, Iwona A. Ciechomska, Bozena Kaminska.

12. **In Vitro Antiproliferative Activity of Extracts of Carlina acaulis subsp. caulescens and Carlina acanthifolia subsp. Utzka (Frontiers in Pharmacology, 2017).**
Maciej Strzemski, **Kamil Wojnicki**, Ireneusz Sowa, Kamila Wojas-Krawczyk, Paweł Krawczyk, Ryszard Kocjan, Justyna Such, Michał Latalski, Artur Wnorowski and Magdalena Wójciak-Kosior.

13. **Identification of new scaffolds with anti-tumor action toward human glioblastoma cells (Med. Chem. Comm. 2016).**
Aleksandra Ellert-Miklaszewska, Sabrina Dallavalle, Loana Musso, Nadine Martinet, **Kamil Wojnicki** and Bozena Kaminska.

14. **Microwave-assisted preparation, structural characterization, lipophilicity, and anti-cancer assay of some hydroxycoumarin derivatives (Monatshefte für chemie, 2015).**
Kinga Ostrowska, Elżbieta Hejchman, Dorota Maciejewska, Agata Włodarczyk, **Kamil Wojnicki**, Dariusz Matosiuk, Agnieszka Czajkowska, Izabela Młynarczuk-Biały, Łukasz Dobrzycki.

## 8. REFERENCES

1.  Aasland, D. et al. 2019. Temozolomide Induces Senescence and Repression of DNA Repair Pathways in Glioblastoma Cells via Activation of ATR–CHK1, p21, and NF-κB. *Cancer Research* 79(1), pp. 99–113.
2.  Ababou, M. 2021. Bloom syndrome and the underlying causes of genetic instability. *Molecular Genetics and Metabolism* 133(1), pp. 35–48.
3.  ABDEL-MONEM, M., DÜRWALD, H. and HOFFMANN-BERLING, H. 1976. Enzymic Unwinding of DNA. *European Journal of Biochemistry* 65(2), pp. 441–449.
4.  Abe, T., Yoshimura, A., Hosono, Y., Tada, S., Seki, M. and Enomoto, T. 2011. The N-terminal region of RECQL4 lacking the helicase domain is both essential and sufficient for the viability of vertebrate cells: Role of the N-terminal region of RECQL4 in cells. *Biochimica et Biophysica Acta (BBA) - Molecular Cell Research* 1813(3), pp. 473–479.
5.  Abu-Libdeh, B. et al. 2022. RECON syndrome is a genome instability disorder caused by mutations in the DNA helicase RECQL1. *The Journal of Clinical Investigation* 132(5).
6.  Ahamad, N., Khan, S., Mahdi, A.T.A. and Xu, Y. 2021. Checkpoint functions of RecQ helicases at perturbed DNA replication fork. *Current Genetics* 67(3), pp. 369–382.
7.  Alzahrani, F.A. et al. 2020. Investigating the pathogenic SNPs in BLM helicase and their biological consequences by computational approach. *Scientific Reports* 10(1), p. 12377.
8.  Amé, J.-C., Spenlehauer, C. and de Murcia, G. 2004. The PARP superfamily. *BioEssays* 26(8), pp. 882–893.
9.  Andrabi, S.A. et al. 2006. Poly(ADP-ribose) (PAR) polymer is a death signal. *Proceedings of the National Academy of Sciences of the United States of America* 103(48), pp. 18308–18313.
10. Annus, T. et al. 2022. Bloom syndrome helicase contributes to germ line development and longevity in zebrafish. *Cell Death & Disease* 13(4), p. 363.
11. Arkaitz, I., Etienne, S. and Juan, M. 2008. Excess MCM proteins protect human cells from replicative stress by licensing backup origins of replication. *Proceedings of the National Academy of Sciences* 105(26), pp. 8956–8961.
12. Arna, A.B. et al. 2022. Synthetic lethal interactions of DEAD/H-box helicases as targets for cancer therapy. *Frontiers in oncology* 12, p. 1087989.
13. Arora, A. et al. 2015. Transcriptomic and Protein Expression Analysis Reveals Clinicopathological Significance of Bloom Syndrome Helicase (BLM) in Breast Cancer. *Molecular Cancer Therapeutics* 14(4), pp. 1057–1065.
14. Arora, A. and Somasundaram, K. 2019. Glioblastoma vs temozolomide: can the red queen race be won? *Cancer Biology & Therapy* 20(8), pp. 1083–1090.
15. Ashworth, A. and Lord, C.J. 2018. Synthetic lethal therapies for cancer: what's next after PARP inhibitors? *Nature Reviews Clinical Oncology* 15(9), pp. 564–576.
16. Ayrapetov, M.K., Gursoy-Yuzugullu, O., Xu, C., Xu, Y. and Price, B.D. 2014. DNA double-strand breaks promote methylation of histone H3 on lysine 9

and transient formation of repressive chromatin. *Proceedings of the National Academy of Sciences* 111(25), pp. 9169–9174.

17. Baker, S.J., Markowitz, S., Fearon, E.R., Willson, J.K. V and Vogelstein, B. 1990. Suppression of Human Colorectal Carcinoma Cell Growth by Wild-Type p53. *Science* 249(4971), pp. 912–915.

18. Barciszewska, A.-M., Gurda, D., Głodowicz, P., Nowak, S. and Naskręt-Barciszewska, M.Z. 2015. A New Epigenetic Mechanism of Temozolomide Action in Glioma Cells. *PLOS ONE* 10(8), p. e0136669.

19. Barefield, C. and Karlseder, J. 2012. The BLM helicase contributes to telomere maintenance through processing of late-replicating intermediate structures. *Nucleic Acids Research* 40(15), pp. 7358–7367.

20. Barnholtz-Sloan, J.S., Ostrom, Q.T. and Cote, D. 2018. Epidemiology of Brain Tumors. *Neurologic Clinics* 36(3), pp. 395–419.

21. Beauséjour, C.M., Krtolica, A., Galimi, F., Narita, M., Lowe, S.W., Yaswen, P. and Campisi, J. 2003. Reversal of human cellular senescence: roles of the p53 and p16 pathways. *The EMBO journal* 22(16), pp. 4212–4222.

22. Bedoui, S., Herold, M.J. and Strasser, A. 2020. Emerging connectivity of programmed cell death pathways and its physiological implications. *Nature Reviews Molecular Cell Biology* 21(11), pp. 678–695.

23. Beltzig, L. et al. 2022a. Senescence Is the Main Trait Induced by Temozolomide in Glioblastoma Cells. *Cancers* 14(9).

24. Beltzig, L., Christmann, M. and Kaina, B. 2022b. Abrogation of Cellular Senescence Induced by Temozolomide in Glioblastoma Cells: Search for Senolytics. *Cells* 11(16).

25. Ben-Porath, I. and Weinberg, R.A. 2005. The signals and pathways activating cellular senescence. *The international journal of biochemistry & cell biology* 37(5), pp. 961–976.

26. Bennett, R.J. and Keck, J.L. 2004. Structure and Function of RecQ DNA Helicases. *Critical Reviews in Biochemistry and Molecular Biology* 39(2), pp. 79–97.

27. Bernstein, K.A., Gangloff, S. and Rothstein, R. 2010. The RecQ DNA Helicases in DNA Repair. *Annual Review of Genetics* 44(1), pp. 393–417.

28. Bian, L., Meng, Y., Zhang, M. and Li, D. 2019. MRE11-RAD50-NBS1 complex alterations and DNA damage response: implications for cancer treatment. *Molecular Cancer* 18(1), p. 169.

29. Bischof, O., Kim, S.H., Irving, J., Beresten, S., Ellis, N.A. and Campisi, J. 2001. Regulation and localization of the Bloom syndrome protein in response to DNA damage. *The Journal of cell biology* 153(2), pp. 367–380.

30. Bisht, P., Kumar, V.U., Pandey, R., Velayutham, R. and Kumar, N. 2022. Role of PARP Inhibitors in Glioblastoma and Perceiving Challenges as Well as Strategies for Successful Clinical Development. *Frontiers in pharmacology* 13, p. 939570.

31. Bohr, V.A. 2008. Rising from the RecQ-age: the role of human RecQ helicases in genome maintenance. *Trends in biochemical sciences* 33(12), pp. 609–620.

32. Bojko, A., Czarnecka-Herok, J., Charzynska, A., Dabrowski, M. and Sikora, E. 2019. Diversity of the Senescence Phenotype of Cancer Cells Treated with Chemotherapeutic Agents. *Cells* 8(12).

33. Bouquet, F., Muller, C. and Salles, B. 2006. The Loss of &gamma;H2AX Signal is a Marker of DNA Double Strand Breaks Repair Only at Low Levels of DNA Damage. *Cell Cycle* 5(10), pp. 1116–1122.

34. Brachet, P.E. et al. 2017. A GINECO phase II study of Navitoclax (ABT 263) in women with platinum resistant/refractory recurrent ovarian cancer (ROC). *Annals of Oncology* 28, p. v347.

35. Brosh, R.M. and Matson, S.W. 2020. History of DNA Helicases. *Genes* 11(3).

36. Bryan, T.M., Englezou, A., Gupta, J., Bacchetti, S. and Reddel, R.R. 1995. Telomere elongation in immortal human cells without detectable telomerase activity. *The EMBO journal* 14(17), pp. 4240–4248.

37. Bryant, H.E. et al. 2005. Specific killing of BRCA2-deficient tumours with inhibitors of poly(ADP-ribose) polymerase. *Nature* 434(7035), pp. 913–917.

38. von Bueren, A.O. et al. 2012. Mismatch repair deficiency: a temozolomide resistance factor in medulloblastoma cell lines that is uncommon in primary medulloblastoma tumours. *British Journal of Cancer* 107(8), pp. 1399–1408.

39. Bythell-Douglas, R. and Deans, A.J. 2021. A Structural Guide to the Bloom Syndrome Complex. *Structure* 29(2), pp. 99–113.

40. Caccese, M. et al. 2020. Mismatch-Repair Protein Expression in High-Grade Gliomas: A Large Retrospective Multicenter Study. *International Journal of Molecular Sciences* 21(18).

41. Caldecott, K.W. 2008. Single-strand break repair and genetic disease. *Nature reviews. Genetics* 9(8), pp. 619–631.

42. Caron, M.-C. et al. 2019. Poly(ADP-ribose) polymerase-1 antagonizes DNA resection at double-strand breaks. *Nature Communications* 10(1), p. 2954.

43. Chan, K.-L., North, P.S. and Hickson, I.D. 2007. BLM is required for faithful chromosome segregation and its localization defines a class of ultrafine anaphase bridges. *The EMBO Journal* 26(14), pp. 3397–3409.

44. Chandrashekar, D.S., Bashel, B., Balasubramanya, S.A.H., Creighton, C.J., Ponce-Rodriguez, I., Chakravarthi, B.V.S.K. and Varambally, S. 2017. UALCAN: A Portal for Facilitating Tumor Subgroup Gene Expression and Survival Analyses. *Neoplasia (New York, N.Y.)* 19(8), pp. 649–658.

45. Chang, J. et al. 2016. Clearance of senescent cells by ABT263 rejuvenates aged hematopoietic stem cells in mice. *Nature Medicine* 22(1), pp. 78–83.

46. Chen, J. et al. 2019. Polyploid Giant Cancer Cells (PGCCs): The Evil Roots of Cancer. *Current cancer drug targets* 19(5), pp. 360–367.

47. Chen, X. et al. 2021. Uncovering an allosteric mode of action for a selective inhibitor of human Bloom syndrome protein. Carter, A. P. and Wolberger, C. eds. *eLife* 10, p. e65339.

48. Chester, N., Kuo, F., Kozak, C., O'Hara, C.D. and Leder, P. 1998. Stage-specific apoptosis, developmental delay, and embryonic lethality in mice homozygous for a targeted disruption in the murine Bloom's syndrome gene. *Genes & development* 12(21), pp. 3382–3393.

49. Chi, Z. et al. 2012. RecQL4 cytoplasmic localization: Implications in mitochondrial DNA oxidative damage repair. *The International Journal of Biochemistry & Cell Biology* 44(11), pp. 1942–1951.

50. Chien, C.-H., Hsueh, W.-T., Chuang, J.-Y. and Chang, K.-Y. 2021. Dissecting the mechanism of temozolomide resistance and its association with the regulatory roles of intracellular reactive oxygen species in glioblastoma. *Journal of Biomedical Science* 28(1), p. 18.

51. Chien, Y. et al. 2011. Control of the senescence-associated secretory phenotype by NF-κB promotes senescence and enhances chemosensitivity. *Genes & development* 25(20), pp. 2125–2136.

52. Childs, B.G., Durik, M., Baker, D.J. and van Deursen, J.M. 2015. Cellular

senescence in aging and age-related disease: from mechanisms to therapy. *Nature Medicine* 21(12), pp. 1424–1435.

53. Choi, S., Yu, Y., Grimmer, M.R., Wahl, M., Chang, S.M. and Costello, J.F. 2018. Temozolomide-associated hypermutation in gliomas. *Neuro-Oncology* 20(10), pp. 1300–1309.

54. Chu, W.K. and Hickson, I.D. 2009. RecQ helicases: multifunctional genome caretakers. *Nature Reviews Cancer* 9(9), pp. 644–654.

55. Ciechomska, I.A. et al. 2023. Exploring Novel Therapeutic Opportunities for Glioblastoma Using Patient-Derived Cell Cultures. *Cancers* 15(5).

56. Collado, M. and Serrano, M. 2010. Senescence in tumours: evidence from mice and humans. *Nature Reviews Cancer* 10(1), pp. 51–57.

57. Coppé, J.-P. et al. 2008. Senescence-Associated Secretory Phenotypes Reveal Cell-Nonautonomous Functions of Oncogenic RAS and the p53 Tumor Suppressor. *PLOS Biology* 6(12), p. e301.

58. Cordin, O., Banroques, J., Tanner, N.K. and Linder, P. 2006. The DEAD-box protein family of RNA helicases. *Gene* 367, pp. 17–37.

59. Croteau, D.L. et al. 2012. RECQL4 localizes to mitochondria and preserves mitochondrial DNA integrity. *Aging Cell* 11(3), pp. 456–466.

60. Croteau, D.L., Popuri, V., Opresko, P.L. and Bohr, V.A. 2014. Human RecQ Helicases in DNA Repair, Recombination, and Replication. *Annual Review of Biochemistry* 83(1), pp. 519–552.

61. Cunniff, C., Bassetti, J.A. and Ellis, N.A. 2017. Bloom's Syndrome: Clinical Spectrum, Molecular Pathogenesis, and Cancer Predisposition. *Molecular Syndromology* 8(1), pp. 4–23.

62. Czarnecka-Herok, J. et al. 2022. Therapy-Induced Senescent/Polyploid Cancer Cells Undergo Atypical Divisions Associated with Altered Expression of Meiosis, Spermatogenesis and EMT Genes. *International Journal of Molecular Sciences* 23(15).

63. Daley, J.M., Chiba, T., Xue, X., Niu, H. and Sung, P. 2014. Multifaceted role of the Topo IIIα–RMI1-RMI2 complex and DNA2 in the BLM-dependent pathway of DNA break end resection. *Nucleic Acids Research* 42(17), pp. 11083–11091.

64. Datta, A. and Brosh, R.M. 2018. New Insights Into DNA Helicases as Druggable Targets for Cancer Therapy. *Frontiers in Molecular Biosciences* 5.

65. Davies, S.L., North, P.S., Dart, A., Lakin, N.D. and Hickson, I.D. 2004. Phosphorylation of the Bloom's syndrome helicase and its role in recovery from S-phase arrest. *Molecular and cellular biology* 24(3), pp. 1279–1291.

66. De, S. et al. 2012. RECQL4 is essential for the transport of p53 to mitochondria in normal human cells in the absence of exogenous stress. *Journal of Cell Science* 125(10), pp. 2509–2522.

67. Demaria, M. et al. 2014. An essential role for senescent cells in optimal wound healing through secretion of PDGF-AA. *Developmental cell* 31(6), pp. 722–733.

68. Demaria, M. et al. 2017. Cellular Senescence Promotes Adverse Effects of Chemotherapy and Cancer Relapse. *Cancer Discovery* 7(2), pp. 165–176.

69. Dietlein, F., Thelen, L. and Reinhardt, H.C. 2014. Cancer-specific defects in DNA repair pathways as targets for personalized therapeutic approaches. *Trends in genetics : TIG* 30(8), pp. 326–339.

70. Dietschy, T. et al. 2009. p300-mediated acetylation of the Rothmund-Thomson-syndrome gene product RECQL4 regulates its subcellular

localization. *Journal of Cell Science* 122(8), pp. 1258–1267.

71. Dikovskaya, D. et al. 2015. Mitotic Stress Is an Integral Part of the Oncogene-Induced Senescence Program that Promotes Multinucleation and Cell Cycle Arrest. *Cell Reports* 12(9), pp. 1483–1496.

72. Dong, F., Soubeyrand, S. and Haché, R.J.G. 2010. Activation of PARP-1 in response to bleomycin depends on the Ku antigen and protein phosphatase 5. *Oncogene* 29(14), pp. 2093–2103.

73. Drosopoulos, W.C., Kosiyatrakul, S.T. and Schildkraut, C.L. 2015. BLM helicase facilitates telomere replication during leading strand synthesis of telomeres. *Journal of Cell Biology* 210(2), pp. 191–208.

74. Du, K., Xia, Q., Heng, H. and Feng, F. 2020. Temozolomide-Doxorubicin Conjugate as a Double Intercalating Agent and Delivery by Apoferritin for Glioblastoma Chemotherapy. *ACS applied materials & interfaces* 12(31), pp. 34599–34609.

75. Du, X. et al. 2021. High BLM Expression Predicts Poor Clinical Outcome and Contributes to Malignant Progression in Human Cholangiocarcinoma. *Frontiers in Oncology* 11.

76. Duan, S., Han, X., Akbari, M., Croteau, D.L., Rasmussen, L.J. and Bohr, V.A. 2020. Interaction between RECQL4 and OGG1 promotes repair of oxidative base lesion 8-oxoG and is regulated by SIRT1 deacetylase. *Nucleic Acids Research* 48(12), pp. 6530–6546.

77. Eladad, S., Ye, T.-Z., Hu, P., Leversha, M., Beresten, S., Matunis, M.J. and Ellis, N.A. 2005. Intra-nuclear trafficking of the BLM helicase to DNA damage-induced foci is regulated by SUMO modification. *Human Molecular Genetics* 14(10), pp. 1351–1365.

78. Ellert-Miklaszewska, A., Ciechomska, I.A. and Kaminska, B. 2021. Synthetic Cannabinoids Induce Autophagy and Mitochondrial Apoptotic Pathways in Human Glioblastoma Cells Independently of Deficiency in TP53 or PTEN Tumor Suppressors. *Cancers* 13(3).

79. Erenpreisa, J. et al. 2005. Segregation of genomes in polyploid tumour cells following mitotic catastrophe. *Cell Biology International* 29(12), pp. 1005–1011.

80. Erenpreisa, J., Salmina, K., Huna, A., Kosmacek, E.A., Cragg, M.S., Ianzini, F. and Anisimov, A.P. 2011. Polyploid tumour cells elicit paradiploid progeny through depolyploidizing divisions and regulated autophagic degradation. *Cell Biology International* 35(7), pp. 687–695.

81. Erenpreisa, J.A., Cragg, M.S., Fringes, B., Sharakhov, I. and Illidge, T.M. 2000. RELEASE OF MITOTIC DESCENDANTS BY GIANT CELLS FROM IRRADIATED BURKITT'S LYMPHOMA CELL LINES. *Cell Biology International* 24(9), pp. 635–648.

82. Erice, O. et al. 2015. MGMT Expression Predicts PARP-Mediated Resistance to Temozolomide. *Molecular cancer therapeutics* 14(5), pp. 1236–1246.

83. Ewald, J.A., Desotelle, J.A., Wilding, G. and Jarrard, D.F. 2010. Therapy-induced senescence in cancer. *Journal of the National Cancer Institute* 102(20), pp. 1536–1546.

84. Fagagna, F. d'Adda di et al. 2003. A DNA damage checkpoint response in telomere-initiated senescence. *Nature* 426(6963), pp. 194–198.

85. Farmer, H. et al. 2005. Targeting the DNA repair defect in BRCA mutant cells as a therapeutic strategy. *Nature* 434(7035), pp. 917–921.

86. Fei, F. et al. 2015. The number of polyploid giant cancer cells and epithelial-mesenchymal transition-related proteins are associated

with invasion and metastasis in human breast cancer. *Journal of Experimental & Clinical Cancer Research* 34(1), p. 158.

87. Feldheim, J., Kessler, A.F., Monoranu, C.M., Ernestus, R.-I., Löhr, M. and Hagemann, C. 2019. Changes of O6-Methylguanine DNA Methyltransferase (MGMT) Promoter Methylation in Glioblastoma Relapse—A Meta-Analysis Type Literature Review. *Cancers* 11(12).

88. Fizazi, K. et al. 2023. Rucaparib or Physician's Choice in Metastatic Prostate Cancer. *New England Journal of Medicine* 388(8), pp. 719–732.

89. Fleury, H. et al. 2019. Exploiting interconnected synthetic lethal interactions between PARP inhibition and cancer cell reversible senescence. *Nature Communications* 10(1), p. 2556.

90. Freund, A., Laberge, R.-M., Demaria, M. and Campisi, J. 2012. Lamin B1 loss is a senescence-associated biomarker. *Molecular Biology of the Cell* 23(11), pp. 2066–2075.

91. Freund, A., Patil, C.K. and Campisi, J. 2011. p38MAPK is a novel DNA damage response-independent regulator of the senescence-associated secretory phenotype. *The EMBO journal* 30(8), pp. 1536–1548.

92. Fu, Y., Foden, J.A., Khayter, C., Maeder, M.L., Reyon, D., Joung, J.K. and Sander, J.D. 2013. High-frequency off-target mutagenesis induced by CRISPR-Cas nucleases in human cells. *Nature Biotechnology* 31(9), pp. 822–826.

93. Fulton, B. et al. 2017. PARADIGM-2: Two parallel phase I studies of olaparib and radiotherapy or olaparib and radiotherapy plus temozolomide in patients with newly diagnosed glioblastoma, with treatment stratified by MGMT status. *Clinical and translational radiation oncology* 8, pp. 12–16.

94. Gao, X. et al. 2019. Berberine attenuates XRCC1-mediated base excision repair and sensitizes breast cancer cells to the chemotherapeutic drugs. *Journal of Cellular and Molecular Medicine* 23(10), pp. 6797–6804.

95. García, S. and Conde, C. 2015. The Role of Poly(ADP-ribose) Polymerase-1 in Rheumatoid Arthritis. *Mediators of inflammation* 2015, p. 837250.

96. Garner, E., Kim, Y., Lach, F.P., Kottemann, M.C. and Smogorzewska, A. 2013. Human GEN1 and the SLX4-associated nucleases MUS81 and SLX1 are essential for the resolution of replication-induced Holliday junctions. *Cell reports* 5(1), pp. 207–215.

97. Gaymes, T.J., North, P.S., Brady, N., Hickson, I.D., Mufti, G.J. and Rassool, F. V 2002. Increased error-prone non homologous DNA end-joining – a proposed mechanism of chromosomal instability in Bloom's syndrome. *Oncogene* 21(16), pp. 2525–2533.

98. German, J. 1997. Bloom's syndrome. XX. The first 100 cancers. *Cancer Genetics and Cytogenetics* 93(1), pp. 100–106.

99. German, J., Archibald, R. and Bloom, D. 1965. Chromosomal Breakage in a Rare and Probably Genetically Determined Syndrome of Man. *Science* 148(3669), pp. 506–507.

100. German, J., Crippa, L.P. and Bloom, D. 1974. Bloom's syndrome. III. Analysis of the chromosome aberration characteristic of this disorder. *Chromosoma* 48(4), pp. 361–366.

101. German, J., Sanz, M.M., Ciocci, S., Ye, T.Z. and Ellis, N.A. 2007. Syndrome-causing mutations of the BLM gene in persons in the Bloom's Syndrome Registry. *Human Mutation* 28(8), pp. 743–753.

102. Germani, F., Bergantinos, C. and Johnston, L.A. 2018. Mosaic Analysis in Drosophila. *Genetics* 208(2), pp. 473–490.

103. Germano, I., Swiss, V. and Casaccia, P. 2010. Primary brain tumors, neural stem cell, and brain tumor cancer cells: where is the link? *Neuropharmacology* 58(6), pp. 903–910.

104. Gong, T., Jia, B., Gu, L. and Yu, T. 2022. KLF5-trancripted miR-125b-5p is involved in enhancing the radio-sensitivity of breast cancer cells by targeting BRCA1. *Molecular & Cellular Toxicology* 18(1), pp. 101–110.

105. González-Gualda, E., Baker, A.G., Fruk, L. and Muñoz-Espín, D. 2021. A guide to assessing cellular senescence in vitro and in vivo. *The FEBS journal* 288(1), pp. 56–80.

106. Gorbalenya, A.E. and Koonin, E. V 1993. Helicases: amino acid sequence comparisons and structure-function relationships. *Current Opinion in Structural Biology* 3(3), pp. 419–429.

107. Goundiam, O. and Basto, R. 2021. Centrosomes in disease: how the same music can sound so different? *Current opinion in structural biology* 66, pp. 74–82.

108. Groden, J. and German, J. 1992. Bloom's syndrome. *Human Genetics* 90(4), pp. 360–367.

109. Guille, M. 1999. Microinjection into Xenopus Oocytes and Embryos BT - Molecular Methods in Developmental Biology: Xenopus and Zebrafish. In: Guille, M. ed. Totowa, NJ: Humana Press, pp. 111–123.

110. Guo, R., Rigolet, P., Zargarian, L., Fermandjian, S. and Xi, X.G. 2005. Structural and functional characterizations reveal the importance of a zinc binding domain in Bloom's syndrome helicase. *Nucleic Acids Research* 33(10), pp. 3109–3124.

111. Gupta, S., De, S., Srivastava, V., Hussain, M., Kumari, J., Muniyappa, K. and Sengupta, S. 2014. RECQL4 and p53 potentiate the activity of polymerase γ and maintain the integrity of the human mitochondrial genome. *Carcinogenesis* 35(1), pp. 34–45.

112. Haince, J.-F., McDonald, D., Rodrigue, A., Déry, U., Masson, J.-Y., Hendzel, M.J. and Poirier, G.G. 2008. PARP1-dependent Kinetics of Recruitment of MRE11 and NBS1 Proteins to Multiple DNA Damage Sites*. *Journal of Biological Chemistry* 283(2), pp. 1197–1208.

113. Han, Z. et al. 2002. Role of p21 in Apoptosis and Senescence of Human Colon Cancer Cells Treated with Camptothecin*. *Journal of Biological Chemistry* 277(19), pp. 17154–17160.

114. Happold, C. et al. 2012. Distinct molecular mechanisms of acquired resistance to temozolomide in glioblastoma cells. *Journal of Neurochemistry* 122(2), pp. 444–455.

115. Hayakawa, S., Kaneko, H., Fukao, T., Kasahara, K., Matsumoto, T., Furuichi, Y. and Kondo, N. 2000. Characterization of the nuclear localization signal in the DNA helicase responsible for Bloom syndrome. *Int J Mol Med* 5(5), pp. 477–561.

116. HAYFLICK, L. and MOORHEAD, P.S. 1961. The serial cultivation of human diploid cell strains. *Experimental cell research* 25, pp. 585–621.

117. He, S. and Sharpless, N.E. 2017. Senescence in Health and Disease. *Cell* 169(6), pp. 1000–1011.

118. Heerma van Voss, M.R., van Diest, P.J. and Raman, V. 2017. Targeting RNA helicases in cancer: The translation trap. *Biochimica et biophysica acta. Reviews on cancer* 1868(2), pp. 510–520.

119. Henson, J.D. and Reddel, R.R. 2010. Assaying and investigating Alternative Lengthening of Telomeres activity in human cells and cancers. *FEBS*

*Letters* 584(17), pp. 3800–3811.

120. Hernandez-Segura, A., Nehme, J. and Demaria, M. 2018. Hallmarks of Cellular Senescence. *Trends in Cell Biology* 28(6), pp. 436–453.

121. Herranz, N. and Gil, J. 2016. Mitochondria and senescence: new actors for an old play. *The EMBO Journal* 35(7), pp. 701–702.

122. Higuchi, F., Nagashima, H., Ning, J., Koerner, M.V.A., Wakimoto, H. and Cahill, D.P. 2020. Restoration of Temozolomide Sensitivity by PARP Inhibitors in Mismatch Repair Deficient Glioblastoma is Independent of Base Excision Repair. *Clinical Cancer Research* 26(7), pp. 1690–1699.

123. Hoki, Y. et al. 2003. Growth retardation and skin abnormalities of the Recql4 -deficient mouse. *Human Molecular Genetics* 12(18), pp. 2293–2299.

124. Holloway, J.K., Morelli, M.A., Borst, P.L. and Cohen, P.E. 2010. Mammalian BLM helicase is critical for integrating multiple pathways of meiotic recombination. *Journal of Cell Biology* 188(6), pp. 779–789.

125. Hu, W., Sung, T., Jessen, B.A., Thibault, S., Finkelstein, M.B., Khan, N.K. and Sacaan, A.I. 2016. Mechanistic Investigation of Bone Marrow Suppression Associated with Palbociclib and its Differentiation from Cytotoxic Chemotherapies. *Clinical Cancer Research* 22(8), pp. 2000–2008.

126. Hunia, J., Gawalski, K., Szredzka, A., Suskiewicz, M.J. and Nowis, D. 2022. The potential of PARP inhibitors in targeted cancer therapy and immunotherapy. *Frontiers in molecular biosciences* 9, p. 1073797.

127. Hunter, C. et al. 2006. A hypermutation phenotype and somatic MSH6 mutations in recurrent human malignant gliomas after alkylator chemotherapy. *Cancer research* 66(8), pp. 3987–3991.

128. Ichikawa, K., Noda, T. and Furuichi, Y. 2002. [Preparation of the gene targeted knockout mice for human premature aging diseases, Werner syndrome, and Rothmund-Thomson syndrome caused by the mutation of DNA helicases]. *Nihon yakurigaku zasshi. Folia pharmacologica Japonica* 119(4), pp. 219–226.

129. Ivancich, M., Schrank, Z., Wojdyla, L., Leviskas, B., Kuckovic, A., Sanjali, A. and Puri, N. 2017. Treating Cancer by Targeting Telomeres and Telomerase. *Antioxidants* 6(1).

130. Ivanov, A., Cragg, M.S., Erenpreisa, J., Emzinsh, D., Lukman, H. and Illidge, T.M. 2003. Endopolyploid cells produced after severe genotoxic damage have the potential to repair DNA double strand breaks. *Journal of Cell Science* 116(20), pp. 4095–4106.

131. Jackson, T.R. et al. 2013. DNA damage causes TP53-dependent coupling of self-renewal and senescence pathways in embryonal carcinoma cells. *Cell Cycle* 12(3), pp. 430–441.

132. Jankowsky, E. and Fairman-Williams, M.E. 2010. Chapter 1 An Introduction to RNA Helicases: Superfamilies, Families, and Major Themes. In: *RNA Helicases*. The Royal Society of Chemistry, pp. 1–31.

133. Jia, S., Xu, X., Zhou, S., Chen, Y., Ding, G. and Cao, L. 2019. Fisetin induces autophagy in pancreatic cancer cells via endoplasmic reticulum stress- and mitochondrial stress-dependent pathways. *Cell Death & Disease* 10(2), p. 142.

134. Jiapaer, S., Furuta, T., Tanaka, S., Kitabayashi, T. and Nakada, M. 2018. Potential Strategies Overcoming the Temozolomide Resistance for Glioblastoma. *Neurologia medico-chirurgica* 58(10), pp. 405–421.

135. Jiricny, J. 2006. The multifaceted mismatch-repair system. *Nature Reviews Molecular Cell Biology* 7(5), pp. 335–346.

136. Johnson, B.E. et al. 2014. Mutational analysis reveals the origin and therapy-driven evolution of recurrent glioma. *Science (New York, N.Y.)* 343(6167), pp. 189–193.

137. Jue, T.R. et al. 2017. Veliparib in combination with radiotherapy for the treatment of MGMT unmethylated glioblastoma. *Journal of translational medicine* 15(1), p. 61.

138. Kalathur, M. et al. 2015. A chemogenomic screening identifies CK2 as a target for pro-senescence therapy in PTEN-deficient tumours. *Nature Communications* 6(1), p. 7227.

139. Kaneko, H. et al. 1997. BLM (the causative gene of Bloom syndrome) protein translocation into the nucleus by a nuclear localization signal. *Biochemical and biophysical research communications* 240(2), pp. 348–353.

140. Kang, M., Park, S., Park, S.-H., Lee, H.G. and Park, J.H. 2022. A Double-Edged Sword: The Two Faces of PARylation. *International journal of molecular sciences* 23(17).

141. Kang, T.-W. et al. 2011. Senescence surveillance of pre-malignant hepatocytes limits liver cancer development. *Nature* 479(7374), pp. 547–551.

142. Karmakar, P. et al. 2006. BLM is an early responder to DNA double-strand breaks. *Biochemical and Biophysical Research Communications* 348(1), pp. 62–69.

143. Kaur, E., Agrawal, R. and Sengupta, S. 2021. Functions of BLM Helicase in Cells: Is It Acting Like a Double-Edged Sword?. *Frontiers in Genetics* 12.

144. Kern, S.E., Pietenpol, J.A., Thiagalingam, S., Seymour, A., Kinzler, K.W. and Vogelstein, B. 1992. Oncogenic forms of p53 inhibit p53-regulated gene expression. *Science (New York, N.Y.)* 256(5058), pp. 827–830.

145. Killoran, M.P. and Keck, J.L. 2006. Sit down, relax and unwind: structural insights into RecQ helicase mechanisms. *Nucleic Acids Research* 34(15), pp. 4098–4105.

146. Kitao, S., Ohsugi, I., Ichikawa, K., Goto, M., Furuichi, Y. and Shimamoto, A. 1998. Cloning of Two New Human Helicase Genes of the RecQ Family: Biological Significance of Multiple Species in Higher Eukaryotes. *Genomics* 54(3), pp. 443–452.

147. Knizhnik, A. V, Roos, W.P., Nikolova, T., Quiros, S., Tomaszowski, K.-H., Christmann, M. and Kaina, B. 2013. Survival and Death Strategies in Glioma Cells: Autophagy, Senescence and Apoptosis Triggered by a Single Type of Temozolomide-Induced DNA Damage. *PLOS ONE* 8(1), p. e55665.

148. Knöfler, M., Haider, S., Saleh, L., Pollheimer, J., Gamage, T.K.J.B. and James, J. 2019. Human placenta and trophoblast development: key molecular mechanisms and model systems. *Cellular and molecular life sciences : CMLS* 76(18), pp. 3479–3496.

149. Koczor, C.A. et al. 2021. Temporal dynamics of base excision/single-strand break repair protein complex assembly/disassembly are modulated by the PARP/NAD(+)/SIRT6 axis. *Cell reports* 37(5), p. 109917.

150. Kong, Y. et al. 2021. BLM helicase inhibition synergizes with PARP inhibition to improve the radiosensitivity of olaparib resistant non-small cell lung cancer cells by inhibiting homologous recombination repair.

*Cancer biology & medicine* 19(8), pp. 1150–1171.

151. Koussounadis, A., Langdon, S.P., Um, I.H., Harrison, D.J. and Smith, V.A. 2015. Relationship between differentially expressed mRNA and mRNA-protein correlations in a xenograft model system. *Scientific Reports* 5(1), p. 10775.

152. Krokan, H.E. and Bjørås, M. 2013. Base excision repair. *Cold Spring Harbor perspectives in biology* 5(4), p. a012583.

153. Król, S.K. et al. 2020. Aberrantly expressed recql4 helicase supports proliferation and drug resistance of human glioma cells and glioma stem cells. *Cancers* 12(10).

154. Krtolica, A., Parrinello, S., Lockett, S., Desprez, P.Y. and Campisi, J. 2001. Senescent fibroblasts promote epithelial cell growth and tumorigenesis: a link between cancer and aging. *Proceedings of the National Academy of Sciences of the United States of America* 98(21), pp. 12072–12077.

155. Krüger, A., Bürkle, A., Hauser, K. and Mangerich, A. 2020. Real-time monitoring of PARP1-dependent PARylation by ATR-FTIR spectroscopy. *Nature communications* 11(1), p. 2174.

156. Kuffer, C., Kuznetsova, A.Y. and Storchová, Z. 2013. Abnormal mitosis triggers p53-dependent cell cycle arrest in human tetraploid cells. *Chromosoma* 122(4), pp. 305–318.

157. Kumar, V., Kumar, A., Mir, K.U.I., Yadav, V. and Chauhan, S.S. 2022. Pleiotropic role of PARP1: an overview. *3 Biotech* 12(1), p. 3.

158. Laberge, R.-M. et al. 2015. MTOR regulates the pro-tumorigenic senescence-associated secretory phenotype by promoting IL1A translation. *Nature cell biology* 17(8), pp. 1049–1061.

159. Lakens, D. 2013. Calculating and reporting effect sizes to facilitate cumulative science: a practical primer for t-tests and ANOVAs. *Frontiers in Psychology* 4, p. 863.

160. Lamborn, K.R. et al. 2008. Progression-free survival: An important end point in evaluating therapy for recurrent high-grade gliomas. *Neuro-Oncology* 10(2), pp. 162–170.

161. Langlois, R.G., Bigbee, W.L., Jensen, R.H. and German, J. 1989. Evidence for increased in vivo mutation and somatic recombination in Bloom's syndrome. *Proceedings of the National Academy of Sciences* 86(2), pp. 670–674.

162. Lau, L., Porciuncula, A., Yu, A., Iwakura, Y. and David, G. 2019. Uncoupling the Senescence-Associated Secretory Phenotype from Cell Cycle Exit via Interleukin-1 Inactivation Unveils Its Protumorigenic Role. *Molecular and cellular biology* 39(12).

163. Lee, B.Y. et al. 2006. Senescence-associated beta-galactosidase is lysosomal beta-galactosidase. *Aging cell* 5(2), pp. 187–195.

164. Lee, J.-J., Kim, B.C., Park, M.-J., Lee, Y.-S., Kim, Y.-N., Lee, B.L. and Lee, J.-S. 2011. PTEN status switches cell fate between premature senescence and apoptosis in glioma exposed to ionizing radiation. *Cell death and differentiation* 18(4), pp. 666–677.

165. Lee, J.W., Harrigan, J., Opresko, P.L. and Bohr, V.A. 2005. Pathways and functions of the Werner syndrome protein. *Mechanisms of Ageing and Development* 126(1), pp. 79–86.

166. Lee, S. et al. 2021. Virus-induced senescence is a driver and therapeutic target in COVID-19. *Nature* 599(7884), pp. 283–289.

167. Leontieva, O. V, Demidenko, Z.N. and Blagosklonny, M. V 2014. Contact inhibition and high cell density deactivate the mammalian target

of rapamycin pathway, thus suppressing the senescence program. *Proceedings of the National Academy of Sciences* 111(24), pp. 8832–8837.

168. Lesueur, P. et al. 2019. Phase I/IIa study of concomitant radiotherapy with olaparib and temozolomide in unresectable or partially resectable glioblastoma: OLA-TMZ-RTE-01 trial protocol. *BMC Cancer* 19, p. NA.

169. Li, F. et al. 2020a. FBP1 loss disrupts liver metabolism and promotes tumorigenesis through a hepatic stellate cell senescence secretome. *Nature Cell Biology* 22(6), pp. 728–739.

170. Li, J. et al. 2018. Fisetin Inhibited Growth and Metastasis of Triple-Negative Breast Cancer by Reversing Epithelial-to-Mesenchymal Transition via PTEN/Akt/GSK3β Signal Pathway. *Frontiers in pharmacology* 9, p. 772.

171. Li, J., Bi, Z., Wang, L., Xia, Y., Xie, Y. and Liu, Y. 2023. Recent Advances in Strategies for Imaging Detection and Intervention of Cellular Senescence. *ChemBioChem* 24(1), p. e202200364.

172. Li, L.-Y., Guan, Y., Chen, X.-S., Yang, J.-M. and Cheng, Y. 2020b. DNA Repair Pathways in Cancer Therapy and Resistance. *Frontiers in pharmacology* 11, p. 629266.

173. Li, M. and Yu, X. 2013. Function of BRCA1 in the DNA Damage Response Is Mediated by ADP-Ribosylation. *Cancer Cell* 23(5), pp. 693–704.

174. Li, X. and Heyer, W.-D. 2008. Homologous recombination in DNA repair and DNA damage tolerance. *Cell Research* 18(1), pp. 99–113.

175. Lima, F.R.S. et al. 2012. Glioblastoma: therapeutic challenges, what lies ahead. *Biochimica et biophysica acta* 1826(2), pp. 338–349.

176. Liu, C., Vyas, A., Kassab, M.A., Singh, A.K. and Yu, X. 2017. The role of poly ADP-ribosylation in the first wave of DNA damage response. *Nucleic acids research* 45(14), pp. 8129–8141.

177. Liu, G. et al. 2018. Clinical characteristics and preliminary morphological observation of 47 cases of primary anorectal malignant melanomas. *Melanoma research* 28(6), pp. 592–599.

178. Liu, L.-L. et al. 2013. Inhibition of mTOR Pathway Sensitizes Acute Myeloid Leukemia Cells to Aurora Inhibitors by Suppression of Glycolytic Metabolism. *Molecular Cancer Research* 11(11), pp. 1326–1336.

179. Liu, X. et al. 2012. Iniparib nonselectively modifies cysteine-containing proteins in tumor cells and is not a bona fide PARP inhibitor. *Clinical cancer research : an official journal of the American Association for Cancer Research* 18(2), pp. 510–523.

180. Lloyd, A.C. 2013. The Regulation of Cell Size. *Cell* 154(6), pp. 1194–1205.

181. Lopez-Beltran, A., Eble, J.N. and Bostwick, D.G. 2005. Pleomorphic giant cell carcinoma of the prostate. *Archives of pathology & laboratory medicine* 129(5), pp. 683–685.

182. Lopez-Sánchez, L.M. et al. 2014. CoCl2, a Mimic of Hypoxia, Induces Formation of Polyploid Giant Cells with Stem Characteristics in Colon Cancer. *PLOS ONE* 9(6), p. e99143.

183. Lord, C.J. and Ashworth, A. 2017. PARP inhibitors: Synthetic lethality in the clinic. *Science (New York, N.Y.)* 355(6330), pp. 1152–1158.

184. Louis, D.N. et al. 2021. The 2021 WHO Classification of Tumors of the Central Nervous System: a summary. *Neuro-oncology* 23(8), pp. 1231–1251.

185. Lu, H. et al. 2016. RECQL4 Promotes DNA End Resection in Repair of DNA Double-Strand Breaks. *Cell Reports* 16(1), pp. 161–173.

186. Lu, H. et al. 2017a. Cell cycle-dependent phosphorylation regulates RECQL4

pathway choice and ubiquitination in DNA double-strand break repair. *Nature Communications* 8(1), p. 2039.

187. Lu, Y. et al. 2017b. Chemosensitivity of IDH1-Mutated Gliomas Due to an Impairment in PARP1-Mediated DNA Repair. *Cancer research* 77(7), pp. 1709–1718.

188. Luijsterburg, M.S. et al. 2012. DDB2 promotes chromatin decondensation at UV-induced DNA damage. *The Journal of cell biology* 197(2), pp. 267–281.

189. Luo, G. et al. 2000. Cancer predisposition caused by elevated mitotic recombination in Bloom mice. *Nature Genetics* 26(4), pp. 424–429.

190. Luong, T.T. and Bernstein, K.A. 2021. Role and Regulation of the RECQL4 Family during Genomic Integrity Maintenance. *Genes* 12(12).

191. Lv, H. et al. 2014. Polyploid giant cancer cells with budding and the expression of cyclin E, S-phase kinase-associated protein 2, stathmin associated with the grading and metastasis in serous ovarian tumor. *BMC cancer* 14, p. 576.

192. M, A., Xavier, J., A S, F., Bisht, P., Murti, K., Ravichandiran, V. and Kumar, N. 2023. Epigenetic basis for PARP mutagenesis in glioblastoma: A review. *European Journal of Pharmacology* 938, p. 175424.

193. Machlus, K.R. and Italiano, J.E.J. 2013. The incredible journey: From megakaryocyte development to platelet formation. *The Journal of cell biology* 201(6), pp. 785–796.

194. Maltseva, E.A., Rechkunova, N.I., Sukhanova, M. V and Lavrik, O.I. 2015. Poly(ADP-ribose) Polymerase 1 Modulates Interaction of the Nucleotide Excision Repair Factor XPC-RAD23B with DNA via Poly(ADP-ribosyl)ation. *The Journal of biological chemistry* 290(36), pp. 21811–21820.

195. Mao, K. and Zhang, G. 2022. The role of PARP1 in neurodegenerative diseases and aging. *The FEBS journal* 289(8), pp. 2013–2024.

196. Mao, Z., Bozzella, M., Seluanov, A. and Gorbunova, V. 2008. DNA repair by nonhomologous end joining and homologous recombination during cell cycle in human cells. *Cell Cycle* 7(18), pp. 2902–2906.

197. Masumoto, H., Muramatsu, S., Kamimura, Y. and Araki, H. 2002. S-Cdk-dependent phosphorylation of Sld2 essential for chromosomal DNA replication in budding yeast. *Nature* 415(6872), pp. 651–655.

198. Mateo, J., Ong, M., Tan, D.S.P., Gonzalez, M.A. and de Bono, J.S. 2013. Appraising iniparib, the PARP inhibitor that never was--what must we learn? *Nature reviews. Clinical oncology* 10(12), pp. 688–696.

199. Maxwell, J.A. et al. 2008. Mismatch repair deficiency does not mediate clinical resistance to temozolomide in malignant glioma. *Clinical cancer research : an official journal of the American Association for Cancer Research* 14(15), pp. 4859–4868.

200. McDaniel, L.D., Chester, N., Watson, M., Borowsky, A.D., Leder, P. and Schultz, R.A. 2003. Chromosome instability and tumor predisposition inversely correlate with BLM protein levels. *DNA Repair* 2(12), pp. 1387–1404.

201. Medagli, B. and Onesti, S. 2013. Structure and Mechanism of Hexameric Helicases BT - DNA Helicases and DNA Motor Proteins. In: Spies, M. ed. New York, NY: Springer New York, pp. 75–95.

202. Metscher, B.D. 2009. MicroCT for comparative morphology: simple staining methods allow high-contrast 3D imaging of diverse non-mineralized animal tissues. *BMC Physiology* 9(1), p. 11.

203. Di Micco, R. et al. 2011. Interplay between oncogene-induced DNA damage

response and heterochromatin in senescence and cancer. *Nature Cell Biology* 13(3), pp. 292–302.

204.  Mimitou, E.P. and Symington, L.S. 2009. Nucleases and helicases take center stage in homologous recombination. *Trends in Biochemical Sciences* 34(5), pp. 264–272.

205.  Mirzayans, R., Andrais, B., Scott, A., Wang, Y.W., Kumar, P. and Murray, D. 2017. Multinucleated Giant Cancer Cells Produced in Response to Ionizing Radiation Retain Viability and Replicate Their Genome. *International Journal of Molecular Sciences* 18(2).

206.  Mitin, N. et al. 2022. A biomarker of aging, p16, predicts peripheral neuropathy in women receiving adjuvant taxanes for breast cancer. *npj Breast Cancer* 8(1), p. 103.

207.  Mo, D. et al. 2016. Human Helicase RECQL4 Drives Cisplatin Resistance in Gastric Cancer by Activating an AKT–YB1–MDR1 Signaling Pathway. *Cancer Research* 76(10), pp. 3057–3066.

208.  Mohammad, S.N. and Hopfinger, A.J. 1980. Chemical reactivity of a methyldiazonium ion with nucleophilic centers of DNA bases. *Journal of Theoretical Biology* 87(2), pp. 401–419.

209.  Moiseeva, O. et al. 2013. Metformin inhibits the senescence-associated secretory phenotype by interfering with IKK/NF-κB activation. *Aging cell* 12(3), pp. 489–498.

210.  Monnat, R.J. 2010. Human RECQ helicases: Roles in DNA metabolism, mutagenesis and cancer biology. *Seminars in Cancer Biology* 20(5), pp. 329–339.

211.  Murali, B. et al. 2018. Inhibition of the Stromal p38MAPK/MK2 Pathway Limits Breast Cancer Metastases and Chemotherapy-Induced Bone Loss. *Cancer research* 78(19), pp. 5618–5630.

212.  Nakayama, H., Nakayama, K., Nakayama, R., Irino, N., Nakayama, Y. and Hanawalt, P.C. 1984. Isolation and genetic characterization of a thymineless death-resistant mutant of Escherichia coli K12: Identification of a new mutation (recQ1) that blocks the RecF recombination pathway. *Molecular and General Genetics MGG* 195(3), pp. 474–480.

213.  Nakayama, T., Blitz, I.L., Fish, M.B., Odeleye, A.O., Manohar, S., Cho, K.W.Y. and Grainger, R.M. 2014. Cas9-based genome editing in Xenopus tropicalis. *Methods in enzymology* 546, pp. 355–375.

214.  Nakayama, Y., Igarashi, A., Kikuchi, I., Obata, Y., Fukumoto, Y. and Yamaguchi, N. 2009. Bleomycin-induced over-replication involves sustained inhibition of mitotic entry through the ATM/ATR pathway. *Experimental Cell Research* 315(15), pp. 2515–2528.

215.  Neftel, C. et al. 2019. An Integrative Model of Cellular States, Plasticity, and Genetics for Glioblastoma. *Cell* 178(4), pp. 835-849.e21.

216.  Nehme, Z., Pasquereau, S., Haidar Ahmad, S., El Baba, R. and Herbein, G. 2022. Polyploid giant cancer cells, EZH2 and Myc upregulation in mammary epithelial cells infected with high-risk human cytomegalovirus. *EBioMedicine* 80, p. 104056.

217.  Neijenhuis, S., Begg, A.C. and Vens, C. 2005. Radiosensitization by a dominant negative to DNA polymerase β is DNA polymerase β-independent and XRCC1-dependent. *Radiotherapy and Oncology* 76(2), pp. 123–128.

218.  Newman, J.A. and Gileadi, O. 2020. RecQ helicases in DNA repair and cancer targets. *Essays in biochemistry* 64(5), pp. 819–830.

219.  Nguyen, G.H. et al. 2013. A Small Molecule Inhibitor of the BLM Helicase Modulates Chromosome Stability in Human Cells. *Chemistry & Biology* 20(1), pp. 55–62.

220.  Nicholas, C., Holger, B., Jan, P., Charlene, M. and Philip, L. 2006. Mutation of the Murine Bloom's Syndrome Gene Produces Global Genome Destabilization. *Molecular and Cellular Biology* 26(17), pp. 6713–6726.

221.  Nientiedt, C., Duensing, A., Zschäbitz, S., Jäger, D., Hohenfellner, M., Stenzinger, A. and Duensing, S. 2021. PARP inhibition in prostate cancer. *Genes, Chromosomes and Cancer* 60(5), pp. 344–351.

222.  Nimonkar, A. V, Özsoy, A.Z., Genschel, J., Modrich, P. and Kowalczykowski, S.C. 2008. Human exonuclease 1 and BLM helicase interact to resect DNA and initiate DNA repair. *Proceedings of the National Academy of Sciences* 105(44), pp. 16906–16911.

223.  Niu, N. et al. 2016. Linking genomic reorganization to tumor initiation via the giant cell cycle. *Oncogenesis* 5(12), pp. e281–e281.

224.  Noble, A., Abu-Daya, A. and Guille, M. 2021. Cryopreservation of Xenopus Sperm and In Vitro Fertilization Using Frozen Sperm Samples. *Cold Spring Harbor Protocols*.

225.  Obrosova, I.G. et al. 2004. Role of poly(ADP-ribose) polymerase activation in diabetic neuropathy. *Diabetes* 53(3), pp. 711–720.

226.  Ochocka, N. et al. 2021. Single-cell RNA sequencing reveals functional heterogeneity of glioma-associated brain macrophages. *Nature Communications* 12(1), p. 1151.

227.  Ochocka, N. et al. 2023. Specialized functions and sexual dimorphism explain the functional diversity of the myeloid populations during glioma progression. *Cell Reports* 42(1).

228.  Oliver, L., Lalier, L., Salaud, C., Heymann, D., Cartron, P.F. and Vallette, F.M. 2020. Drug resistance in glioblastoma: are persisters the key to therapy? *Cancer Drug Resistance* 3(3), pp. 287–301.

229.  Ong, D.S.T. et al. 2017. PAF promotes stemness and radioresistance of glioma stem cells. *Proceedings of the National Academy of Sciences* 114(43), pp. E9086–E9095.

230.  Opresko, P.L., von Kobbe, C., Laine, J.-P., Harrigan, J., Hickson, I.D. and Bohr, V.A. 2002. Telomere-binding protein TRF2 binds to and stimulates the Werner and Bloom syndrome helicases. *The Journal of biological chemistry* 277(43), pp. 41110–41119.

231.  Opresko, P.L., Mason, P.A., Podell, E.R., Lei, M., Hickson, I.D., Cech, T.R. and Bohr, V.A. 2005. POT1 Stimulates RecQ Helicases WRN and BLM to Unwind Telomeric DNA Substrates*. *Journal of Biological Chemistry* 280(37), pp. 32069–32080.

232.  Ossovskaya, V., Koo, I.C., Kaldjian, E.P., Alvares, C. and Sherman, B.M. 2010. Upregulation of Poly (ADP-Ribose) Polymerase-1 (PARP1) in Triple-Negative Breast Cancer and Other Primary Human Tumor Types. *Genes & cancer* 1(8), pp. 812–821.

233.  Ostrom, Q.T., Cioffi, G., Gittleman, H., Patil, N., Waite, K., Kruchko, C. and Barnholtz-Sloan, J.S. 2019. CBTRUS Statistical Report: Primary Brain and Other Central Nervous System Tumors Diagnosed in the United States in 2012-2016. *Neuro-oncology* 21(Suppl 5), pp. v1–v100.

234.  Ouyang, K.J., Woo, L.L., Zhu, J., Huo, D., Matunis, M.J. and Ellis, N.A. 2009.

SUMO Modification Regulates BLM and RAD51 Interaction at Damaged Replication Forks. *PLOS Biology* 7(12), p. e1000252.

235. Paez-Ribes, M., González-Gualda, E., Doherty, G.J. and Muñoz-Espín, D. 2019. Targeting senescent cells in translational medicine. *EMBO molecular medicine* 11(12), p. e10234.

236. Pan, X., Ye, P., Yuan, D.S., Wang, X., Bader, J.S. and Boeke, J.D. 2006. A DNA Integrity Network in the Yeast Saccharomyces cerevisiae. *Cell* 124(5), pp. 1069–1081.

237. Pandya, K.G., Patel, M.R. and Lau-Cam, C.A. 2010. Comparative study of the binding characteristics to and inhibitory potencies towards PARP and in vivo antidiabetogenic potencies of taurine, 3-aminobenzamide and nicotinamide. *Journal of Biomedical Science* 17(1), p. S16.

238. Park, C.-K. et al. 2012. The Changes in MGMT Promoter Methylation Status in Initial and Recurrent Glioblastomas. *Translational oncology* 5(5), pp. 393–397.

239. Park, G.-B., Jeong, J.-Y. and Kim, D. 2019a. Gliotoxin Enhances Autophagic Cell Death via the DAPK1-TAp63 Signaling Pathway in Paclitaxel-Resistant Ovarian Cancer Cells. *Marine Drugs* 17(7).

240. Park, J., Shim, J.-K., Yoon, S.-J., Kim, S.H., Chang, J.H. and Kang, S.-G. 2019b. Transcriptome profiling-based identification of prognostic subtypes and multi-omics signatures of glioblastoma. *Scientific Reports* 9(1), p. 10555.

241. Parrish, K.E. et al. 2015. Efficacy of PARP Inhibitor Rucaparib in Orthotopic Glioblastoma Xenografts Is Limited by Ineffective Drug Penetration into the Central Nervous System. *Molecular cancer therapeutics* 14(12), pp. 2735–2743.

242. Parsons, D.W. et al. 2008. An integrated genomic analysis of human glioblastoma multiforme. *Science (New York, N.Y.)* 321(5897), pp. 1807–1812.

243. Patel, A.G., De Lorenzo, S.B., Flatten, K.S., Poirier, G.G. and Kaufmann, S.H. 2012. Failure of iniparib to inhibit poly(ADP-Ribose) polymerase in vitro. *Clinical cancer research : an official journal of the American Association for Cancer Research* 18(6), pp. 1655–1662.

244. Patel, D.S., Misenko, S.M., Her, J. and Bunting, S.F. 2017. BLM helicase regulates DNA repair by counteracting RAD51 loading at DNA double-strand break sites. *Journal of Cell Biology* 216(11), pp. 3521–3534.

245. Peiris-Pagès, M., Sotgia, F. and Lisanti, M.P. 2015. Chemotherapy induces the cancer-associated fibroblast phenotype, activating paracrine Hedgehog-GLI signalling in breast cancer cells. *Oncotarget; Vol 6, No 13*.

246. Petkovic, M., Dietschy, T., Freire, R., Jiao, R. and Stagljar, I. 2005. The human Rothmund-Thomson syndrome gene product, RECQL4, localizes to distinct nuclear foci that coincide with proteins involved in the maintenance of genome stability. *Journal of Cell Science* 118(18), pp. 4261–4269.

247. Petsalaki, E., Dandoulaki, M., Morrice, N. and Zachos, G. 2014. Chk1 protects against chromatin bridges by constitutively phosphorylating BLM serine 502 to inhibit BLM degradation. *Journal of cell science* 127(Pt 18), pp. 3902–3908.

248. Poll, E.H. and Benbow, R.M. 1988. A DNA helicase from Xenopus laevis ovaries. *Biochemistry* 27(24), pp. 8701–8706.

249. Pollak, M.N. 2012. Investigating metformin for cancer prevention

and treatment: the end of the beginning. *Cancer discovery* 2(9), pp. 778–790.

250. Potapova, T. and Gorbsky, G.J. 2017. The Consequences of Chromosome Segregation Errors in Mitosis and Meiosis. *Biology* 6(1).

251. Qu, Y., Zhang, L., Rong, Z., He, T. and Zhang, S. 2013. Number of glioma polyploid giant cancer cells (PGCCs) associated with vasculogenic mimicry formation and tumor grade in human glioma. *Journal of Experimental & Clinical Cancer Research* 32(1), p. 75.

252. Quan Li, Pan Zhang, Yu-Ni Zhang, Hui-Xiao Hu1, Jun-Fang Yan, Ai-Hua Shen, and B.-R.H. 2022. Aberrant Expression of BLM Correlates with Malignant Progression and Immune Infiltration in Pancreatic Adenocarcinoma. *Cancer Screening and Prevention*.

253. Rahman, M. et al. 2022. Selective Vulnerability of Senescent Glioblastoma Cells to BCL-XL Inhibition. *Molecular Cancer Research* 20(6), pp. 938–948.

254. Rao, S.G. and Jackson, J.G. 2016. SASP: Tumor Suppressor or Promoter? Yes! *Trends in cancer* 2(11), pp. 676–687.

255. Rapp, M., Baernreuther, J., Turowski, B., Steiger, H.-J., Sabel, M. and Kamp, M.A. 2017. Recurrence Pattern Analysis of Primary Glioblastoma. *World neurosurgery* 103, pp. 733–740.

256. Ray Chaudhuri, A. and Nussenzweig, A. 2017. The multifaceted roles of PARP1 in DNA repair and chromatin remodelling. *Nature reviews. Molecular cell biology* 18(10), pp. 610–621.

257. Rivera, A.L. et al. 2010. MGMT promoter methylation is predictive of response to radiotherapy and prognostic in the absence of adjuvant alkylating chemotherapy for glioblastoma. *Neuro-Oncology* 12(2), pp. 116–121.

258. Roberson, R.S., Kussick, S.J., Vallieres, E., Chen, S.-Y.J. and Wu, D.Y. 2005. Escape from Therapy-Induced Accelerated Cellular Senescence in p53-Null Lung Cancer Cells and in Human Lung Cancers. *Cancer Research* 65(7), pp. 2795–2803.

259. Rogers, C.M., Wang, J.C.-Y., Noguchi, H., Imasaki, T., Takagi, Y. and Bochman, M.L. 2017. Yeast Hrq1 shares structural and functional homology with the disease-linked human RecQ4 helicase. *Nucleic Acids Research* 45(9), pp. 5217–5230.

260. Romero-Zamora, D. and Hayashi, M.T. 2023. A non-catalytic N-terminus domain of WRN prevents mitotic telomere deprotection. *Scientific Reports* 13(1), p. 645.

261. Rose, M., Burgess, J.T., O'Byrne, K., Richard, D.J. and Bolderson, E. 2020. PARP Inhibitors: Clinical Relevance, Mechanisms of Action and Tumor Resistance. *Frontiers in Cell and Developmental Biology* 8.

262. Rosenthal, A.S. et al. 2010. Discovery of ML216, a Small Molecule Inhibitor of Bloom (BLM) Helicase. Bethesda (MD): National Center for Biotechnology Information (US); 2010–. PMID: 24027802.

263. Ruchert, J.M., Brady, M.M., McMahan, S., Lacey, K.J., Latta, L.C., Sekelsky, J. and Stoffregen, E.P. 2022. Blm helicase facilitates rapid replication of repetitive DNA sequences in early Drosophila development. *Genetics* 220(1).

264. Ruggiero, A. et al. 2020. Temozolomide and oral etoposide in children with recurrent malignant brain tumors. Drugs Context. 2020 Jun 2;9:2020-3-1. PMID: 32547627; PMCID: PMC7271709.

265. Ruscetti, T., Lehnert, B.E., Halbrook, J., Le Trong, H., Hoekstra, M.F., Chen, D.J.

and Peterson, S.R. 1998. Stimulation of the DNA-dependent protein kinase by poly(ADP-ribose) polymerase. *The Journal of biological chemistry* 273(23), pp. 14461–14467.

266. Sajesh, B. V and McManus, K.J. 2015. Targeting SOD1 induces synthetic lethal killing in BLM- and CHEK2 -deficient colorectal cancer cells. *Oncotarget; Vol 6, No 29.*

267. Salam, R. et al. 2023. Cellular senescence in malignant cells promotes tumor progression in mouse and patient Glioblastoma. *Nature Communications* 14(1), p. 441.

268. Saleh, T. et al. 2020. Clearance of therapy-induced senescent tumor cells by the senolytic ABT-263 via interference with BCL-X(L) -BAX interaction. *Molecular oncology* 14(10), pp. 2504–2519.

269. Saleh, T., Carpenter, V.J., Bloukh, S. and Gewirtz, D.A. 2022. Targeting tumor cell senescence and polyploidy as potential therapeutic strategies. *Seminars in Cancer Biology* 81, pp. 37–47.

270. Sangrithi, M.N., Bernal, J.A., Madine, M., Philpott, A., Lee, J., Dunphy, W.G. and Venkitaraman, A.R. 2005. Initiation of DNA Replication Requires the RECQL4 Protein Mutated in Rothmund-Thomson Syndrome. *Cell* 121(6), pp. 887–898.

271. Sanoff, H.K. et al. 2014. Effect of Cytotoxic Chemotherapy on Markers of Molecular Age in Patients With Breast Cancer. *JNCI: Journal of the National Cancer Institute* 106(4), p. dju057.

272. Sarbajna, S., Davies, D. and West, S.C. 2014. Roles of SLX1–SLX4, MUS81–EME1, and GEN1 in avoiding genome instability and mitotic catastrophe. *Genes & Development* 28(10), pp. 1124–1136.

273. Schärer, O.D. 2013. Nucleotide excision repair in eukaryotes. *Cold Spring Harbor perspectives in biology* 5(10), p. a012609.

274. Schenk, K.M., Reuss, J.E., Choquette, K. and Spira, A.I. 2019. A review of canakinumab and its therapeutic potential for non-small cell lung cancer. *Anti-cancer drugs* 30(9), pp. 879–885.

275. Schmitt, C.A., Wang, B. and Demaria, M. 2022. Senescence and cancer — role and therapeutic opportunities. *Nature Reviews Clinical Oncology* 19(10), pp. 619–636.

276. Schnöller, L.E. et al. 2022. Integrative analysis of therapy resistance and transcriptomic profiling data in glioblastoma cells identifies sensitization vulnerabilities for combined modality radiochemotherapy. *Radiation Oncology* 17(1), p. 79.

277. Schurman, S.H. et al. 2009. Direct and indirect roles of RECQL4 in modulating base excision repair capacity. *Human Molecular Genetics* 18(18), pp. 3470–3483.

278. Schwarzenbach, C. et al. 2021. Targeting c-IAP1, c-IAP2, and Bcl-2 Eliminates Senescent Glioblastoma Cells Following Temozolomide Treatment. *Cancers* 13(14).

279. Sengupta, S. et al. 2004. Functional interaction between BLM helicase and 53BP1 in a Chk1-mediated pathway during S-phase arrest. *Journal of Cell Biology* 166(6), pp. 801–813.

280. Shamanna, R.A. et al. 2014. RECQ helicase RECQL4 participates in non-homologous end joining and interacts with the Ku complex. *Carcinogenesis* 35(11), pp. 2415–2424.

281. Shao, X., Joergensen, A.M., Howlett, N.G., Lisby, M. and Oestergaard, V.H. 2020. A distinct role for recombination repair factors in an early cellular

response to transcription–replication conflicts. *Nucleic Acids Research* 48(10), pp. 5467–5484.

282. Sharma, S., Yao, H.-P., Zhou, Y.-Q., Zhou, J., Zhang, R. and Wang, M.-H. 2014. Prevention of BMS-777607-induced polyploidy/senescence by mTOR inhibitor AZD8055 sensitizes breast cancer cells to cytotoxic chemotherapeutics. *Molecular Oncology* 8(3), pp. 469–482.

283. Shimamoto, A., Nishikawa, K., Kitao, S. and Furuichi, Y. 2000. Human RecQ5β, a large isomer of RecQ5 DNA helicase, localizes in the nucleoplasm and interacts with topoisomerases 3α and 3β. *Nucleic Acids Research* 28(7), pp. 1647–1655.

284. Shimono, J. et al. 2018. Clinicopathological analysis of polyploid diffuse large B-cell lymphoma. *PloS one* 13(4), p. e0194525.

285. Shorrocks, A.-M.K. et al. 2021. The Bloom syndrome complex senses RPA-coated single-stranded DNA to restart stalled replication forks. *Nature Communications* 12(1), p. 585.

286. Sidana, S. et al. 2019. Tetraploidy is associated with poor prognosis at diagnosis in multiple myeloma. *American journal of hematology* 94(5), pp. E117–E120.

287. Singh, D.K. et al. 2010. The involvement of human RECQL4 in DNA double-strand break repair. *Aging Cell* 9(3), pp. 358–371.

288. Singh, D.K. et al. 2012. The human RecQ helicases BLM and RECQL4 cooperate to preserve genome stability. *Nucleic Acids Research* 40(14), pp. 6632–6648.

289. Singleton, M.R., Dillingham, M.S. and Wigley, D.B. 2007. Structure and Mechanism of Helicases and Nucleic Acid Translocases. *Annual Review of Biochemistry* 76(1), pp. 23–50.

290. Sirois, I. et al. 2019. A Unique Morphological Phenotype in Chemoresistant Triple-Negative Breast Cancer Reveals Metabolic Reprogramming and PLIN4 Expression as a Molecular Vulnerability. *Molecular cancer research : MCR* 17(12), pp. 2492–2507.

291. Sokolov, A. V et al. 2021. Brain Cancer Drug Discovery: Clinical Trials, Drug Classes, Targets, and Combinatorial Therapies. *Pharmacological reviews* 73(4), pp. 1–32.

292. Sottoriva, A. et al. 2013. Intratumor heterogeneity in human glioblastoma reflects cancer evolutionary dynamics. *Proceedings of the National Academy of Sciences of the United States of America* 110(10), pp. 4009–4014.

293. Strobel, H. et al. 2019. Temozolomide and Other Alkylating Agents in Glioblastoma Therapy. *Biomedicines* 7(3).

294. Stupp, R. et al. 2005. Radiotherapy plus concomitant and adjuvant temozolomide for glioblastoma. *The New England journal of medicine* 352(10), pp. 987–996.

295. Stupp, R. et al. 2009. Effects of radiotherapy with concomitant and adjuvant temozolomide versus radiotherapy alone on survival in glioblastoma in a randomised phase III study: 5-year analysis of the EORTC-NCIC trial. *The Lancet. Oncology* 10(5), pp. 459–466.

296. Stupp, R., Brada, M., van den Bent, M.J., Tonn, J.-C. and Pentheroudakis, G. 2014. High-grade glioma: ESMO Clinical Practice Guidelines for diagnosis, treatment and follow-up. *Annals of oncology : official journal of the European Society for Medical Oncology* 25 Suppl 3, pp. iii93-101.

297. Sturzenegger, A., Burdova, K., Kanagaraj, R., Levikova, M., Pinto, C., Cejka, P.

and Janscak, P. 2014. DNA2 cooperates with the WRN and BLM RecQ helicases to mediate long-range DNA end resection in human cells. *The Journal of biological chemistry* 289(39), pp. 27314–27326.

298. Sugrue, M.M., Shin, D.Y., Lee, S.W. and Aaronson, S.A. 1997. Wild-type p53 triggers a rapid senescence program in human tumor cells lacking functional p53. *Proceedings of the National Academy of Sciences* 94(18), pp. 9648–9653.

299. Sulkowski, P.L. et al. 2017. 2-Hydroxyglutarate produced by neomorphic IDH mutations suppresses homologous recombination and induces PARP inhibitor sensitivity. *Science translational medicine* 9(375).

300. Sundaram, M., Guernsey, D.L., Rajaraman, M.M. and Rajaraman, R. 2004. Neosis: a novel type of cell division in cancer. *Cancer biology & therapy* 3(2), pp. 207–218.

301. Tan, J., Wang, X., Phoon, L., Yang, H. and Lan, L. 2020. Resolution of ROS-induced G-quadruplexes and R-loops at transcriptionally active sites is dependent on BLM helicase. *FEBS Letters* 594(9), pp. 1359–1367.

302. Tan, Q. et al. 2021. RNF8 ubiquitinates RecQL4 and promotes its dissociation from DNA double strand breaks. *Oncogenesis* 10(3), p. 24.

303. Tavera-Tapia, A. et al. 2019. RECQL5: Another DNA helicase potentially involved in hereditary breast cancer susceptibility. *Human Mutation* 40(5), pp. 566–577.

304. The Cancer Genome Atlas Research Network 2008. Comprehensive genomic characterization defines human glioblastoma genes and core pathways. *Nature* 455(7216), pp. 1061–1068.

305. Thomas, C. et al. 2019. Hit and run versus long-term activation of PARP-1 by its different domains fine-tunes nuclear processes. *Proceedings of the National Academy of Sciences of the United States of America* 116(20), pp. 9941–9946.

306. Thompson, B. 2007. Effect sizes, confidence intervals, and confidence intervals for effect sizes. *Psychology in the Schools* 44(5), pp. 423–432.

307. van Thuijl, H.F. et al. 2015. Evolution of DNA repair defects during malignant progression of low-grade gliomas after temozolomide treatment. *Acta Neuropathologica* 129(4), pp. 597–607.

308. Tikoo, S. et al. 2013. Ubiquitin-dependent recruitment of the Bloom Syndrome helicase upon replication stress is required to suppress homologous recombination. *The EMBO Journal* 32(12), pp. 1778–1792.

309. Tomaszewski, W., Sanchez-Perez, L., Gajewski, T.F. and Sampson, J.H. 2019. Brain Tumor Microenvironment and Host State: Implications for Immunotherapy. *Clinical cancer research : an official journal of the American Association for Cancer Research* 25(14), pp. 4202–4210.

310. Tripathi, V. et al. 2018. MRN complex-dependent recruitment of ubiquitylated BLM helicase to DSBs negatively regulates DNA repair pathways. *Nature Communications* 9(1), p. 1016.

311. Umate, P., Tuteja, N. and Tuteja, R. 2011. Genome-wide comprehensive analysis of human helicases. *Communicative & Integrative Biology* 4(1), pp. 118–137.

312. Veith, S. and Mangerich, A. 2015. RecQ helicases and PARP1 team up in maintaining genome integrity. *Ageing research reviews* 23(Pt A), pp. 12–28.

313. Verhaak, R.G.W. et al. 2010. Integrated genomic analysis identifies clinically relevant subtypes of glioblastoma characterized

by abnormalities in PDGFRA, IDH1, EGFR, and NF1. *Cancer cell* 17(1), pp. 98–110.

314. Viziteu, E., Kassambara, A., Pasero, P., Klein, B. and Moreaux, J. 2016. RECQ helicases are deregulated in hematological malignancies in association with a prognostic value. *Biomarker Research* 4(1), p.3.

315. Votino, C., Laudanna, C., Parcesepe, P., Giordano, G., Remo, A., Manfrin, E. and Pancione, M. 2017. Aberrant BLM cytoplasmic expression associates with DNA damage stress and hypersensitivity to DNA-damaging agents in colorectal cancer. *Journal of gastroenterology* 52(3), pp. 327–340.

316. Vuong, H.G., Nguyen, T.Q., Ngo, T.N.M., Nguyen, H.C., Fung, K.-M. and Dunn, I.F. 2020. The interaction between TERT promoter mutation and MGMT promoter methylation on overall survival of glioma patients: a meta-analysis. *BMC Cancer* 20(1), p. 897.

317. Walbert, T. et al. 2010. Combination of 6-thioguanine, capecitabine, and celecoxib with temozolomide or lomustine for recurrent high-grade glioma. *Journal of Clinical Oncology* 28(15_suppl), p. 2057.

318. Wang, B., Kohli, J. and Demaria, M. 2020a. Senescent Cells in Cancer Therapy: Friends or Foes? *Trends in cancer* 6(10), pp. 838–857.

319. Wang, C.-X. et al. 2020b. Design, Synthesis, and Evaluation of New Quinazolinone Derivatives that Inhibit Bloom Syndrome Protein (BLM) Helicase, Trigger DNA Damage at the Telomere Region, and Synergize with PARP Inhibitors. *Journal of Medicinal Chemistry* 63(17), pp. 9752–9772.

320. Wang, H., Li, S., Zhang, H., Wang, Y., Hao, S. and Wu, X. 2018. BLM prevents instability of structure-forming DNA sequences at common fragile sites. *PLOS Genetics* 14(11), p. e1007816.

321. Wang, J., Chen, J. and Gong, Z. 2013a. TopBP1 controls BLM protein level to maintain genome stability. *Molecular cell* 52(5), pp. 667–678.

322. Wang, L., Lankhorst, L. and Bernards, R. 2022. Exploiting senescence for the treatment of cancer. *Nature Reviews Cancer* 22(6), pp. 340–355.

323. Wang, Q. et al. 2013b. Polyploidy road to therapy-induced cellular senescence and escape. *International Journal of Cancer* 132(7), pp. 1505–1515.

324. Wang, Q. et al. 2017. Tumor Evolution of Glioma-Intrinsic Gene Expression Subtypes Associates with Immunological Changes in the Microenvironment. *Cancer cell* 32(1), pp. 42-56.e6.

325. Wang, Y., Cortez, D., Yazdi, P., Neff, N., Elledge, S.J. and Qin, J. 2000. BASC, a super complex of BRCA1-associated proteins involved in the recognition and repair of aberrant DNA structures. *Genes & development* 14(8), pp. 927–939.

326. Was, H. et al. 2017. Bafilomycin A1 triggers proliferative potential of senescent cancer cells in vitro and in NOD/SCID mice. *Oncotarget* 8(6), pp. 9303–9322.

327. Watt, P.M., Hickson, I.D., Borts, R.H. and Louis, E.J. 1996. SGS1, a Homologue of the Bloom's and Werner's Syndrome Genes, Is Required for Maintenance of Genome Stability in Saccharomyces cerevisiae. *Genetics* 144(3), pp. 935–945.

328. Wei, H. and Yu, X. 2016. Functions of PARylation in DNA Damage Repair Pathways. *Genomics, proteomics & bioinformatics* 14(3), pp. 131–139.

329. White-Gilbertson, S. et al. 2020. Tamoxifen is a candidate first-in-class inhibitor of acid ceramidase that reduces amitotic division in polyploid giant cancer cells—Unrecognized players in tumorigenesis. *Cancer*

*Medicine* 9(9), pp. 3142–3152.

330. Wiley, C.D. et al. 2021. Oxylipin biosynthesis reinforces cellular senescence and allows detection of senolysis. *Cell Metabolism* 33(6), pp. 1124-1136.e5.

331. Wilson, T.A., Karajannis, M.A. and Harter, D.H. 2014. Glioblastoma multiforme: State of the art and future therapeutics. *Surgical neurology international* 5, p. 64.

332. Witzens-Harig, M., Memmer, M.L., Dreyling, M. and Hess, G. 2013. A phase I/II trial to evaluate the safety, feasibility and activity of salvage therapy consisting of the mTOR inhibitor Temsirolimus added to standard therapy of Rituximab and DHAP for the treatment of patients with relapsed or refractory diffuse large c. *BMC cancer* 13, p. 308.

333. Wu, J., Capp, C., Feng, L. and Hsieh, T. 2008. Drosophila homologue of the Rothmund–Thomson syndrome gene: Essential function in DNA replication during development. *Developmental Biology* 323(1), pp. 130–142.

334. Wu, L., Davies, S.L., Levitt, N.C. and Hickson, I.D. 2001. Potential Role for the BLM Helicase in Recombinational Repair via a Conserved Interaction with RAD51*. *Journal of Biological Chemistry* 276(22), pp. 19375–19381.

335. Wu, W. et al. 2010. Joint NCCTG and NABTC prognostic factors analysis for high-grade recurrent glioma. *Neuro-Oncology* 12(2), pp. 164–172.

336. Xie, J. et al. 2022. The Roles of RNA Helicases in DNA Damage Repair and Tumorigenesis Reveal Precision Therapeutic Strategies. *Cancer Research* 82(5), pp. 872–884.

337. Xu, X. and Liu, Y. 2009. Dual DNA unwinding activities of the Rothmund–Thomson syndrome protein, RECQ4. *The EMBO Journal* 28(5), pp. 568–577.

338. Xu, X., Rochette, P.J., Feyissa, E.A., Su, T. V and Liu, Y. 2009. MCM10 mediates RECQ4 association with MCM2-7 helicase complex during DNA replication. *The EMBO Journal* 28(19), pp. 3005–3014.

339. Yan, H. et al. 2009. IDH1 and IDH2 mutations in gliomas. *The New England journal of medicine* 360(8), pp. 765–773.

340. Yan, H. et al. 2023. The Heterogeneous Cellular States of Glioblastoma Stem Cells Revealed by Single Cell Analysis. *Stem Cells* 41(2), pp. 111–125.

341. Yang, J., Liu, M., Hong, D., Zeng, M. and Zhang, X. 2021. The Paradoxical Role of Cellular Senescence in Cancer. *Frontiers in Cell and Developmental Biology* 9.

342. Yang, P. et al. 2015. IDH mutation and MGMT promoter methylation in glioblastoma: results of a prospective registry. *Oncotarget* 6(38), pp. 40896–40906.

343. Yin, A., Zhang, L., Cheng, J., Dong, Y., Liu, B., Han, N. and Zhang, X. 2014. The Predictive but Not Prognostic Value of MGMT Promoter Methylation Status in Elderly Glioblastoma Patients: A Meta-Analysis. *PLOS ONE* 9(1), p. e85102.

344. Yin, Q.-K. et al. 2019. Discovery of Isaindigotone Derivatives as Novel Bloom's Syndrome Protein (BLM) Helicase Inhibitors That Disrupt the BLM/DNA Interactions and Regulate the Homologous Recombination Repair. *Journal of Medicinal Chemistry* 62(6), pp. 3147–3162.

345. Zach, L., Yedidia-Aryeh, L. and Goldberg, M. 2022. Estrogen and DNA damage modulate mRNA levels of genes involved in homologous recombination repair in estrogen-deprived cells. *Journal of Translational Genetics and Genomics* 6(2), pp. 266–280.

346. Zack, T.I. et al. 2013. Pan-cancer patterns of somatic copy number

alteration. *Nature Genetics* 45(10), pp. 1134–1140.

347. Zhang, D., Wang, Y. and Zhang, S. 2014a. Asymmetric cell division in polyploid giant cancer cells and low eukaryotic cells. *BioMed research international* 2014, p. 432652.

348. Zhang, J., Qiao, Q., Xu, H., Zhou, R. and Liu, X. 2022a. Human cell polyploidization: The good and the evil. *Seminars in Cancer Biology* 81, pp. 54–63.

349. Zhang, L., Pitcher, L.E., Prahalad, V., Niedernhofer, L.J. and Robbins, P.D. 2022b. Targeting cellular senescence with senotherapeutics: senolytics and senomorphics. *The FEBS Journal* n/a(n/a).

350. Zhang, S. et al. 2021. BKM120 sensitizes glioblastoma to the PARP inhibitor rucaparib by suppressing homologous recombination repair. *Cell Death & Disease* 12(6), p. 546.

351. Zhang, S., Mercado-Uribe, I., Xing, Z., Sun, B., Kuang, J. and Liu, J. 2014b. Generation of cancer stem-like cells through the formation of polyploid giant cancer cells. *Oncogene* 33(1), pp. 116–128.

352. Zhou, Y. et al. 2021. Parthanatos and its associated components: Promising therapeutic targets for cancer. *Pharmacological research* 163, p. 105299.

353. Zhu, X., Chen, H., Yang, Y., Xu, C., Zhou, J., Zhou, J. and Chen, Y. 2018. Distinct prognosis of mRNA expression of the five RecQ DNA-helicase family members - RECQL, BLM, WRN, RECQL4, and RECQL5 - in patients with breast cancer. *Cancer management and research* 10, pp. 6649–6668.

354. Zlotnik, A. 2004. Chemokines in neoplastic progression. *Seminars in cancer biology* 14(3), pp. 181–185.

355. Zou, H., Stoppani, E., Volonte, D. and Galbiati, F. 2011. Caveolin-1, cellular senescence and age-related diseases. *Mechanisms of Ageing and Development* 132(11), pp. 533–542.